

VOL. 19 NO. 4 DECEMBER 1968
COMPLETING VOLUME 19
PUBLISHED MONTHLY

JOURNAL OF

ELECTROANALYTICAL CHEMISTRY AND INTERFACIAL ELECTROCHEMISTRY

International Journal devoted to all Aspects
of Electroanalytical Chemistry, Double Layer
Studies, Electrokinetics, Colloid Stability, and
Electrode Kinetics.

EDITORIAL BOARD:

- J. O'M. BOCKRIS (Philadelphia, Pa.)
G. CHARLOT (Paris)
B. E. CONWAY (Ottawa)
P. DELAHAY (New York)
A. N. FRUMKIN (Moscow)
L. GIERST (Brussels)
M. ISHIBASHI (Kyoto)
W. KEMULA (Warsaw)
H. L. KIES (Delft)
J. J. LINGANE (Cambridge, Mass.)
J. LYKLEMA (Wageningen)
G. W. C. MILNER (Harwell)
R. H. OTTEWILL (Bristol)
J. E. PAGE (London)
R. PARSONS (Bristol)
C. N. REILLEY (Chapel Hill, N.C.)
G. SEMERANO (Padua)
M. VON STACKELBERG (Bonn)
I. TACHI (Kyoto)
P. ZUMAN (Prague)

E L S E V I E R

GENERAL INFORMATION

Types of contributions

- (a) Original research work not previously published in other periodicals.
- (b) Reviews on recent developments in various fields.
- (c) Short communications.
- (d) Bibliographical notes and book reviews.

Languages

Papers will be published in English, French or German.

Submission of papers

Papers should be sent to one of the following Editors:

Professor J. O'M. BOCKRIS, John Harrison Laboratory of Chemistry,
University of Pennsylvania, Philadelphia 4, Pa. 19104, U.S.A.

Dr. R. H. OTTEWILL, Department of Chemistry, The University, Bristol 8, England.

Dr. R. PARSONS, Department of Chemistry, The University, Bristol 8, England.

Professor C. N. REILLEY, Department of Chemistry,
University of North Carolina, Chapel Hill, N.C. 27515, U.S.A.

Authors should preferably submit two copies in double-spaced typing on pages of uniform size. Legends for figures should be typed on a separate page. The figures should be in a form suitable for reproduction, drawn in Indian ink on drawing paper or tracing paper, with lettering etc. in thin pencil. The sheets of drawing or tracing paper should preferably be of the same dimensions as those on which the article is typed. Photographs should be submitted as clear black and white prints on glossy paper. Standard symbols should be used in line drawings, the following are available to the printers:



All references should be given at the end of the paper. They should be numbered and the numbers should appear in the text at the appropriate places.
A summary of 50 to 200 words should be included.

Reprints

Fifty reprints will be supplied free of charge. Additional reprints (minimum 100) can be ordered at quoted prices. They must be ordered on order forms which are sent together with the proofs.

Publication

The *Journal of Electroanalytical Chemistry and Interfacial Electrochemistry* appears monthly. For 1969, each volume has 3 issues and 4 volumes will appear. Subscription price: \$ 70.00 or Sfr. 304.00 per year; \$ 17.50 or Sfr. 76.00 per volume; plus postage. Additional cost for copies by air mail available on request. For advertising rates apply to the publishers.

Subscriptions

Subscriptions should be sent to:

ELSEVIER SEQUOIA S.A., P.O. Box 851, 1001 Lausanne 1, Switzerland

*In continuation of a
well-known book series:*

ORGANOMETALLIC CHEMISTRY REVIEWS

SECTION B ANNUAL SURVEYS

A new Elsevier Sequoia Journal

The "Annual Surveys of Organometallic Chemistry" (Seydel-King) published so far in book form have been the standard reference work for, and unanimously appraised by, any scientist or researcher, teacher or student wanting to keep abreast with the progress made in all fields of organometallic chemistry.

In order to channel through these annual surveys to the reader faster than a book appearing only once a year would permit, their continuation is now published in the form of a journal entitled **Organometallic Chemistry Reviews — Section B — Annual Surveys** (three to four issues to the volume, one volume per year). The first volume is Vol. 4, the three volumes of the book series now being back volumes to the Journal.

The Journal "Organometallic Chemistry Reviews" published since 1966 will continue as **Organometallic Chemistry Reviews — Section A — Subject Reviews.**

Publishers:



Elsevier Sequoia S.A.

4 Avenue Ruchonnet P.O. Box 851
1001 LAUSANNE 1 Switzerland

From A to Z

Keep updated on all developments
in Organometallic Chemistry

Actinides
Aluminium
Antimony
Arsenic

Beryllium
Bismuth
Boron

Cadmium
Calcium
Chromium
Cobalt
Copper

Ferrocene

Gallium
Germanium
Gold

Hafnium

Indium
Iridium
Iron

Lanthanides
Lead
Lithium

Magnesium
Manganese

Mercury
Molybdenum

Nickel
Niobium

Osmium
Osmocene

Palladium
Platinum
Potassium

Rhenium
Rhodium
Ruthenium
Ruthenocene

Sodium
Silicon
Silver

Tantalum
Technetium
Thallium
Tin
Titanium
Tungsten

Vanadium

Zinc
Zirconium

The Authors:

D. Seydel
R.B. King

E.C. Ashby
R.W. Bott
E.J. Bulten
F. Calderazzo
G.O. Doak
J.J. Eisch
L.D. Freedman
W.H. Glaze
J.G. Luyten
D.S. Matteson
J.G. Noltes
L.C. Willemse



**Organometallic Chemistry Reviews
Section B
Annual Surveys**

Order Form

Please detach and complete this form, and return it to your usual subscription agent or to: Elsevier Sequoia S.A., P. O. Box 851, 1001 Lausanne 1, Switzerland.

Please enter my/our order for the items marked "X" below
Subscriptions to be entered: until cancelled for current year only.

Opinions on Organometallic Chemistry Reviews – Annual Surveys

“... worth having on the bookshelf.”

(Nature)

“... invaluable to anyone working in the field ...”

(Analytica Chimica Acta)

«Die übersichtliche, klare Darstellung und die kritische, sachkundige Auswahl werden dieser Reihe einen festen Platz überall dort sichern, wo Interesse an der Organometall-Chemie besteht.»

(Österr. Chemiker-Zeitung)

“The value of this ready reference work to those working on organometallic chemistry can hardly be overestimated.”

(Chemistry and Industry)

Subscription to **Organometallic Chemistry Reviews, Section B, Annual Surveys** (Sfrs 83.50 = approx. US\$ 19.80 or £ 8.7.0 incl. postage) starting with Vol. 4, No. 1, 1968.

Seydel/King: “Annual Surveys of Organometallic Chemistry”, Vol. 1 (covering the year 1964).

id., Vol. 2 (covering the year 1965).

id., Vol. 3 (covering the year 1966).

Please note: The preceding three items are the back volumes of Organometallic Chemistry Reviews, Section B, Annual Surveys. Prices will be quoted on request.

Subscription to Organometallic Chemistry Reviews, Section A, Subject Reviews (Sfrs 70.50 = approx. US\$ 16.30 or £ 7.1.0. incl. postage).

Organometallic Chemistry Reviews, Section A, Vol. 1, 1966 (Back Volume) Sfrs 76.25 = approx. US\$ 17.50 or £ 7.12.6. incl. postage.

Organometallic Chemistry Reviews, Section A, Vol. 2, 1967 (Back Volume) Sfrs 76.25 = approx. US\$ 17.50 or £ 7.12.6. incl. postage.

Payment: check enclosed please send invoice

Please send me/us a free sample copy of: Organometallic Chemistry Reviews — Section A — Subject Reviews Organometallic Chemistry Reviews — Section B — Annual Surveys.

Date: _____ Signature: _____

Name: _____

Company or Institution: _____

Street or P. O. Box: _____

City: _____ Zip Code/Postal Number: _____

Country: _____

Please note: All invoices will be made out in Swiss Francs. Foreign currency equivalents given for guidance only and subject to change. Payments in currency other than Swiss Francs are welcome at official Swiss exchange rate on day of payment.

25 ก.พ. 2512

Order Form

(see overleaf)

Please send me/us also further information on following Elsevier Sequoia Journals:

- Journal of Organometallic Chemistry
- Journal of Electroanalytical Chemistry and Interfacial Electrochemistry
- Journal of the Less-Common Metals
- Materials Science and Engineering
- Powder Technology
- Thin Solid Films
- Wear / Usure / Verschleiss

Your name and address on the back of this form, please!

Please complete this form and return it to your usual subscription agent or to:
Elsevier Sequoia S.A., P.O. Box 851, 1001 Lausanne 1, Switzerland.

SUBSCRIPTION INFORMATION

Organometallic Chemistry Reviews Section B — Annual Surveys

(1 volume per year; 3-4 issues to the volume; 1968 = Vol. 4)

Subscription rates:

Sales price	Sfrs 78.—
Postage	<u>Sfrs 5.50</u>
Total	<u>Sfrs 83.50</u>

Organometallic Chemistry Reviews Section A — Subject Reviews

(1 volume per year, 4 issues to the volume; 1968 = Vol. 3)

Subscription rates:

Sales price	Sfrs 65.—
Postage	<u>Sfrs 5.50</u>
Total	<u>Sfrs 70.50</u>

Back Volumes:

Sales prices	Sfrs 72.00
Postage & handling	<u>Sfrs 4.25</u>
Total	<u>Sfrs 76.25</u> per volume

For further information
please contact:

Elsevier Sequoia S.A.

4 Av. Ruchonnet, P.O. Box 851
1001 Lausanne 1, Switzerland

Telephone: (021) 23 72 13
Cables: ELSEVIER Lausanne



Elsevier Sequoia S.A.

P.O. Box 851
CH-1001 LAUSANNE 1
Switzerland

THE FORMATION OF METAL LAYERS

D. J. ASTLEY, J. A. HARRISON AND H. R. THIRSK

School of Chemistry, University of Newcastle upon Tyne, Newcastle upon Tyne, NE1 7RU (England)

(Received April 5th, 1968)

INTRODUCTION

In the electrochemical study of metal deposition, considerable difficulties arise owing to the complex structure of the underlying metal. Recent studies by BUDIEWSKI *et al.*¹ show that when silver is deposited on to dislocation-free filaments of silver, grown from a single crystal into a capillary, it grows in a simple manner uncomplicated by previous surface geometry, *i.e.*, by two-dimensional nucleation and growth of steps of monomolecular height across the surface. Normally, single crystals have sufficient dislocations in their surface to make them unsuitable for the investigation of the kinetics of metal deposition². ASTLEY *et al.*³ have shown that when metals are grown on inert carbon substrates, the initial stages of growth may be studied when the currents are controlled by the kinetics of the electrocrystallization reaction, and interpretation of the phenomenon as a phase change is possible.

If metal is deposited on to an inert substrate it can be certain that when current flows, material grows on the surface and can be removed without affecting the substrate. This is particularly true in the case of potential sweep and pulse measurements when the new potential regions are reached in very short times and the current flow to form a layer is characteristic of the nucleation and growth of the layer. In favourable conditions one would expect to be able to separate out the various parameters. This method is particularly powerful at low coverage before the complex outward growth of the layer could interfere.

SCHMIDT AND GYGAX⁴ have recently reported phenomena observed under potential sweep conditions when various metallic cations are reduced at inert metal electrodes. They obtained either two or one current/voltage peaks according to the system chosen and interpreted the results in terms of adsorption of metal governed by a Langmuir isotherm. According to the isotherm chosen, either linearized or full, they were able to predict the number of peaks obtained with a sweep profile. These so-called pseudo-capacitance peaks have also been similarly explained by HALE AND GREEF⁵, who offered an analysis in terms of interactive adsorption to account for the double-peaked nature of the current/voltage profile obtained for the system of hydrogen atom adsorption on noble metals. Our own experience shows that whenever new phases are formed, one must expect nucleation and growth to take some part, and look for crystallization processes to be involved in the phenomena observed by SCHMIDT AND GYGAX. It therefore seems pertinent to investigate these systems as involving crystal growth phenomena, and to extend the scope of the

techniques used to include the potentiostatic pulse method as a means of identifying them as such.

EXPERIMENTAL

The polycrystalline silver (Matthey spectrographically pure) and the single silver crystal (111 face) (Metals Research, Royston, Herts) electrodes were electro-polished potentiostatically in a cyanide bath by a method similar to that used by SHUTTLEWORTH *et al.*⁶. The lead electrode (99.99% purity) was electropolished in a fluoroborate bath by a method similar to that used by MOULEN⁷. The sides of the electrodes were insulated with Lacomit. Glassware was cleaned with a chromic/sulphuric acid mixture and rinsed thoroughly with triply-distilled water. All solutions were prepared using triply-distilled water. Lead solutions were made up from once-recrystallised A.R. lead nitrate and acetate in supporting electrolytes of once-recrystallised A.R. potassium chloride and sodium acetate, respectively. The sodium acetate solutions were acidified with A.R. acetic acid. Thallous solutions were made up from A.R. thallous sulphate and once-recrystallised A.R. potassium chloride. Cadmium solutions were made up from twice-recrystallised cadmium perchlorate, prepared by dissolving the precipitated hydroxide in A.R. perchloric acid, and once-recrystallised A.R. sodium perchlorate. White Spot purity nitrogen was passed through the solutions for 30 min before measurements were made. In some cases purified charcoal was added to the solutions and this made essentially no difference.

The potentials to be applied to the electrodes were set on the potentiostat with respect to the Ag/AgCl electrode in 1 M KCl solution (except for the case of the cadmium perchlorate solution where 1 M NaCl was used). The liquid junctions between the reference electrode solutions and the cell solutions were achieved by the use of a glass sinter.

A Luggin capillary was used with the reference to monitor the potential at the working electrode. The cell was designed so that the working electrode was parallel to the auxiliary electrode—a Pt spade in a compartment separated by a glass sinter.

The potentiostat (Type TR70-2A), and wave-form generator (Type RB1) were both transistorized (Chemical Electronics Co., Newcastle-upon-Tyne). The wave-form generator provided both single and double pulses, and also a linear potential sweep profile. Current-time transients under pulse conditions for long times were obtained by recording the observed current on the potentiostat microammeter as a function of time (measured using a stop-clock). Short time transients were observed oscillographically and were photographed, as were the current-voltage peaks observed under linear sweep conditions with the horizontal deflection plates connected for external voltage amplification.

RESULTS

The effect of applying a linear potential sweep profile from a suitable initial potential (anodic to the deposition potential for the cation involved) for the deposition of Pb on Ag from Cl⁻ solution is shown in Fig. 1a. The formation of two peaks is a characteristic feature of this system. It is found that the charge under the first peak for a polycrystalline silver substrate decreases with increasing sweep rate but

is of the order one would expect for a two-dimensional monolayer of Pb (*ca.* 280 $\mu\text{C cm}^{-2}$). In the case of the single Ag crystal, the charge is quite constant up to a sweep rate of 3 V/sec and is about 370 $\mu\text{C cm}^{-2}$. The charge under the second peak is a factor five to ten times that under the first peak, clearly corresponding to multilayer formation. The effect of using an acetate electrolyte in place of chloride (Fig. 1b), is to

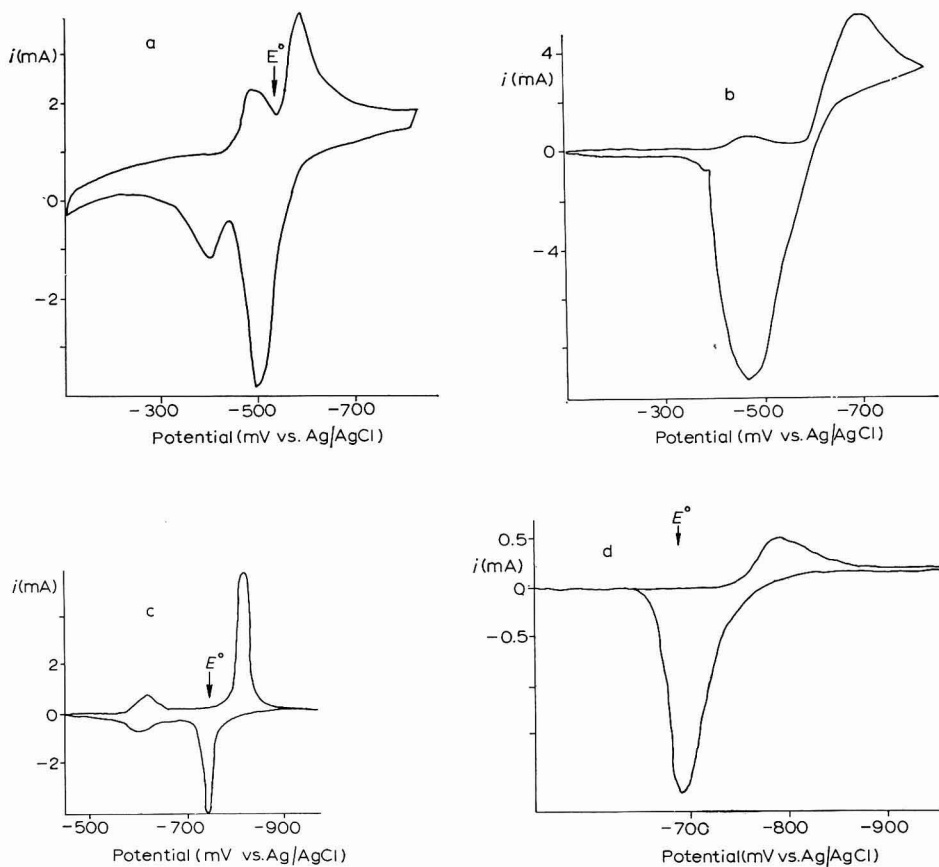


Fig. 1. (a), Double-peaked system for the deposition of Pb on a single Ag crystal (111 face, electro-polished) from a $3 \cdot 10^{-3} M$ $\text{Pb}(\text{NO}_3)_2/1 M$ KCl soln. at a sweep rate of 3 V/sec; (b), deposition of Pb on a polycrystalline electropolished Ag electrode from a $3 \cdot 10^{-2} M$ $\text{Pb}(\text{OAc})_2/1 M$ $\text{NaOAc}/0.1 M$ AcOH soln. at a sweep rate of 300 mV/sec; (c), deposition of Tl on a polycrystalline electropolished Ag electrode from a $8.75 \cdot 10^{-4} M$ $\text{TICl}/1 M$ KCl soln. at a sweep rate of 300 mV/sec; (d), deposition of Cd on a polycrystalline electropolished Pb electrode from a $8.3 \cdot 10^{-3} M$ $\text{Cd}(\text{ClO}_4)_2/1 M$ NaClO_4 soln. at a sweep rate of 30 mV/sec.

decrease the magnitude of the peak currents, possibly by preceding chemical reaction, though the charge under the peaks seems little affected. The formation of two peaks is thus a function of the depolarising ion and not the anion medium in which the reduction is conducted.

A second system in which two peaks are observed under sweep conditions is

that for the reduction of Tl^+ on Ag (Fig. 1c). The charge under the first peak is again equivalent to that due to a two-dimensional monolayer (*ca.* 200 $\mu\text{C cm}^{-2}$), the second peak being the multilayer formation with charge a factor four larger. A system which gives rise to only one peak under potential sweep is that of Cd on to Pb (Fig. 1d). The charge under this peak is equivalent to about ten to thirty two-dimensional monolayers.

The thermodynamic reversible potentials for the systems, measured for bulk Pb in the same solution for the Pb/Ag case and obtained from the literature⁸ for $\text{Tl(s)}/\text{TiCl}$ and $\text{Cd}^{2+}/\text{Cd(s)}$, are marked on the graphs as E^0 .

The monolayer peaks form anodic to E^0 . There is evidence in the electrochemical formation of mercury salts that the reversible potential of a monolayer occurs cathodic to the thermodynamic reversible potential for the bulk salt. For example, in the formation of Hg_2HPO_4 , the first monolayer occurs approximately 40 mV cathodic to the thermodynamic reversible potential⁹. It seems likely that when a metal is deposited on an inert substrate a similar effect could occur, and there is no reason to suppose that the first layer is the adsorption of discrete atoms rather than the formation of a crystalline phase.

The potential difference between the peaks is large, about 120 mV for Pb/Ag and 200 mV for Tl/Ag. It seems unlikely that these magnitudes could be explained in terms of adsorption isotherms.

BERZINS AND DELAHAY¹⁰ predict that the peak current (i_p) for the reversible deposition of an insoluble reductant with constant activity should be proportional to the square root of the sweep rate (ω). Plots of i_p against $\omega^{\frac{1}{2}}$ for the first and second peaks for the deposition of Pb on Ag (Figs. 2a and b), show that linearity is achieved for the second peak, but that a higher dependence of i_p on ω is suggested for the first peak. A similar situation is observed for the deposition of Tl on Ag (Fig. 2c and d). The assumption of a constant reductant activity would be justified for the second peak, when there is already a full monolayer of reductant available, but not for the first peak. A mathematical analysis of the formation of a partial monolayer under sweep conditions is possible, but has not been attempted in the present work.

It might be suspected from the above values of the charge under the peaks, representing either a monolayer or multilayer, that typical nucleation and growth processes are involved in these sweep regions. To test this, potentiostatic pulses were applied, starting from potentials well anodic to the reversible potential of the cation in solution and jumping to various positions within the sweep range. This should identify where nucleation and growth of the metal controls the current. It is well known that the electrochemical formation of a new phase leads to rising current/time transients in a potentiostatic pulse experiment, which are a function of the number and geometry of the nuclei, the growth rate at the boundary, and any possible diffusion processes.

The results of applying pulses at various potentials are shown in Fig. 3a and b. These are plotted as i vs. $t^{-\frac{1}{2}}$. The potentials extend through the monolayer and multilayer region. In the monolayer region, the curves are essentially diffusion-controlled, but with two striking differences. The curves do not go through the $i/t^{-\frac{1}{2}}$ origin but at $i=0$, cut the $t^{-\frac{1}{2}}$ -axis at finite times. At low overpotentials the plots show curvature. To compare the results with theory a model can be taken in which the change of activity of the metal on the surface is controlled by linear diffusion

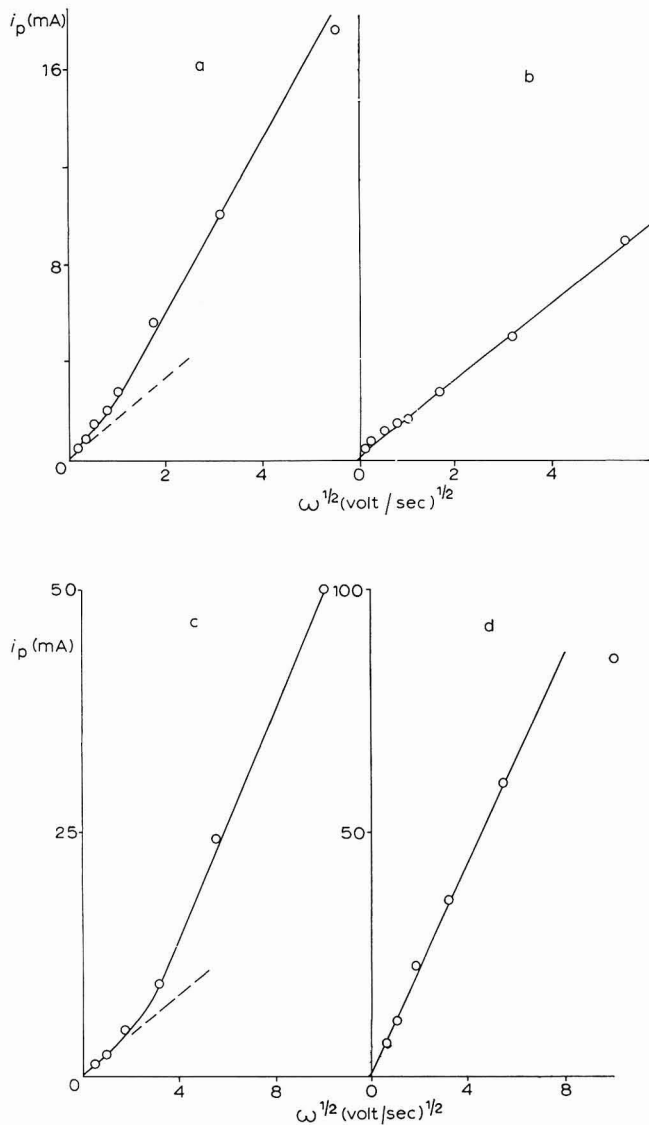


Fig. 2. Plot of peak current (i_p) vs. (sweep rate) $^{1/2}$ [$\omega^{1/2}$] for: (a), the peaks observed for Pb on polycrystalline Ag from a $3 \cdot 10^{-3} M$ $Pb(NO_3)_2/1 M$ KCl soln. for the first peak; (b), second peak; (c), for the peaks observed for Tl on polycrystalline Ag from a $8.75 \cdot 10^{-4} M$ $TlCl/1 M$ KCl soln. for the first peak; (d), second peak.

and the Nernst equation. The equations to be solved are:

$$\partial C_{(X,t)} / \partial t = D (\partial^2 C_{(X,t)} / \partial X^2) \quad (1)$$

where $C_{(X,t)}$ is the concentration of the metal ion at a distance, X , perpendicular from the electrode and at a time, t .

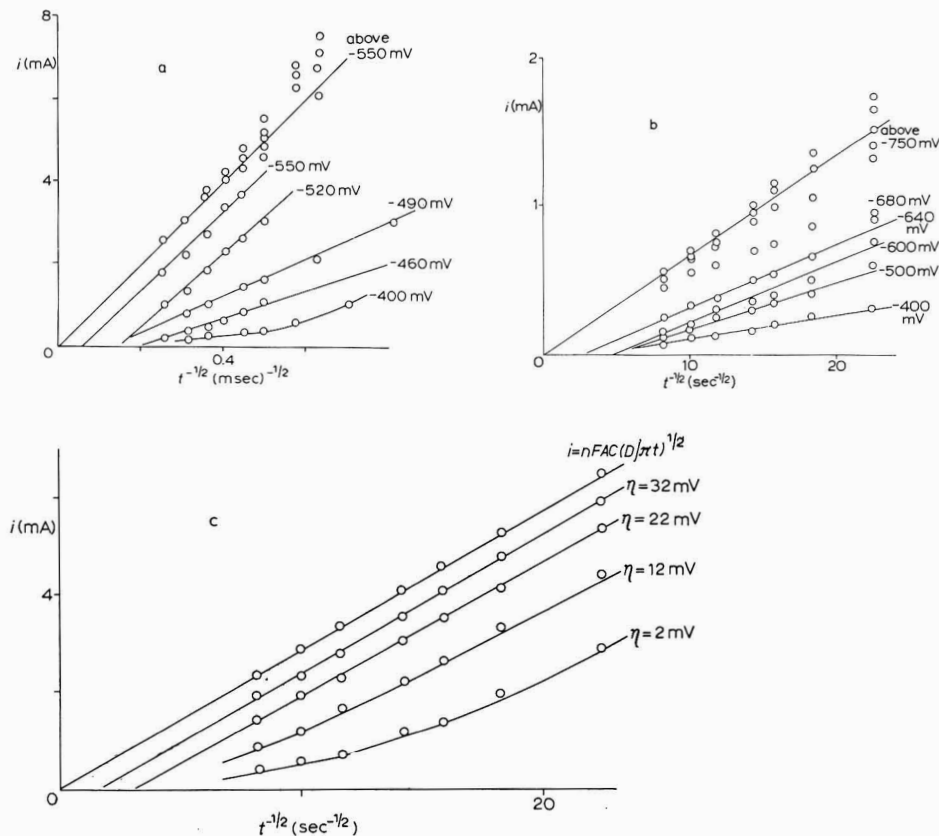


Fig. 3. Plot of current at short times *vs.* t^{-1} for: (a), Pb on polycrystalline Ag from a $3 \cdot 10^{-3} M$ $Pb(NO_3)_2/1 M$ KCl soln.; (b), Tl on polycrystalline Ag from a $6 \cdot 10^{-4} M$ $TlCl/1 M$ KCl soln.; (c), plot of the currents *vs.* t^{-1} predicted by eqn. (4).

The rate of change of the activity (*a*) of the deposit will be related to the flux at the interface,

$$\frac{da_{(t)}}{dt} = (AD/m)(\partial C_{(0,t)}/\partial x) \quad (2)$$

where *A* is the electrode area and *m* is the number of moles of deposit at monolayer coverage. If one assumes a linearized Langmuir isotherm with the Nernst equation to apply to the electrode reaction

$$C_{(0,t)}/C = a_{(t)} \exp(-nF\eta/RT) \quad (3)$$

where η is the overpotential, positive for a cathodic reaction, and *C* is the bulk concentration. The overpotential is defined with respect to normal thermodynamic equilibrium when $a=1$ and $C_{(0,t)}=C$.

Simultaneous solution of eqns. (1), (2) and (3) by the Laplace Transform method, where the Laplace transform of a function $f(t)$ is defined as

$$\tilde{f}(p) = \int_0^\infty f(t) \exp(-pt) dt$$

leads to

$$\partial \bar{C}(0,p)/\partial x = (C/D^{\frac{1}{2}})\{1/(p^{\frac{1}{2}} + CD^{\frac{1}{2}}(A/m)\exp(-nF\eta/RT))\}$$

Inversion leads to the expression for i ,

$$i = nFAC\sqrt{D/\pi t} - [(nFA^2C^2D/m)\exp(-nF\eta/RT)] \\ \times \exp[\{C^2DA^2\exp(-2nF\eta/RT)\}t/m^2] \operatorname{erfc}[\{CD^{\frac{1}{2}}A\exp(-nF\eta/RT)\}t^{\frac{1}{2}}/m]] \quad (4)$$

This expression may also be derived from the results obtained by DELAHAY AND TRACHTENBERG¹¹ for the kinetics of adsorption of neutral substances on electrodes using the linearized isotherm. Their results show that this simplification is only really justified with $C < ca. 10^{-4} M$. However, an exact solution is not possible using the complete isotherm, though REINMUTH¹² produced a series solution. For low concentrations, REINMUTH found good agreement between the result predicted for the full and linearized isotherm up to 50% coverage. The assumption of linear diffusion conditions is somewhat uncertain if separate nuclei are considered present on the electrode surface. Under these conditions, hemispherical diffusion zones would spread out into the solution.

The form of the $i/t^{-\frac{1}{2}}$ plots predicted by eqn. (4) for the parameters corresponding to the Pb/Ag deposition, ($C = 3 \cdot 10^{-3} M$, $A = 0.28 \text{ cm}^2$, $m = 1.9 \cdot 10^{-10} \text{ moles}$), is shown in Fig. 3c. Totally diffusion-controlled currents are much more rapidly achieved by this equation for increasing cathodic overpotentials than those reached for the deposition of Pb and Tl on to Ag in Fig. 3a and b; nevertheless, the curves reproduce qualitatively the characteristics of the experimental curves. The theoretical plots are curved at low overpotentials and intersect the $t^{-\frac{1}{2}}$ -axis. The parameter that can be varied in eqn. (4) is m . The value of m chosen in calculating Fig. 3c is that expected for a two-dimensional plane of lead atoms packed as the basal plane of the close packed cubic lattice. If m is increased twice, the overpotential to reach the limiting diffusion rate calculated from

$$i = nFAC\sqrt{D/\pi t}$$

is 30 mV, and when m is halved the overpotential becomes 60 mV.

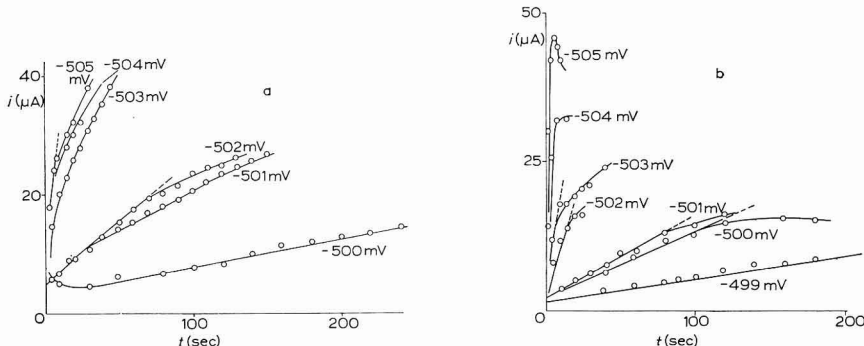


Fig. 4. Typical cathodic i vs. t transients obtained with $3.4 \cdot 10^{-3} M$ $\text{Pb}(\text{NO}_3)_2/1 M$ KCl soln. on polycrystalline Ag. (a), no prepulse; (b), with a prepulse of -700 mV (ref. Ag/AgCl) for 10 msec.

Pulsing into the multilayer region and at longer times for Pb/Ag, Tl/Ag and Cd/Pb, produces rising transients of the form shown in Fig. 4a for the deposition of Pb on to Ag. Rising transients are characteristic features in the formation of new phases, being due to nucleation and crystal growth processes. These transients are extremely potential-dependent and plots of current at constant time (and charge) show steep Tafel slopes (Fig. 5a). The slopes for the transients on the polycrystalline electrodes are $(4\text{--}6 \text{ mV})^{-1}$; for the deposition of Pb on to the single silver crystal the slope is less steep, $(12 \text{ mV})^{-1}$.

When nucleation and growth occur in an electrochemical process, it is often possible to investigate the growth process by forming the nuclei at a large potential prepulse and following the growth of these nuclei at small overpotentials where essentially no more nucleation occurs. In this case, prepulsing to 200 mV more cathodic than the growing potential for a series of short times from 3 to 300 msec gave the unexpected result that prepulsing did not increase the growth current transients significantly, as in Fig. 4b. The potential-dependence was also not very much affected. This is shown in Fig. 5b. Similarly, prepulsing to the lower cathodic region in the first peak region in an attempt to produce a monolayer coverage, had no effect upon the potential-dependence of the transients rising in the second peak region.

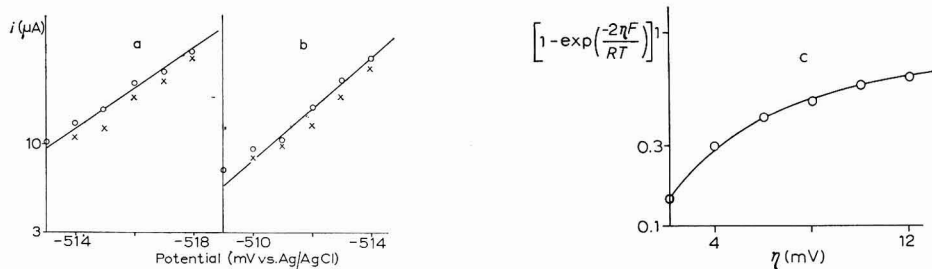


Fig. 5. Plot of current at fixed time, in the rising transient potential range, *vs.* potential for Pb on a single Ag crystal for $3 \cdot 10^{-3} M$ $\text{Pb}(\text{NO}_3)_2$ /1 M KCl soln. (a), no prepulse, $\times = 10$ sec, $\circ = 15$ sec; (b), prepulse -700 mV, 30 msec, $\times = 10$ sec, $\circ = 15$ sec; (c), plot of the function $[1 - \exp(-2\eta F/RT)]^{1/2}$ *vs.* potential.

It is impossible to explain such steep potential-dependencies in terms of any clear electrochemical process. The steepest slope for a $2e^-$ process, without diffusion control, at the periphery of the nuclei, for the current plotted at fixed charge as a function of potential (this approximates to a planar electrode, *i.e.*, constant interfacial area) is $(30 \text{ mV})^{-1}$. However, when diffusion in a Nernst diffusion layer of thickness, δ , controls the current,

$$i = \{nFAD/\delta\}C(1 - \exp[-nF\eta/RT]) \quad (5)$$

for a reversible electrochemical reaction at the surface. Figure 5c shows the potential-dependence of eqn. (5). It seems most probable that the nuclei do, in fact, grow from a Nernst diffusion layer. This arises because the metal is dense and rapidly depletes the solution in its neighbourhood. The current into each nucleus is then independent of the nucleus geometry. This fits well with the observed *at* time-dependence, which means progressive nucleation, each new nucleus bringing an equal increment in

current. The fact that prepulsing has no effect must mean that the rate of nucleation is controlled by the generation of defects in the surface of the deposited nuclei. A crude model in which the nucleus is considered as a growing hemisphere would give the surface area proportional to $t^{\frac{3}{2}}$ for constant flux. If it is assumed that the number of defects generated is directly dependent on the surface area, then the rate of nucleation is just $t^{\frac{3}{2}}$. The volume will, however, be far from hemispherical and in practice $t^{\frac{3}{2}}$ would scarcely be distinguishable from $i \propto t$. The potential-dependence can now be understood as arising from eqn. (5).

The model of defect generation accounts for the somewhat less steep potential-dependencies obtained for the single silver crystal substrate. The smoother surface of the single crystal would produce a lower number of three-dimensional nuclei at a fixed time than those produced on the polycrystalline substrate where greater surface irregularities would tend to present a greater surface area for nuclei formation. The reduction of the number of nuclei, and hence the number of defects at any time, would be reflected by lower potential-dependencies.

DISCUSSION

Since crystal growth cannot be a controlling factor in the deposition of soluble metal on to pure mercury, it would be expected that the deposition Pb/Hg would show one peak under sweep conditions. This has been observed in the literature¹³ and is confirmed by our measurements on Hg.

Since rising transients are observed under potentiostatic pulse conditions in the second peak region for Pb and Tl on to Ag and for the peak region for Cd/Pb, it seems evident that nucleation and growth of the new phase must be controlling factors in these regions. An inspection of the unit cell dimensions and crystal habits for the (deposited metal/substrate metal) systems investigated by SCHMIDT AND GYGAX⁴ reveal the connection between the interplay of the crystallographic features and the number of peaks observed under sweep conditions.

Nothing is, in fact, known about the metal monolayer structure, but the charge suggests that it is a two-dimensional layer. This is probably epitaxially fitted to the substrate metal. From Table 1 it seems that large differences in lattice dimen-

TABLE 1

A COMPARISON OF THE CRYSTALLOGRAPHIC PARAMETERS FOR DEPOSIT/SUBSTRATE INVESTIGATED BY SCHMIDT AND GYGAX⁴

No. of peaks	Deposited metal	Crystal habit	Unit cell dimension a_D (\AA)	Substrate metal	Crystal habit	Unit cell dimension a_s (\AA)	$(a_D - a_s)$ (\AA)
2	Pb	Cubic	4.95	Ag	Cubic	4.09	+0.86
2	Pb	Cubic	4.95	Cu	Cubic	3.61	+1.34
2	Tl(α)	Cubic	3.88	Au	Cubic	4.08	-0.2
2	Tl	Cubic	3.88	Ag	Cubic	4.09	-0.21
2	Tl	Cubic	3.88	Cu	Cubic	3.61	+0.27
1	Tl	Cubic	3.88	Sn	Tetragonal	5.82	-1.94
1	Cd	Hexagonal	2.96	Bi	Hexagonal	4.53	-1.57
1	Cd	Hexagonal	2.96	Pb	Cubic	4.95	-2
1	Cd	Hexagonal	2.96	Sn	Tetragonal	5.82	-2.86

sion between the substrate and the metal film preclude the monolayer peak, as this is energetically unfavourable. In the cases where the monolayer forms, some considerable potential difference is necessary before the layer can nucleate and grow further in a three-dimensional nucleation which grows with the preferred lattice dimensions of the bulk metal.

ACKNOWLEDGEMENT

One of us (D.J.A.) wishes to thank the Science Research Council for the provision of a Research Studentship.

SUMMARY

The deposition phenomena observed in the electrodeposition of deposits of Pb, Tl and Cd on to inert substrates of silver and lead are described for potentiostatic conditions. Under sweep conditions, Pb/Ag and Tl/Ag give rise to two peaks, whereas Cd/Pb gives only one. The first peaks are ascribed to the formation of monolayers of metal following the substrate profile; the second peak to multilayer formation with the deposit profile. Systems with large crystallographic dimensional differences are predicted to have only one peak. Phenomena observed in the first peak region are explained in terms of the growth of partial monolayers. Crystal growth processes are observed in the second peak-region, and the peak region for Cd/Pb, with extreme potential-dependence. This dependence is interpreted in terms of a fixed diffusion layer effect with the Nernst equation controlling the concentration at the interface. A model of defect generation explains the time-dependence of the transients.

REFERENCES

- 1 E. BUDĘWSKI, W. BOSTANOFF, T. VITANOFF, Z. STOINOFF, A. KOTZEWKA AND R. KAISCHEW, *Phys. State Solidi*, **13** (1966) 577.
- 2 M. FLEISCHMANN AND J. A. HARRISON, *Electrochim. Acta*, **11** (1966) 749.
- 3 D. J. ASTLEY, J. A. HARRISON AND H. R. THIRSK, *Trans. Faraday Soc.*, **64** (1968) 192.
- 4 E. SCHMIDT AND H. R. GYGAX, *J. Electroanal. Chem.*, **12** (1966) 300; *Helv. Chim. Acta*, **49** (1965) 733; **48** (1965) 1178; **48** (1965) 1584.
- 5 J. M. HALE AND R. GREEF, *Electrochim. Acta*, **12** (1967) 1409.
- 6 R. SHUTTLEWORTH, R. KING AND B. CHALMERS, *Metal Treat. Drop Forging*, **14** (1957) 161.
- 7 A. W. MOULEN, *J. Electrochem. Soc.*, **99** (1952) 133C.
- 8 *Stability Constants of Metal-ion Complexes*, *Chem. Soc. London, Spec. Publ.* **17** (1964).
- 9 R. D. ARMSTRONG, M. FLEISCHMANN AND J. W. OLDFIELD, *J. Electroanal. Chem.*, **14** (1967) 235.
- 10 T. BERZINS AND P. DELAHAY, *J. Am. Chem. Soc.*, **75** (1953) 555.
- 11 P. DELAHAY AND I. TRACHTENBERG, *J. Am. Chem. Soc.*, **79** (1957) 2355.
- 12 W. H. REINMUTH, *J. Phys. Chem.*, **65** (1961) 473.
- 13 C. A. STREULI AND W. D. COOKE, *Anal. Chem.*, **25** (1953) 1691.

ÉTUDE THÉORIQUE DE L'UTILISATION DE L'IMPÉDANCE OPÉRATIONNELLE DANS LES MÉTHODES TRANSITOIRES*

EUGÈNE LEVART ET EMMANUEL POIRIER D'ANGÉ D'ORSAY

Laboratoire d'Electrolyse du C.N.R.S., 92, Bellevue (France)

(Reçu le 30. janvier, 1968; sous forme revisée, le 4. juin, 1968)

CONSIDÉRATIONS GÉNÉRALES

La possibilité de relier les données impulsionales à la notion d'impédance est connue en électricité¹. Elle a aussi été signalée en électrochimie² mais n'a fait l'objet d'aucune étude approfondie bien qu'un procédé consistant à calculer l'impédance à partir de telles données ait déjà été proposé^{2,3}. Ceci nous a conduit à élaborer une méthode de traitement des données impulsionales en terme d'impédance^{4,5} qu'on se propose ici d'analyser plus en détail et de comparer avec les autres méthodes utilisées habituellement en cinétique électrochimique.

Les méthodes impulsionales consistent à relever la réponse transitoire résultant de l'application d'une perturbation donnée au système étudié. A une perturbation en tension correspond une réponse en courant et réciproquement. Pour la détermination de l'impédance, les données expérimentales doivent être obtenues dans les conditions de linéarité entre ces deux grandeurs. Bien que les systèmes électrochimiques ne remplissent en général pas cette condition, on peut, par approximation, les considérer comme linéaires pour de faibles perturbations. Il est alors possible d'assimiler chaque processus élémentaire de la réaction d'électrode à un circuit électrique composé d'éléments exclusivement linéaires (dont le nombre peut être selon le cas fini ou infini) tels que des résistances, des capacités et même exceptionnellement des self-inductances³. L'impédance de chaque circuit ainsi défini caractérise le processus élémentaire envisagé. Dans tout ce qui suivra, on se limitera à l'étude des seuls phénomènes linéaires.

Si l'on veut faire abstraction de la méthode expérimentale utilisée, on sait qu'il faut substituer à la notion classique de l'impédance définie en régime sinusoïdal permanent, celle, plus générale, de l'impédance opérationnelle définie par :

$$Z(s) = U(s)/J(s) \quad (1)$$

où $U(s)$ et $J(s)$ sont, respectivement, la tension et le courant, transformés au moyen d'un paramètre opérationnel s . $Z(s)$, par définition, ne dépend ni de la nature ni de la forme du signal perturbateur (tant que la condition de linéarité reste respectée). Elle ne dépend pas non plus de la transformation opérationnelle employée. Par

* Les travaux exposés dans cet article constituent une partie de la thèse de Doctorat ès-Sciences physiques de Mr. POIRIER D'ANGÉ D'ORSAY (Paris, 1966), adresse actuelle : Centre de Recherches, S.E.V. MARCHAL, 31, Toulouse (France).

exemple, dans toute expression $Z(s)$ obtenue par la transformation de Laplace, on peut remplacer s par $j\omega$ et on retrouve alors l'expression de l'impédance classique valable pour le régime sinusoïdal de fréquence ω . En raison de la corrélation qui existe entre s et $j\omega$, on donne souvent par la suite à s le nom de fréquence opérationnelle.

La transformation de Laplace convient particulièrement bien non seulement pour établir des expressions analytiques $Z(s)$ par résolution des équations phénoménologiques caractérisant les mécanismes électrochimiques étudiés, mais surtout pour obtenir à partir des données expérimentales impulsionales les valeurs numériques de $U(s)$ et $J(s)$ nécessaires au calcul de $Z(s)$. Rappelons que la transformation de Laplace fait correspondre à une fonction $f(t)$ la fonction transformée $F(s)$ définie par :

$$F(s) = \int_0^{\infty} f(t) \exp(-st) dt, \quad (2)$$

les valeurs de s utilisables étant celles des nombres réels et complexes dont la partie réelle est positive et suffisamment grande pour rendre convergente l'intégrale de définition.

Divers moyens permettant de calculer les valeurs du courant et de la tension transformés ont déjà été proposés²⁻⁶. Nous avons récemment mis au point un procédé graphique simple consistant à intégrer les surfaces délimitées par les valeurs de la réponse impulsionale, retracées suivant une abscisse $\exp(-st)$. Les résultats d'une étude expérimentale effectuée à l'aide de ce procédé seront présentés dans un prochain article⁷. Les diagrammes, $Z=f(s)$, ainsi obtenus y seront confrontés avec les expressions théoriques correspondant à différents types de réactions d'électrode.

Dans le présent article, on se propose d'établir un certain nombre de ces expressions en considérant tout d'abord le cas des valeurs purement réelles de s , puis on traitera brièvement des possibilités intéressantes, elles aussi, de l'emploi des valeurs complexes de s . Il sera montré que l'emploi de l'impédance opérationnelle permet d'élucider de façon satisfaisante le mécanisme de réactions d'électrode assez compliquées, en particulier de celles comportant des étapes chimiques, hétérogènes ou homogènes, associées. Or cette élucidation était à peu près impossible à l'aide des équations classiques décrivant les réponses transitoires en fonction du temps⁸⁻¹⁰.

ÉQUATIONS DE L'IMPÉDANCE OPÉRATIONNELLE DANS LE CAS DES VALEURS RÉELLES DE s

1. Contribution de la double couche électrochimique

Si l'on considère un système électrochimique comme équivalent à un circuit électrique (Fig. 1) dont la branche non faradique est constituée par une capacité de double couche, C_d , indépendante de s , on peut écrire la relation suivante pour l'impédance opérationnelle d'un tel circuit :

$$Z = r_e + 1/(1/Z_f + C_d s) \quad (3)$$

Dans cette équation, r_e représente la résistance pure du système, située en général dans l'électrolyte et Z_f l'impédance faradique. Pour l'instant, il n'est pas nécessaire de préciser la composition de la branche faradique dont les éléments constitutifs correspondent aux paramètres caractéristiques de la réaction dont est

le siège l'électrode considérée. Dans la méthode proposée, la détermination des valeurs de ces paramètres fait appel à la confrontation du diagramme expérimental de l'impédance opérationnelle avec les expressions $Z = f(s)$ établies théoriquement pour les différents mécanismes réactionnels envisagés. Dans le cas de réactions d'électrode

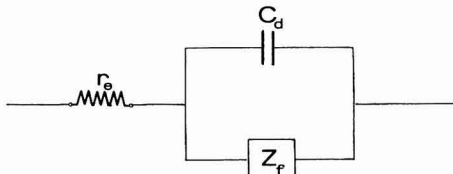


Fig. 1. Schéma équivalent d'une électrode. Cas général. (r_e), résistance d'électrolyte; (C_d), capacité de double couche; (Z_f), impédance faradique.

d'un certain degré de complexité, il est souvent plus aisément d'utiliser pour cela le diagramme de l'impédance faradique, extrait préalablement de celui de l'impédance globale, plutôt que ce dernier, et de le comparer avec les expressions théoriques $Z_f = f(s)$ correspondantes.

Le calcul de Z_f à partir de Z selon (3) nécessite la connaissance de la valeur de la résistance, r_e , et celle de la capacité de double couche, C_d . Le plus souvent, la détermination de C_d s'effectue sur l'électrode en l'absence de constituants électroactifs du système; il est parfois possible de l'effectuer en leur présence lorsque la durée de la mesure peut être choisie suffisamment courte pour que l'admittance faradique $1/Z_f$, dont l'ordre en s est toujours inférieur à 1, puisse être négligée devant le terme $C_{ds}s$. En effet, pour s assez élevé (t assez faible), l'éqn. (3) se réduit à:

$$Z \approx r_e + 1/C_{ds} \quad (4)$$

Quand cette dernière formule est vérifiée, elle permet aisément de déterminer à la fois r_e et C_d . En effet, la résistance, r_e , correspond à la limite à fréquence infinie de l'impédance globale. Si cette limite n'est pas atteinte aux erreurs près pour les plus hautes fréquences opérationnelles utilisées, la valeur de r_e peut être obtenue par extrapolation à fréquence infinie du graphe $Z = f(1/s)$. D'autre part, la capacité, C_d , peut être déterminée aux fréquences opérationnelles élevées à partir de la pente de la portion rectiligne de ce même graphe.

La constance de la valeur C_d par rapport à la fréquence, en présence d'une réaction d'électrode, est un problème très débattu. C'est ainsi que, pour le cas d'une réaction d'électrode comportant une adsorption spécifique, on a proposé récemment¹¹⁻¹² des traitements théoriques tenant compte d'une variation de C_d avec la fréquence. Toutefois, les idées sur ce point semblent encore sujettes à révision¹³⁻¹⁷.

Dans le présent travail, on admet que la capacité de double couche est déterminée en présence des constituants électroactifs du système aux fréquences opérationnelles élevées. La valeur ainsi trouvée est utilisée, dans tout le domaine de s , pour calculer Z_f à l'aide de l'éqn. (3). Le procédé décrit est justifié a posteriori lorsque l'erreur qui en résulte sur les valeurs de Z_f obtenues est faible, ce qui se trouve être souvent le cas pour les électrodes liquides. De toute manière la validité du procédé proposé peut être vérifiée dans la plupart des cas à l'aide d'équations, telles que éqn. (11) ou (16), valables dans tout le spectre de s .

2. Réactions d'électrode avec contrôle mixte par transfert et diffusion

Le cas le plus simple d'une réaction d'électrode, contrôlée seulement par le transport massique par diffusion a fait l'objet d'une précédente étude⁵. De même, on a déjà brièvement traité le cas du contrôle mixte par transfert de charges et diffusion^{4,5}; aussi, donnera-t-on ici seulement quelques précisions supplémentaires sur ce dernier cas en raison de son importance pratique.

Rappelons tout d'abord certaines conditions générales, valables pour toutes les réactions d'électrode, $Ox + ne \rightleftharpoons Red$, étudiées ici. L'interface de l'électrode est plane (une sphère de rayon suffisamment grand peut par approximation être assimilée à un plan). Un électrolyte support est toujours présent en grand excès, ce qui permet de considérer comme négligeables l'influence de la couche diffuse et celle de la migration des espèces électroactives. On suppose aussi négligeable l'effet de la convection. On peut donc considérer que le transport des espèces électroactives s'effectue par diffusion semi-infinie linéaire. Ceci est valable très généralement jusqu'à des fréquences opérationnelles extrêmement basses (durée de mesure dépassant plusieurs secondes).

Désignons par c_{Ox} et c_{Red} les concentrations à l'interface ($x=0$), variables avec le temps, et par c_{Ox}^0 et c_{Red}^0 les concentrations à l'équilibre. Pour la réaction d'électrode ainsi définie, la relation linéaire suivante entre le courant faradique, I_f , et la surtension η est valable dans le domaine des faibles surtensions:

$$I_f = A i_0 (c_{Red}/c_{Red}^0 - c_{Ox}/c_{Ox}^0 + \eta n F / RT) \quad (5)$$

A représentant l'aire de l'électrode, i_0 la densité de courant d'échange; R , T et F ayant leur signification habituelle.

Compte tenu de (5), la résolution des équations différentielles de Fick:

$$\frac{\partial c_{Red}}{\partial t} = D_{Red} \frac{\partial^2 c_{Red}}{\partial x^2} \quad \text{et} \quad \frac{\partial c_{Ox}}{\partial t} = D_{Ox} \frac{\partial^2 c_{Ox}}{\partial x^2} \quad (6)$$

avec les conditions aux limites: celles égalant à $t=0$ et pour $x \rightarrow \infty$ les concentrations à leur valeur d'équilibre et celles exprimant l'égalité des flux à l'interface ($x=0$):

$$I_f = AnF D_{Red} \left(\frac{\partial c_{Red}}{\partial x} \right)_{x=0} = -AnF D_{Ox} \left(\frac{\partial c_{Ox}}{\partial x} \right)_{x=0} \quad (7)$$

conduit à l'expression suivante de l'impédance faradique^{4,5}

$$Z_f = r_t + ms^{-\frac{1}{2}} = r_t + (m_{Ox} + m_{Red})s^{-\frac{1}{2}} \quad (8)$$

avec

$$m_{Ox} = RT/An^2 F^2 c_{Ox}^0 D_{Ox}^{\frac{1}{2}} \quad \text{et} \quad m_{Red} = RT/An^2 F^2 c_{Red}^0 D_{Red}^{\frac{1}{2}} \quad (9)$$

et r_t , résistance de transfert donnée par:

$$r_t = RT/AnF i_0. \quad (10)$$

Remarquons que le terme $ms^{-\frac{1}{2}}$ de l'éqn. (8) a la forme de l'impédance d'une ligne de transmission RC semi-infinie; ceci était d'ailleurs prévisible¹⁸ d'après l'analogie formelle existant entre les équations différentielles correspondantes. Le circuit électrique équivalent à l'électrode considérée est schématisé sur la Fig. 2 où $LT_{\infty}^{RC}_{Ox}$ et $LT_{\infty}^{RC}_{Red}$ désignent deux lignes de transmission, équivalentes respectivement à la diffusion de Ox et à la diffusion de Red.

D'après (3) et (8), on obtient:

$$Z - r_e = (r_t + ms^{-\frac{1}{2}}) / (1 + mC_d s^{\frac{1}{2}} + r_t C_d s) \quad (11)$$

Cette équation, valable dans tout le domaine de s , peut servir de base pour calculer les trois paramètres: m , r_t et C_d , et pour vérifier leur invariance en fonction de s .

La résistance de l'électrolyte, r_e , ayant été préalablement déterminée par la limite à fréquence infinie de l'impédance globale [voir formule (4)], nous proposons pour déterminer les autres paramètres le procédé opératoire suivant.

(a) *Détermination de m.* En développant (11) autour de $s=0$, on obtient:

$$Z - r_e \approx r_t + ms^{-\frac{1}{2}} - m^2 C_d \quad (12)$$

On peut donc obtenir m par la pente de la portion rectiligne apparaissant sur le diagramme $Z=f(s^{-\frac{1}{2}})$ (Fig. 3) vers les plus basses fréquences opérationnelles. Par ailleurs, comme le terme $m^2 C_d$ est souvent négligeable, l'extrapolation de cette droite à fréquence infinie donne une indication sur la valeur de r_t .

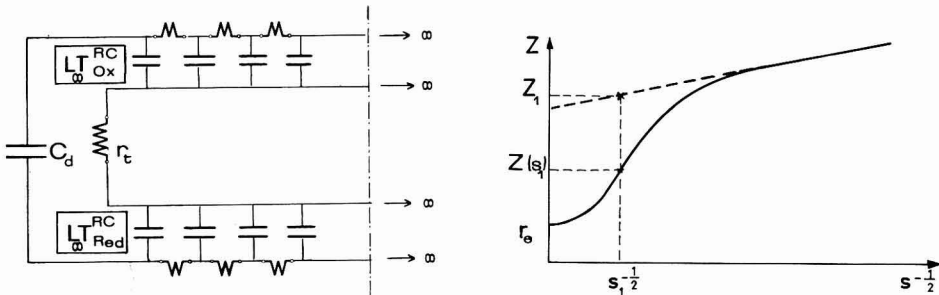


Fig. 2. Cas du contrôle mixte par transfert et diffusion. $L T_\infty^{RC} Ox$ et $L T_\infty^{RC} Red$, lignes de transmission équivalentes à la diffusion de l'espèce Ox et de l'espèce Red.

Fig. 3. Contrôle mixte par transfert et diffusion. Courbe $Z = f(s^{-\frac{1}{2}})$.

Si l'on s'intéresse aux valeurs des coefficients de diffusion, D_{Ox} et D_{Red} , leur calcul nécessite, conformément à (9), de séparer le paramètre global m en ses deux parties, m_{Ox} et m_{Red} . Cette séparation peut être effectuée par l'étude à concentration c_{Ox} ou c_{Red} variable. En effet, l'extrapolation à $c \rightarrow \infty$ du diagramme $m=f(1/c)$ fournit la valeur du terme correspondant au constituant dont la concentration a été maintenue constante. Bien entendu, lorsque l'un des termes se trouve être négligeable devant l'autre, la valeur globale de m se confond avec le terme prédominant⁵.

(b) *Détermination de r_t .* Dans le domaine des s élevés ($s^{\frac{1}{2}} \gg m/r_t$), on peut déterminer r_t à l'aide d'une des deux relations suivantes:

$$1/(Z - r_e) \approx C_d s + 1/r_t \quad (13)$$

$$1/(Z - r_e)s \approx C_d + 1/r_t s \quad (14)$$

La première d'entre elles exprime la variation de $1/(Z - r_e)$ (admittance d'électrode) en fonction de s , la seconde la variation de $1/(Z - r_e)s$ ("capacité" d'électrode) en fonction de s^{-1} . Les deux permettent de déterminer r_t (la première par extrapolation à

$s=0$, la seconde par la pente de la droite obtenue) avec une précision supérieure à celle qui résulte de l'extrapolation à $s \rightarrow \infty$ de la droite (12).

(c) *Détermination de C_d .* Les deux diagrammes précédents (13) et (14) fournissent dans le domaine des s élevés une valeur de C_d plus précise que celle que l'on obtiendrait à partir de la pente du diagramme $Z=f(s^{-1})$ suivant la formule (4). Cette valeur est égale dans le premier cas [utilisation de la formule (13)] à la pente de la droite obtenue et dans l'autre cas à l'ordonnée à l'origine du diagramme (14). L'amélioration de la précision par rapport à l'emploi de la formule (4) est due à la correction préalable de la chute ohmique et n'est effective que dans la mesure où r_e peut être connu avec une précision suffisante.

On peut aussi calculer C_d en utilisant le domaine des s moyens où la courbe $Z=f(s^{-1})$ s'écarte progressivement du prolongement de sa portion rectiligne (Fig. 3). En effet, pour un point quelconque (Z_1, s_1) situé sur ce prolongement, on a d'après (11) et (12):

$$Z_1 = r_e + (Z(s_1) - r_e) / \{1 - [Z(s_1) - r_e] C_d s_1\} - m^2 C_d. \quad (15)$$

Comme r_e et m ont été précédemment déterminés et que $Z(s_1)$ résulte de la transformation des fonctions $V(t)$ et $I(t)$ accessibles expérimentalement, l'éqn. (15), du second degré par rapport à C_d , permet de calculer à nouveau ce paramètre pour toutes les valeurs de s situées dans le domaine considéré. La valeur trouvée doit être constante aux erreurs près et égale à la valeur déterminée dans le domaine des s élevés.

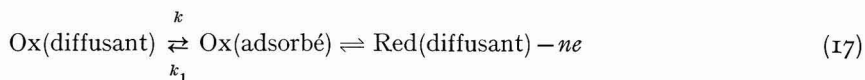
(d) *Opérations de contrôle.* Les valeurs des paramètres ainsi obtenues doivent être vérifiées à l'aide des formules recouvrant la totalité du spectre expérimental. Ces opérations peuvent conduire à un réajustement des valeurs choisies. Le calcul de C_d d'après (15) constitue un premier contrôle pour les valeurs de r_e et m . Une vérification de la valeur de C_d peut être effectuée en éliminant de l'impédance expérimentale les contributions de r_e et de C_d suivant la formule (3) et en représentant les valeurs ainsi calculées de Z_t en fonction de s^{-1} . D'après (8), le diagramme obtenu doit être une droite s'étendant sur tout le domaine exploré de s ; sa pente et son ordonnée à l'origine permettent de préciser les valeurs de r_t et de m . Une autre vérification, déjà signalée sous une forme un peu différente⁴, consistera à représenter la "capacité" d'électrode $1/(Z - r_e)s$ en fonction de sa composante faradique $1/(r_t + ms^{-1})s$ calculée à l'aide des valeurs choisies de r_t et de m :

$$1/(Z - r_e)s = 1/(r_t + ms^{-1})s + C_d. \quad (16)$$

Là encore, le diagramme obtenu doit être une droite recouvrant tout le domaine exploré de s . Son ordonnée à l'origine permet de préciser la valeur de C_d . Les éqns. (8) et (16) valables dans tout le spectre opérationnel permettent ainsi de vérifier le bien-fondé du processus simple envisagé.

3. Réaction d'électrode avec contrôle mixte par transfert, diffusion et adsorption spécifique des espèces réagissantes

Considérons le cas d'une réaction d'électrode comportant une étape d'adsorption spécifique d'une espèce réagissante, par exemple de l'espèce Ox. Supposons que le seul mode réactionnel possible soit:



(avec k =constante de vitesse d'adsorption et k_1 =constante de vitesse de désorption).

On obtient par résolution des équations de Fick avec les conditions aux limites envisagées dans ce cas, le résultat suivant:

$$Z_t = r_t + Z_{\text{Red}} + Z_{\text{Ox}}, \quad (18)$$

où

$$Z_{\text{Red}} = m_{\text{Red}} s^{-\frac{1}{2}} \quad (19)$$

est l'impédance de diffusion de l'espèce Red, et

$$Z_{\text{Ox}} = (r_{\text{aox}} + m_{\text{ox}} s^{-\frac{1}{2}}) / (1 + m_{\text{ox}} C_{\text{aox}} s^{\frac{1}{2}} + r_{\text{aox}} C_{\text{aox}} s) \quad (20)$$

l'impédance mixte de diffusion et d'adsorption spécifique de l'espèce Ox, tandis que m_{ox} et m_{Red} conservent les mêmes définitions qu'en l'absence d'adsorption [éqn. (9)]. D'une façon analogue à ce qui a été établi pour le régime sinusoïdal¹¹, il est possible de démontrer que l'expression de l'impédance Z_{Ox} reste la même quelle que soit la forme de l'isotherme d'adsorption.

Par exemple, dans le cas d'une isotherme de Langmuir, les expressions de r_{aox} et C_{aox} , qui représentent, respectivement, la résistance et la capacité d'adsorption de l'espèce Ox (Fig. 4), sont les suivantes:

$$r_{\text{aox}} = RT / An^2 F^2 k \gamma_{\text{ox}}^0 \quad (21)$$

et

$$C_{\text{aox}} = \gamma_{\text{ox}}^0 A n^2 F^2 / RT \quad (22)$$

avec γ_{ox}^0 concentration superficielle de l'adsorbat (recouvrement) à l'équilibre.

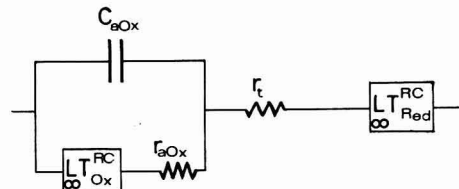


Fig. 4. Contrôle mixte par transfert, diffusion et adsorption spécifique de l'espèce Ox. r_{aox} et C_{aox} , résistance et capacité d'adsorption de l'espèce Ox.

Des expressions analogues peuvent être obtenues pour d'autres types d'isothermes¹⁹.

Le terme Z_{Ox} dans l'éqn. (20) a exactement la même forme que $Z - r_e$ dans l'éqn. (11) (analogie déjà signalée en régime sinusoïdal²⁰) et les équations établies pour le cas précédent peuvent donc s'appliquer ici. Ainsi, ayant calculé Z_t à partir de Z au moyen de l'éqn. (3), on détermine les inconnues par le mode opératoire suivant.

(a) *Détermination des paramètres de diffusion.* En développant (20) autour de $s=0$, on obtient, compte tenu de (18) et (19):

$$Z_t \approx r_t + r_{\text{aox}} + (m_{\text{ox}} + m_{\text{Red}}) s^{-\frac{1}{2}} - m_{\text{ox}}^2 C_{\text{aox}} \quad (23)$$

La pente du diagramme, $Z_t = f(s^{-\frac{1}{2}})$, donne donc directement la valeur de m . La séparation de ce paramètre en m_{ox} et m_{Red} est possible, comme dans le cas précédent, par l'étude effectuée en fonction de c_{ox} ou de c_{Red} et par extrapolation à $c \rightarrow \infty$

des valeurs de Z_f obtenues. Contrairement au cas précédent, cette séparation est ici indispensable pour les déterminations qui suivent.

(b) *Détermination de r_t .* Pour les fréquences assez élevées, telles que $r_{aox}C_{aoxs} \gg 1$, on a par analogie avec (4) :

$$Z_f - Z_{Red} \approx r_t + 1/C_{aoxs} \quad (24)$$

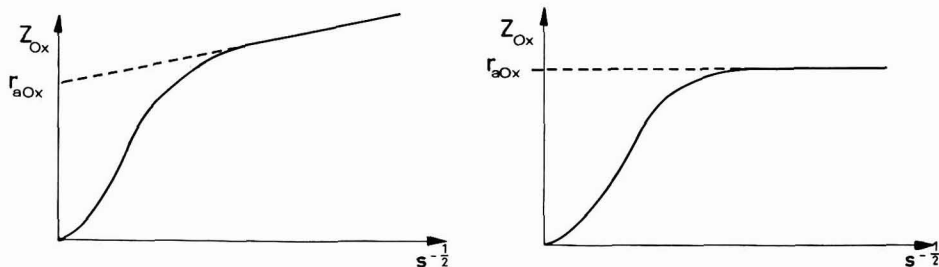
Les valeurs de Z_{Red} ayant été déterminées par (19), la représentation du premier terme de la relation (24) en fonction de s^{-1} donne donc r_t par l'ordonnée à l'origine et aussi C_{aox} par la pente.

(c) *Détermination des paramètres d'adsorption.* Connaissant r_t et Z_{Red} , on peut calculer Z_{Ox} à l'aide de l'éqn. (18). Comme il est d'autre part possible, par analogie avec (14), d'écrire la relation suivante, valable pour $s^{\frac{1}{2}} \gg m_{Ox}/r_{aox}$:

$$1/Z_{Oxs} \approx C_{aox} + 1/r_{aoxs} \quad (25)$$

on voit que la représentation de $1/Z_{Oxs}$ ("capacité" d'oxydation) en fonction de $1/s$ permet à la fois de calculer r_{aox} et de vérifier la valeur de C_{aox} obtenue par (24).

On peut encore se servir de la formule de base (20), valable dans tout le domaine de s ; elle permet, en effet, ayant déterminé au préalable m_{Ox} et Z_{Ox} , de calculer les deux paramètres d'adsorption, r_{aox} et C_{aox} , par deux équations du second degré, la relation (20) ayant été écrite pour deux valeurs de s . Bien entendu, il est aussi possible d'utiliser pour le calcul des paramètres d'adsorption les équations analogues aux éqns. (13), (15) et (16). L'allure caractéristique des courbes $Z_{Ox} = f(s^{-\frac{1}{2}})$ est représentée sur les Figs. 5 (cas général) et 6 (cas particulier $m_{Ox} \rightarrow 0$).



Figs. 5-6. Contrôle mixte par transfert, diffusion et adsorption spécifique de l'espèce Ox. (5) Courbe $Z_{Ox} = f(s^{-\frac{1}{2}})$. (6) Courbe $Z_{Ox} = f(s^{-\frac{1}{2}})$ pour $m_{Ox} \rightarrow 0$.

L'adsorption spécifique des deux espèces réagissantes Ox et Red se traite facilement si on suppose qu'il n'y a pas d'interaction entre les deux adsorptions (pour le cas de l'interaction cf. refs. 11 et 21). En effet, l'impédance s'exprime dans ce cas par l'éqn. (18) dans laquelle le terme Z_{Red} prend une forme identique à celle du terme Z_{Ox} :

$$Z_{Red} = (r_{aRed} + m_{Red}s^{-\frac{1}{2}})/(1 + m_{Red}C_{aRed}s^{\frac{1}{2}} + r_{aRed}C_{aRed}s) \quad (26)$$

L'étude de Z_f au moyen de développements limités pour les valeurs extrêmes de s ($s \rightarrow 0$ ou $s \rightarrow \infty$) reste encore possible^{20,22,23}, mais le recours à une machine à calculer semble être dans ce cas plus intéressant car il permet la confrontation avec l'expérience dans tout le domaine des fréquences opérationnelles. D'une façon générale, ce dernier procédé de détermination des paramètres caractéristiques d'une équation

d'électrode doit être préféré dès qu'il s'agit d'équations comportant un grand nombre d'inconnues.

4. Réaction d'électrode avec contrôle mixte par transfert, diffusion et réaction chimique homogène

Considérons une réaction d'électrode comportant une étape chimique homogène dans laquelle est impliquée, par exemple, la substance électroactive Ox:



Si on suppose la substance S_2 en excès, la vitesse de cette réaction est donnée par:

$$v = v_0 [(c_1/c_1^0)^{\rho_1} - (c_{\text{Ox}}/c_{\text{Ox}}^0)^{\rho}] \quad (28)$$

avec $v_0 = k(c_{\text{Ox}}^0)^\rho = k_1(c_1^0)^\rho$ = vitesse d'équilibre, ρ et ρ_1 étant les ordres de réaction respectifs de l'espèce Ox et S_1^{24} .

Pour de faibles perturbations, l'éqn. (28) peut s'écrire $v = v_0(\rho_1 g_1 - \rho g_{\text{Ox}})$, g_{Ox} et g_1 représentant les accroissements relatifs de concentration des espèces Ox et S_1 , et la résolution des équations différentielles de base avec les conditions aux limites envisagées nous donne:

$$Z_f = r_t + m_{\text{Red}} s^{-\frac{1}{2}} + Z_{\text{Ox}} \quad (29)$$

avec

$$Z_{\text{Ox}} = \frac{2^{\frac{1}{2}} m_{\text{Ox}}}{D_{\text{Ox}}^{\frac{1}{2}} b} \left(\frac{s - \frac{1}{2} D_{\text{Ox}} (a - b) + h}{(a + b)^{\frac{1}{2}}} - \frac{s - \frac{1}{2} D_{\text{Ox}} (a + b) + h}{(a - b)^{\frac{1}{2}}} \right), \quad (30)$$

ayant posé:

$$a = h/D_{\text{Ox}} + h_1/D_1 + s(I/D_{\text{Ox}} + I/D_1), \quad (31)$$

$$b = \left[\left(\frac{h}{D_{\text{Ox}}} + \frac{h_1}{D_1} \right)^2 + 2s \left(\frac{h}{D_{\text{Ox}}} - \frac{h_1}{D_1} \right) \left(\frac{I}{D_{\text{Ox}}} - \frac{I}{D_1} \right) + \left(\frac{I}{D_{\text{Ox}}} - \frac{I}{D_1} \right)^2 s^2 \right]^{\frac{1}{2}} \quad (32)$$

$$h = v_0 \nu \rho / c_{\text{Ox}}^0 \quad h_1 = v_0 \nu_1 \rho_1 / c_1^0 \quad (33)$$

Dans ces équations, D_1 est le coefficient de diffusion de la substance S_1 ; D_{Ox} , m_{Ox} et m_{Red} gardent leurs précédentes définitions.

Pour $s \rightarrow \infty$, l'éqn. (30) se simplifie en:

$$Z_{\text{Ox}} \approx m_{\text{Ox}} s^{-\frac{1}{2}}, \quad (34)$$

expression bien connue de la diffusion pure. Elle se simplifie aussi pour $s \rightarrow 0$ en:

$$Z_{\text{Ox}} \approx m_{\text{Ox}}' s^{-\frac{1}{2}} + r_h \quad (35)$$

avec:

$$m_{\text{Ox}}' = m_{\text{Ox}} h D_{\text{Ox}}^{\frac{1}{2}} / (h + h_1)^{\frac{1}{2}} (h_1 D_{\text{Ox}} + h D_1)^{\frac{1}{2}} \quad (36)$$

$$r_h = m_{\text{Ox}} h D_1^{\frac{1}{2}} / (h_1 D_{\text{Ox}} + h D_1)^{\frac{1}{2}} \quad (37)$$

r_h = résistance de réaction chimique homogène.

On voit que, dans le cas général (Fig. 7), Z_{Ox} est linéaire en fonction de $s^{-\frac{1}{2}}$ aussi bien pour $s \rightarrow \infty$ que pour $s \rightarrow 0$ mais avec des pentes différentes; pour des s moyens l'expression est assez compliquée et le recours à une machine à calculer est alors nécessaire.

Les deux cas particuliers suivants sont intéressants²⁴:

(a) $D_{\text{Ox}} = D_1$. L'équation générale (30) se simplifie en:

$$Z_{\text{Ox}} = m_{\text{Ox}} \frac{1}{(h+h_1)} \left[\frac{h}{(h+h_1+s)^{\frac{1}{2}}} + h_1 s^{-\frac{1}{2}} \right] \quad (38)$$

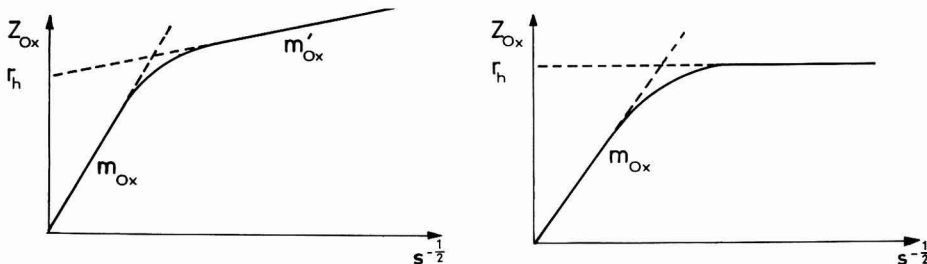
Pour $s \rightarrow 0$, l'éqn. (35) reste valable mais m_{Ox}' et r_h s'écrivent:

$$m_{\text{Ox}}' = m_{\text{Ox}} c_{\text{Ox}^0}/c_{\text{Ox}^0} + (\nu \rho / \nu_1 \rho_1) c_1^0 \quad (39)$$

$$r_h = m_{\text{Ox}} h / (h + h_1)^{\frac{1}{2}} \quad (40)$$

Pour $s \rightarrow \infty$, l'expression de Z_{Ox} reste inchangée (éqn. (34)). De plus, dans le domaine des s un peu moins élevés, on a:

$$Z_{\text{Ox}} = Z_{\text{Ox}} + \frac{1}{2} m_{\text{Ox}} h s^{-\frac{3}{2}} \quad (41)$$



Figs. 7-8. Contrôle mixte par transfert, diffusion et réaction chimique homogène concernant l'espèce Ox. (7) Courbe $Z_{\text{Ox}} = f(s^{-\frac{1}{2}})$. (8) Courbe $Z_{\text{Ox}} = f(s^{-\frac{1}{2}})$ pour $c_{\text{Ox}^0} \ll c_1^0$.

On voit donc que, dans ce cas particulier, la détermination de tous les paramètres est facile.

(b) $c_{\text{Ox}^0} \ll c_1^0$ avec $D_{\text{Ox}} = D_1$. L'équation générale (30) se simplifie alors en:

$$Z_{\text{Ox}} = m_{\text{Ox}} (h + s)^{-\frac{1}{2}} \quad (42)$$

qui donne aux limites, d'une part l'éqn. (34) pour $s \rightarrow \infty$, et d'autre part pour $s \rightarrow 0$:

$$Z_{\text{Ox}} = r_h \approx m_{\text{Ox}} h^{-\frac{1}{2}} \quad (43)$$

Dans ce cas, la détermination des paramètres est particulièrement facile (Fig. 8).

ÉQUATIONS DE L'IMPÉDANCE OPÉRATIONNELLE DANS LE CAS DES VALEURS COMPLEXES DE S

Il a toujours été supposé jusqu'à maintenant que les valeurs prises par la fréquence opérationnelle étaient purement réelles. L'emploi de valeurs complexes pour s peut s'avérer intéressant, par exemple pour mieux mettre en évidence la différence entre plusieurs types possibles de réactions d'électrode.

Le paramètre s étant, dans ce cas, de la forme $s = x + jy$, il en résulte que l'impédance opérationnelle s'écrit:

$$Z(x + jy) = Z_r(x, y) + jZ_i(x, y) \quad (44)$$

On a donc de nouvelles fonctions caractéristiques dans chaque cas particulier:

$$Z_r = f(x) \text{ et } Z_i = f(x) \quad \text{pour } y = \text{Cte}, \quad (45)$$

$$Z_r = f(y) \text{ et } Z_i = f(y) \quad \text{pour } x = \text{Cte}. \quad (46)$$

Le déphasage opérationnelle est aussi intéressant à considérer:

$$\operatorname{tg} \psi = Z_i/Z_r = f(x) \quad \text{pour } y = \text{Cte}, \quad (47)$$

$$\operatorname{tg} \psi = Z_i/Z_r = f(y) \quad \text{pour } x = \text{Cte}. \quad (48)$$

Prenons comme exemple des nouvelles possibilités ainsi offertes le cas d'une réaction hétérogène d'adsorption spécifique dans le cas particulier où la diffusion des espèces réagissantes est négligeable. Si on remplace s par $x + jy$ dans l'éqn. (20) dans le cas où $m_{\text{ox}} = 0$, on obtient pour Z_{ox} :

$$Z_r = r_{\text{aox}}(1 + xC_{\text{aox}}r_{\text{aox}})/\{(1 + xC_{\text{aox}}r_{\text{aox}})^2 + y^2C_{\text{aox}}^2r_{\text{aox}}^2\} \quad (49)$$

$$Z_i = -yC_{\text{aox}}r_{\text{aox}}^2/\{(1 + xC_{\text{aox}}r_{\text{aox}})^2 + y^2C_{\text{aox}}^2r_{\text{aox}}^2\} \quad (50)$$

d'où:

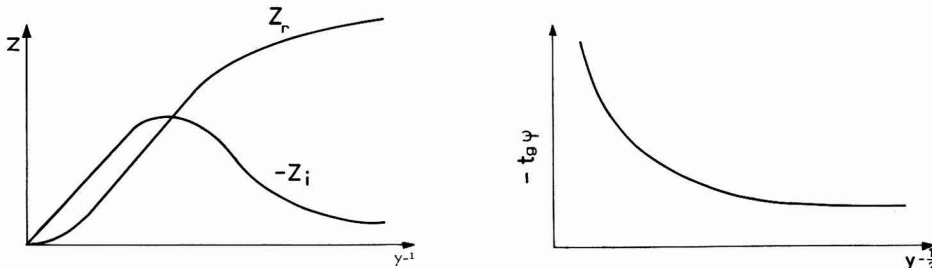
$$\operatorname{tg} \psi = -yC_{\text{aox}}r_{\text{aox}}/(1 + xC_{\text{aox}}r_{\text{aox}}) \quad (51)$$

Etudions les courbes $Z_r = f(y)$ et $-Z_i = f(y)$ pour $x = \text{Cte}$ (Fig. 9). Ces deux courbes partent toutes deux de zéro pour $y \rightarrow \infty$ et dans ce domaine on a: $Z_r = K_r y^{-2}$ et $-Z_i = K_i y^{-1}$. Elles se trouvent à nouveau confondues au maximum de Z_i . Les coordonnées de ce point sont:

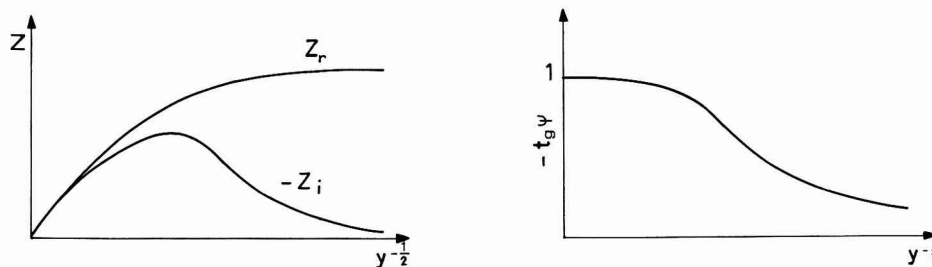
$$Z_i^{\max} = r_{\text{aox}}/2(1 + xC_{\text{aox}}r_{\text{aox}}) = \frac{1}{2}Z_r^{\max} \quad (52)$$

$$y_1 = (1 + xC_{\text{aox}}r_{\text{aox}})/C_{\text{aox}}r_{\text{aox}} \quad (53)$$

La courbe $\operatorname{tg} \psi = f(y)$ à $x = \text{Cte}$ est représentée sur la Fig. 10.



Figs. 9-10. Contrôle mixte par transfert et adsorption spécifique de l'espèce Ox, avec $m_{\text{ox}} \rightarrow 0$. (9) Courbes Z_r et $Z_i = f(y^{-1})$ pour $x = \text{Cte}$. (10) Courbe $\operatorname{tg} \psi = f(y^{-1})$ pour $x = \text{Cte}$.



Figs. 11-12. Contrôle mixte par transfert, diffusion et réaction homogène concernant l'espèce Ox avec $c_{\text{ox}}^0 \ll c_1^0$. (11) Courbe Z_r et $Z_i = f(y^{-1})$. (12) Courbe $\operatorname{tg} \psi = f(y)$ avec $x = \text{Cte}$.

Comme autre exemple, on peut citer le cas particulier d'une réaction homogène associée lorsque $c_{ox}^0 \ll c_1^0$. L'équation (42) exploitée pour des valeurs complexes de s nous donne²², pour $Z_r = f(y)$ et $-Z_i = f(y)$ avec $x = \text{Cte}$, les courbes représentées sur la Fig. 11. Partant toutes les deux de zéro pour $y \rightarrow \infty$ et ceci linéairement en $y^{-\frac{1}{2}}$, elles ne se recoupent pas. De plus, $\operatorname{tg} \psi = f(y)$ pour $x = \text{Cte}$ a l'allure représentée sur la Fig. 12.

En comparant les courbes caractéristiques de l'impédance opérationnelle, obtenues dans le cas des valeurs réelles de s d'une part (Figs. 6 et 8) et dans le cas des valeurs complexes d'autre part (Figs. 9 et 11), on voit que les différences entre les effets d'une réaction hétérogène ou homogène ressortent plus nettement dans ce dernier cas. L'emploi des valeurs complexes du paramètre opérationnel s semble donc pouvoir permettre une meilleure élucidation des phénomènes étudiés.

CONCLUSION

La particularité de la méthode d'étude des réactions d'électrode, proposée ici, réside dans le fait que l'identification du type de la réaction et la détermination de ses paramètres caractéristiques sont effectuées par confrontation, dans l'état transformé, du diagramme expérimental de l'impédance opérationnelle avec les expressions théoriques $Z = f(s)$ établies pour divers types de réaction d'électrode. La mise en oeuvre de la méthode présente donc deux aspects complémentaires: l'un expérimental et l'autre théorique.

Le premier est relatif à l'obtention du diagramme $Z = f(s)$ pour le système électrochimique étudié. Pour cela, les courbes expérimentales $I = f(t)$ et $V = f(t)$, obtenues dans les conditions de linéarité, c'est-à-dire avec des perturbations suffisamment faibles, sont soumises, par exemple graphiquement, à la transformation de Laplace. Le rapport de la valeur ainsi trouvée pour la tension transformée sur celle du courant transformé représente l'impédance du système étudié pour la fréquence opérationnelle choisie. En répétant la même opération avec un certain nombre de valeurs de la variable s , on obtient le diagramme expérimental de l'impédance, $Z = f(s)$.

En ce qui concerne le second aspect, on a préféré établir ici les expressions théoriques de l'impédance directement à partir des équations phénoménologiques, plutôt que d'utiliser la possibilité de remplacer la variable $j\omega$ par s dans les équations de l'impédance classique déjà connues dans certains cas. Ceci a été fait pour montrer la généralité et la simplicité de l'emploi de la variable opérationnelle s .

Pour que la confrontation du diagramme expérimental avec les expressions théoriques soit aussi complète que possible, l'exploitation de tout le domaine des fréquences opérationnelles accessibles expérimentalement est nécessaire, chaque partie de ce domaine ayant son importance particulière. C'est ainsi que, dans la plupart des cas, la capacité de double couche et la résistance d'électrolyte sont déterminées grâce à l'emploi des valeurs de s les plus élevées, tandis que les paramètres de la diffusion sont obtenus dans le domaine des basses fréquences opérationnelles. Enfin, le domaine des valeurs intermédiaires de s permet d'identifier le type particulier de réaction étudiée et d'en préciser les étapes et leurs constantes de vitesse.

Les avantages de la méthode proposée par rapport aux procédés classiques d'exploitation des mesures impulsionales sont nombreux.

C'est ainsi que, pour une réaction de type transfert-diffusion, dans la méthode potentiostatique, le courant d'échange est habituellement déterminé à partir d'une portion rectiligne qui doit apparaître, conformément à la théorie, sur la courbe expérimentale, $I = f(t^1)$, portion limitée du côté des temps courts par la fin de la charge de double couche et du côté des temps longs par la validité de l'approximation mathématique utilisée^{25,26}. Bien que divers efforts aient été faits pour permettre la détermination correcte de cette portion rectiligne²² et aussi pour l'allonger, par exemple en accélérant expérimentalement la charge de double couche^{27,28}, elle reste souvent dans la pratique assez mal définie et peut même, dans le cas des réactions rapides, être tout-à-fait inobservable. De plus, lorsque la résistance de l'électrolyte n'est pas négligeable et dans le cas où la montée en tension du potentiostat n'est pas suffisamment rapide, les résultats obtenus risquent d'être entachés d'erreurs considérables^{22,29-31}, à moins que l'on ne recoure à des perfectionnements tels que la compensation automatique de la chute ohmique³² ou la méthode potentiostatique différentielle³⁰. Enfin, la mesure de la capacité de double couche n'est pas possible par la méthode classique. De même, la méthode galvanostatique simple ne peut être utilisée que grâce à des approximations mathématiques du même genre que celles auxquelles fait appel la méthode potentiostatique. En revanche, avec l'emploi de l'impédance opérationnelle, ces difficultés n'existent plus, le recours aux approximations mathématiques précédentes n'étant pas nécessaire et la forme du signal appliquée n'ayant pas d'importance. A l'aide d'équations simples, valables dans tout le domaine du spectre opérationnel, la méthode proposée permet de tester facilement la présence du contrôle mixte par transfert et diffusion et rend donc possible la détermination des trois paramètres fondamentaux, m , r_t et C_a , pour des réactions d'électrode bien plus rapides que celles exploitables par les procédés classiques.

Dans le cas d'une réaction d'électrode comportant, en plus du transfert et de la diffusion, une étape d'adsorption spécifique, la possibilité de déterminer les paramètres de l'adsorption par les procédés classiques étaient tout-à-fait problématique¹⁰. Comme il a été montré ici, cette possibilité est réelle dans le cas de l'utilisation de l'impédance opérationnelle. Cependant, les calculs étant parfois assez compliqués, le recours à une machine à calculer est recommandé lorsqu'il s'agit d'explorer tout le domaine de s , ce qui est indispensable quand on veut vérifier la présence éventuelle de deux étapes d'adsorption spécifique.

Dans le cas d'une réaction d'électrode comportant entre autres une étape chimique homogène, les procédés classiques ne permettaient pas en général de déterminer les paramètres de cette dernière^{8,9}. Toutefois pour la méthode potentiostatique, certains cas particuliers ont été traités récemment³³. Grâce à l'emploi de l'impédance opérationnelle, des cas bien plus généraux peuvent être traités et les paramètres de la réaction homogène calculés.

Mais c'est la possibilité d'étudier une réaction électrochimique quelconque, à condition d'en pouvoir postuler les différentes étapes, qui constitue le principal avantage du traitement des informations impulsionales en terme d'impédance opérationnelle. Il suffit pour cela, après avoir assimilé le système électrochimique étudié à un circuit électrique composé de résistances, capacités, lignes de transmissions et éventuellement de self-inductances, d'en déterminer la fonction analytique, $Z(s)$. La confrontation de cette expression avec le diagramme obtenu expérimentalement peut alors être faite à l'aide d'un ordinateur, ce qui permet de calculer les paramètres

caractéristiques des étapes constitutifs de la réaction étudiée³⁴. Ceci n'était pas possible par l'exploitation classique des mesures impulsionales par suite des difficultés en général insurmontables d'établir des expressions analytiques rigoureuses en fonction du temps⁶.

Si l'on compare maintenant la méthode proposée avec la méthode classique de détermination de l'impédance en régime sinusoïdal, on peut constater que, sur le plan théorique, les deux méthodes offrent évidemment les mêmes possibilités et que c'est seulement sur le plan de la confrontation avec l'expérience que des différences se font jour. C'est ainsi que, pour une réaction donnée, on obtient en général une expression de l'impédance opérationnelle, $Z(s) = p_1(s)/p_2(s)$, ayant la forme d'un rapport de polynomes aux puissances positives, négatives, entières et fractionnaires de s . Cette expression est utilisable telle quelle et permet une confrontation facile avec l'expérience. Au contraire, dans le cas du régime sinusoïdal, pour effectuer cette confrontation, il faut représenter l'impédance sous la forme $Z(j\omega) = Z_r(\omega) + jZ_i(\omega)$ où Z_r et Z_i sont des rapports de polynomes en ω de degré plus élevé que les polynomes p_1 et p_2 de départ²⁴. Un autre avantage sur le plan de la confrontation est la possibilité d'utiliser dans la méthode opérationnelle, non seulement les équations établies pour les valeurs réelles de s , mais aussi toutes celles concernant les valeurs complexes de s .

Enfin, sur le plan des techniques expérimentales utilisées il a été montré^{5,34} qu'avec un appareillage unique et très simple, il est possible d'explorer par la méthode proposée un domaine de fréquences qui, partant pratiquement du courant continu, atteint quelques MHz, tandis que les mesures en régime sinusoïdal nécessitent pour cela l'emploi de plusieurs montages plus compliqués et d'une mise au point délicate. En revanche la précision des mesures est actuellement meilleure en régime sinusoïdal, du moins dans le domaine des fréquences acoustiques par suite de l'utilisation d'un pont, tandis que les mesures impulsionales se font encore à l'écran d'un oscilloscope et concernent la valeur totale de la grandeur mesurée. Mais, les techniques expérimentales évoluent très vite, et il n'est donc pas possible de conclure fermement en faveur de l'une ou de l'autre de ces méthodes sur des critères purement expérimentaux.

En résumé, la mesure de l'impédance, qu'elle soit classique en courant alternatif, ou opérationnelle par les méthodes transitoires, nous paraît être, la méthode la plus adaptée à l'étude des réactions d'électrode d'une certaine complexité et, en particulier, de celles dans lesquelles interviennent en plus du transfert et de la diffusion des réactions chimiques, homogènes ou hétérogènes. Pour cela, il faut, bien entendu, explorer tout le domaine des fréquences accessibles expérimentalement. Les exploitations faites dans un domaine restreint de temps ou de fréquences peuvent, en effet, conduire à des résultats incomplets et à des interprétations erronées.

REMERCIEMENTS

Les auteurs remercient Monsieur le Professeur M. BONNEMAY pour l'intérêt qu'il a porté à ce travail et les conseils qu'il leur a donnés.

RÉSUMÉ

On analyse les différents aspects d'une méthode originale de traitement des données impulsionales qui consiste à confronter dans l'état transformé le diagramme

expérimental d'impédance avec les expressions théoriques établies en fonction de la fréquence opérationnelle pour les différents mécanismes réactionnels possibles. Le diagramme expérimental est obtenu par la transformation de Laplace à partir de la courbe de réponse résultant de l'application d'une faible perturbation au système électrochimique étudié. On propose des procédés permettant la détermination des différents paramètres électriques du système, en particulier dans le cas d'une réaction chimique homogène ou hétérogène associée. En plus de l'utilisation des valeurs purement réelles de la fréquence opérationnelle, la possibilité de l'emploi des valeurs complexes de celle-ci est envisagée. La méthode proposée est comparée avec la méthode classique d'impédance en régime sinusoïdal et avec les procédés habituels d'exploitation des mesures transitoires.

SUMMARY

The different aspects of an original method of treatment of pulse data that compares in the transient state the experimental impedance diagram with the theoretical expressions established as a function of the operational frequency for different possible mechanisms, have been discussed. The experimental diagram is obtained by a Laplace transform starting from the curve of the response resulting from the application of a weak perturbation to the electrochemical system studied. Procedures for the determination of the different electrical parameters of the system (in particular the case of a homogeneous or heterogeneous associated chemical reaction) have been proposed. In addition to the use of purely real values of the operational frequency, the possibility of using complex values is envisaged. The proposed method is compared with the classical impedance method in a sinusoidal system and with the usual procedures employing transient measurements.

BIBLIOGRAPHIE

- 1 J. MIKUSINSKI, *Operational Calculus*, Pergamon Press, Londres, 1959, p. 73.
- 2 W. LORENZ, *Z. Physik. Chem. Leipzig*, 205 (1956) 311.
- 3 D. SCHUHMAN, *Publ. Sci. Tech. Min. Air, France*, No. 145, 1965.
- 4 E. POIRIER d'ANGÉ d'ORSAY, *Compt. Rend.*, 260 (1965) 5266.
- 5 E. LEVART ET E. POIRIER d'ANGÉ d'ORSAY, *J. Electroanal. Chem.*, 12 (1966) 277.
- 6 M. D. WIJNEN, *Rec. Trav. Chim.*, 79 (1960) 1203.
- 7 E. LEVART ET E. POIRIER d'ANGÉ d'ORSAY, *J. Electroanal. Chem.*, à paraître.
- 8 H. MATSUDA, P. DELAHAY ET M. KLEINERMAN, *J. Am. Chem. Soc.*, 81 (1959) 6379.
- 9 P. DELAHAY ET S. OKA, *J. Am. Chem. Soc.*, 82 (1960) 329; appendice par H. MATSUDA.
- 10 H. MATSUDA ET P. DELAHAY, *Collection Czech. Chem. Commun.*, 25 (1960) 2977.
- 11 M. SENDA ET P. DELAHAY, *J. Phys. Chem.*, 65 (1961) 1580.
- 12 G. C. BARKER, *Symposium on Electrode Processes*, edited by E. YEAGER, J. Wiley, New York, 1961, p. 343.
- 13 P. DELAHAY, *J. Phys. Chem.*, 70 (1966) 2067 et 2373.
- 14 P. DELAHAY, *J. Electrochem. Soc.*, 113 (1966) 967, discussion *ibid.*, p. 971.
- 15 P. DELAHAY ET G. C. SUSBIELLES, *J. Phys. Chem.*, 70 (1966) 3150.
- 16 P. DELAHAY, K. HOLUB, G. SUSBIELLES ET G. TESSARI, *J. Phys. Chem.*, 71 (1967) 779.
- 17 K. HOLUB, G. TESSARI ET P. DELAHAY, *J. Phys. Chem.*, 71 (1967) 2612.
- 18 G. C. BARKER, 14^e réunion du CITCE, Moscou, 1963.
- 19 D. SCHUHMAN, communication privée.
- 20 A. M. BATICLE ET F. PERDU, *Compt. Rend.*, 260 (1965) 5258.
- 21 E. D. BELOKOLOOS, *Elektrokhimiya*, 1 (1965) 498.
- 22 E. POIRIER d'ANGÉ d'ORSAY, Thèse, Paris, 1966.
- 23 A. M. BATICLE ET F. PERDU, *J. Electroanal. Chem.*, 12 (1966) 15.
- 24 H. GERISCHER, *Z. Physik. Chem. Leipzig*, 198 (1951) 286.

- 25 H. GERISCHER ET W. VIELSTICH, *Z. Physik. Chem. N.F.*, 3 (1955) 16.
- 26 H. GERISCHER ET K. E. STAUBACH, *Z. Elektrochem.*, 61 (1957) 789.
- 27 M. BONNEMAY, E. LEVART, A. A. PILLA ET E. POIRIER D'ANGE D'ORSAY, *Compt. Rend.*, 256 (1963) 4008; *Electrochim. Acta*, 8 (1963) 805.
- 28 A. BEWICK ET M. FLEISCHMANN, *Electrochim. Acta*, 8 (1963) 89.
- 29 H. LAITINEN, R. P. TISCHER ET D. K. ROE, *J. Electrochem. Soc.*, 107 (1960) 546.
- 30 M. COSTA, *Electrochim. Acta*, 11 (1966) 169.
- 31 K. B. OLDHAM, *J. Electroanal. Chem.*, 11 (1966) 171.
- 32 M. BONNEMAY, E. LEWARTOWICZ, A. A. PILLA ET E. POIRIER D'ANGE D'ORSAY, *Compt. Rend.*, 255 (1962) 914.
- 33 R. KOOPMANN, *Ber. Bunsenges. Physik. Chem.*, 70 (1966) 121.
- 34 M. SAVY, *Electrochim. Acta*, 13 (1968) 1359.

J. Electroanal. Chem., 19 (1968) 335-350

ELECTROCHEMISTRY OF THE NICKEL OXIDE ELECTRODE PART VIII*. STOICHIOMETRY OF THIN FILM OXIDE LAYERS

B. E. CONWAY AND M. A. SATTAR

Department of Chemistry, University of Ottawa, Ottawa (Canada)

(Received February 19th, 1968; in revised form, June 25th, 1968)

INTRODUCTION

Much of the early work on the nickel oxide electrode, in particular that of ZEDNER¹ and FOERSTER², was concerned with establishing the stoichiometry of species involved in the oxidation and reduction reactions and the extent to which water was involved in these processes. More complete studies of stoichiometry of bulk oxides in the charged and discharged states at electrodes have been made recently, *e.g.*, by chemical methods^{3–5}, combined chemical and electrochemical methods⁶ (the previous papers in this series), by chemical and magnetochemical procedures⁷, and by chemical and differential thermal analysis⁸. In most of these studies, bulk nickel oxide was used but JONES AND WYNNE-JONES⁵ used thick films of electrochemically or chemically deposited nickel oxide on a basis metal such as nickel wire or foil, or platinum. They determined the “active oxygen**” iodometrically. Nickel was estimated⁵ by an argentometric method or by the dimethylglyoxime procedure. Both these methods present difficulties when used for microanalysis of thin film oxide materials and, moreover, metallic nickel itself dissolves slowly in the acidic medium. In spite of these problems, however, their results are found to be in satisfactory agreement with later findings by other workers^{6–8}. They⁵ observed that, with increasing potential, the “active oxygen” content increased and at the highest potential the final product had a mean stoichiometry “NiO_{1.8}”. The “fully-discharged” electrode was found, however, to contain some residual “active oxygen”, and hysteresis was always observed between the extents of charge held at a given potential in the charging and discharging processes.

CONWAY AND BOURGAULT^{6,9}, using precipitated nickel hydroxide in sintered plaque electrodes in various concentrations of KOH, observed that the electrode could be oxidized to the formal state, NiO_{1.57}, in the strongest solution (14.6 M) at 25° and to smaller extents in more dilute solutions and/or at lower potentials.

* Parts I–IV have appeared previously and are listed in ref. 6. Parts V, VI and VII are in press (*Electrochim. Acta*, 1968/69) and are concerned with potentiostatic-step oxidation studies at nickel and the kinetics of oxygen evolution on thin films of nickel oxide in relation to the stoichiometry of the layers.

** Active oxygen, [O], may be defined as the oxidizing equivalents of the nickel oxide which are determinable by release *e.g.*, of iodine from acid solutions of iodide. This oxygen is thus determinable iodometrically. It is also (see later) the quantity of O beyond that corresponding to the divalent state of nickel in the oxide and is thus determinable by other suitable reductants.

The condition of nickel oxide electrodes in the charged and discharged states has been examined by various physical methods including X-ray diffraction analysis^{10,11}, ellipsometry¹² for thin passive layers on nickel anodes in sulphuric acid, and infrared absorption spectrometry¹³. Results from the latter work are of special interest since they indicate¹³ the formation of mixtures, rather than solid solutions, of the various oxides of nickel during the charging process.

Interest in thin film nickel oxide material studied in the present work arises in relation to: (a) stoichiometries and "active oxygen" content of thin layer materials; (b) constitution of thin layers in relation of self-passivation effects in anodic oxygen evolution (Part V¹⁴) and to passivation of the metal itself; (c) internal concentration polarisation effects which may arise with respect to the two or more states of oxidation of nickel (Ni(II), Ni(III), Ni(IV)) in *bulk* oxide material; hence, comparatively, the behaviour of thin film material may be of special interest; (d) possible avoidance of local isolation of reducible material on discharge, a situation that tends to occur in bulk impregnated plaques at high rates of discharge; (e) the ellipsometric results at nickel electrodes, studied by BOCKRIS *et al.*¹² and (f) the possible use of thin film cathode materials for pulsed charge and discharge conditions¹⁵ where high rate, short duration electrical fluxes are involved.

CHEMICAL AND ELECTROCHEMICAL CHARACTERISATION OF THIN FILM NICKEL OXIDE

In general, characterisation of thin film oxide materials by electrochemical means alone is unsatisfactory and usually inadequate for description of the stoichiometry and mean state of oxidation of thin film materials. Accordingly, we have investigated and employed some chemical analytical procedures which can be used in ways complementary to the electrochemical and ellipsometric techniques.

(a) Electrochemical studies

Electrochemical reductive transients were carried out on previously anodized nickel electrodes using a cell of the kind previously described. A potentiostatic pre-treatment programme (Fig. 1) for electrochemical formation of oxide on a fresh sur-

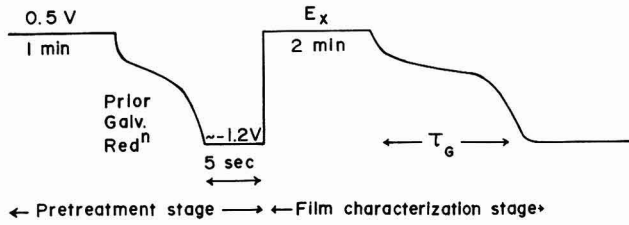


Fig. 1. Schematic electrochemical pre-treatment programme.

face was applied to all electrodes. At the end of the first (pre-treatment) step and the following cathodic reduction, a clean metal surface is produced*. It is on this surface that the oxide film for experimental study is formed in the second potential step (Fig.

* This was demonstrated experimentally by showing that the amount of nickel chemically determinable in the oxide film before and immediately after the first galvanostatic discharge was the same, and the determinable nickel (corrected for Ni dissolution; see below) became negligible after 5 sec of H₂ evolution.

i) and reduced in the final galvanostatic reduction transient for oxide film characterisation. The electrical procedures used were based on previously published techniques¹⁶.

Electrodes were prepared from wires of Spectrograde nickel, previously degreased in benzene vapour for 24 h. They were then sealed in glass in vacuum (10^{-7} mm Hg) or in H_2 at *ca.* 600°. No systematic difference between the behaviour of these two types of electrodes was found.

The solutions used were prepared by dissolving analytical-grade KOH in triply-distilled water. For purification, pre-electrolysis at 20 mA cm^{-2} was carried out for at least 24 h at a large sacrificial electrode. Good reproducibility between different electrodes in the same solution, and in different solutions of the same composition, was regularly attained in most of the measurements.

Hg/HgO reference electrodes were employed with aq. KOH of the same concentration as that used in the nickel anode compartment. This electrode has a potential of +0.925(8) V *vs.* hydrogen electrode in the same solution ($a_{H_2O}=1$).

The electrochemical charge, q , for oxide reduction was measured in cathodic transients by the fast differential galvanostatic method¹⁶. The transition time, τ_G , and hence q , was determined by measuring the peak-to-peak distance between the capacity minima. Comparative results on the surface oxide formation were also obtained by a potentiostatic step charging method described elsewhere¹⁴ and by the potentiodynamic method. Under the conditions employed in the present work, rather thinner oxide films were formed (see below) than in some of the experiments of JONES AND WYNNE-JONES⁵.

Before the oxides were dissolved in the course of the subsequent chemical determination of the amount of nickel oxidized in the formation of the anodic film, the charge for electrochemical reduction of the active "O" for *each* electrode and for *each* potential was determined in six separate experiments; mean values are reported. For each potential, a different electrode was used.

The rate of increase of the active "O" associated with the oxide film was also estimated from measurements of the oxide reduction charge as a function of the time of prior anodic potentiostatic polarisation (see below). All reductive transients were taken in solutions outgassed with purified N_2 and through which N_2 was vigorously bubbled.

Loss of charge. There is always a certain loss of electrochemically reducible material, particularly at potentials higher than 0.5 V, $E_{Hg/HgO}$, by a self-discharge mechanism⁶ which competes with the electrochemical reduction during determination of oxide charge in a galvanostatic cathodic pulse; the extent depends on the transition time associated with the pulse. In order to determine this loss of electrochemically active oxide material, experiments were performed in which the electrode was polarized potentiostatically to a certain potential for a definite period of time after the pre-treatment programme (Fig. 1); the electrode was then kept on open-circuit for various known periods of time, τ_D , (regulated electronically) after the lapse of which, a fast galvanostatic cathodic pulse was automatically applied.

The oxide reduction charges passed in the cathodic pulses were determined, and hence the amounts of electrochemically reducible material remaining after various τ_D were deduced. A plot of charge *vs.* τ_D was made, from which the amount of electrochemically reducible material in the absence of self-discharge could be estimated by extrapolation, (Fig. 2). It is found (as expected) that the extent of loss of cathodically re-

ducible material is potential-dependent⁶. Corrections for this self-discharge effect were therefore introduced into the calculation of the stoichiometry of the oxide for several potentials, for the purpose of comparing the stoichiometries attained in the thin films studied in the present work with the stoichiometric data obtained by ourselves and other workers for thicker or bulk oxide material where self-discharge effects are less significant in short times. Some potentiodynamic oxidation and reduction measurements were also made to examine reversibility of the oxidation/reduction processes at thin oxide films on nickel.

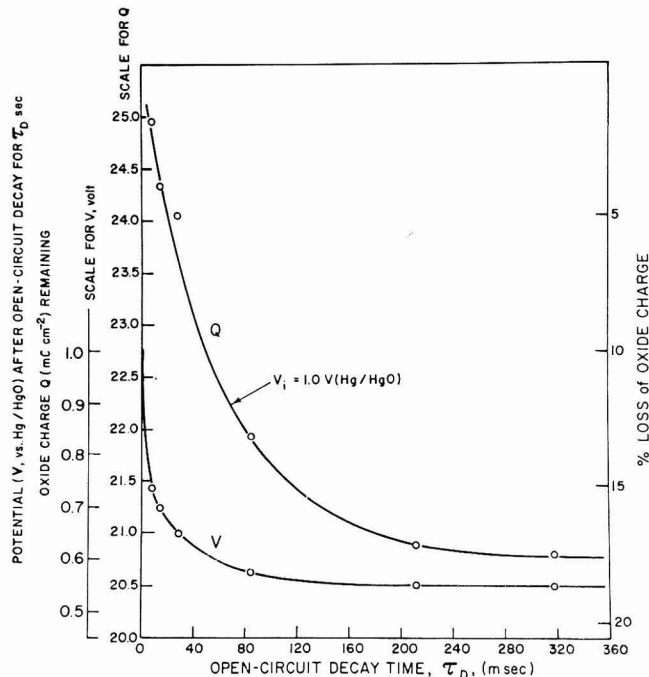


Fig. 2. Reducible oxide charge, Q , remaining after self-discharge for times, τ_D , for initial potential, 1.0 V (thin film Ni oxide at wire electrodes, 2 M aq. KOH, 28°).

(b) Chemical analysis experiments

Methods were sought which would give a complete and rapid stripping of the oxide film without appreciable continuing attack of the metal. Two reagents were employed in separate types of experiment: aq. KCN for complexation of nickel¹⁷; aq. N_2H_4 for reduction of the oxide and complexation of nickel. The latter reagent was employed first in a chemical method for determination of the active oxygen. The use of dimethylglyoxime was also investigated but the method was insufficiently sensitive as a colorimetric procedure for nickel determination and the quantities of nickel were too small for gravimetric analysis.

Two types of electrodes were used: (i) wire electrodes as described above and (ii) pure nickel wire gauze electrodes of large area; the latter were formed in a cylindrical shape, cleaned in an aq. ammonia-hydrazine mixture and then washed in distilled water several times until free from hydrazine.

Method (i). The amount of nickel metal oxidized in the formation of the anodic film was determined by dissolving the oxide film in a known volume of 0.5% KCN solution. The oxide electrode was kept in the complexing solution for controlled times in the range 2–5 min during which period the oxide film dissolved completely giving a bright nickel surface. The absorbance of the complex $[\text{Ni}(\text{CN})_4]^{2-}$ was measured¹⁷ at 268 nm and the amount of nickel derived from the oxide was calculated from a Beer–Lambert calibration plot. Corrections for dissolution of metallic nickel in the 0.5% KCN solution were made. From knowledge of the amount of nickel, and the active oxygen content of the film determined electrochemically, the stoichiometry of the oxide was deduced.

Method (ii). In the second method, the electrode was polarized as described above, and the oxide was then reductively dissolved in a known volume of standard (0.02 M) hydrazine solution (or ammoniacal hydrazine to complete the dissolution of nickel in the film) which was first deoxygenated by bubbling pure nitrogen in order to prevent oxidation of hydrazine by atmospheric oxygen and to minimize oxidation of metallic nickel. Hydrazine reduces higher-valent nickel in the oxide to the divalent state which then dissolves as a complex.

Ideally, if no other side reactions occur leading to loss of hydrazine (see below), then determination of the amount of hydrazine reacted would enable the quantity of available active oxygen, [O], to be calculated ($\text{N}_2\text{H}_4 + 2 \text{O} \rightarrow \text{N}_2 + 2 \text{H}_2\text{O}$). It also enables the complexed nickel to be determined (see below). Hydrazine can be quantitatively estimated before and after the experiment by determination with iodate, and a number of experiments were carried out by this procedure.

Determinations were first made on precipitated nickel oxide ($\text{Ni}_{\text{aq.}}^{2+} + \text{KOH}$ with potassium hypobromite) in order to determine both nickel (by KCN) and [O] by means of hydrazine. The results were encouraging (Fig. 3) in so far as at relatively short treatment times (up to 30 min) a constant value of the active oxygen: nickel ratio

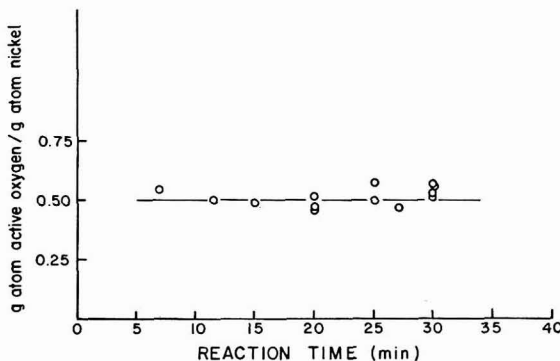


Fig. 3. [O]: Ni ratio from determinations on precipitated nickel oxide (Ni by KCN, [O] by N_2H_4) as a function of reaction time up to 30 min.

(=0.5, corresponding to “ Ni_2O_3 ” or $\text{NiO}\cdot\text{OH}$) was obtained. However, after longer times (Fig. 4), a substantial increase of this value became evident. It is known that hydrazine decomposes to N_2 and NH_3 through the reaction, $3 \text{N}_2\text{H}_4 \rightarrow \text{N}_2 + 4 \text{NH}_3$, a process which is catalysed in the dry state by NiO ¹⁸, and the high apparent values of

TABLE 1

ACTIVE OXYGEN BY HYDRAZINE AND BY ELECTROCHEMICAL REDUCTION
(Large nickel gauze electrode, 2 M KOH, 22°)

Potential vs. Hg/HgO (V)	Amount of Ni in oxide film (spectrometry) ($\mu\text{g atom}$)	Electrochemically reducible oxide charge (mC)	Active oxygen (electrochemical equiv.) ($\mu\text{g atom}$)	Loss of hydrazine ($\mu\text{g atom}$)	Active oxygen (equiv. to hydrazine loss) ($\mu\text{g atom}$)
0.6	2.236	6578*	34.1*	20.34	40.7
0.5	1.432	2154*	11.2*	10.39	20.8
0.4	0.8	178.8	0.93	5.15	10.3
0.3	0.805	100.9	0.52	18.98	38.0

* These data were obtained in the oxygen evolution region; they may hence include some charge for reduction of molecular O_2 which might have been entrapped in the gauze.

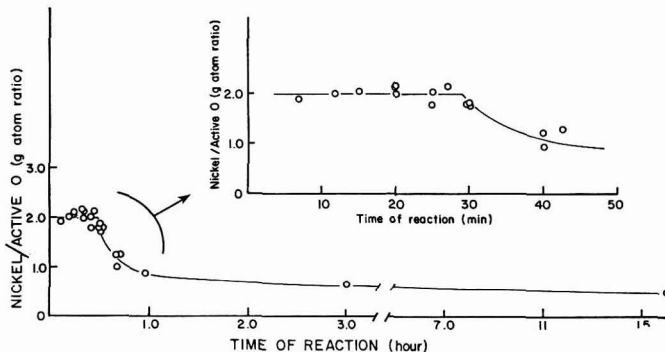


Fig. 4. Ni : [O] ratio from determination on precipitated nickel oxide over a wider time range.

the [O]: Ni ratio may arise because some N_2H_4 becomes lost by catalytic decomposition, in addition to the expected loss by reaction with [O].

Application to large area oxidized nickel gauze electrodes stripped for controlled times in aq. N_2H_4 gave the results shown in Table 1; the chemically determined active "O" is seen to be much larger than the electrochemically determined values, based on cathodic reduction. Here, some of the loss of N_2H_4 may be due to catalytic decomposition by the underlying metal once the oxide film is stripped. Hence, it was concluded that the oxidative loss of N_2H_4 in reductive stripping cannot be used as a reliable method for determination of [O] at nickel electrodes. Cathodic reduction must therefore remain the preferred method, since reaction with iodide in acid media is relatively unsatisfactory for thin film oxide owing to corrosion of the underlying metal. However, for use of the cathodic reduction method for determining [O], it is first necessary to ascertain the extent of reduction of the oxide in a cathodic pulse (see below).

For an alternative estimation of nickel, a small portion of the original solution, after reductive complexation of the oxides with hydrazine, was evaporated to dryness in a dish on a water bath; the residue was dissolved in a known volume of 0.5% KCN solution and determined as the $[\text{Ni}(\text{CN})_4]^{2-}$ complex.

Corrections for loss of nickel by corrosion

The amount of nickel resulting from dissolution of the oxide was corrected for the microquantity (Q_{Ni}) of nickel metal which also dissolves on account of corrosion in 0.5% KCN and in N_2H_4 solutions (Fig. 5). Q_{Ni} was determined as a function of time ($\tau_{dis.}$) for which the electrode was kept in the solution (Fig. 5). In this experiment, the complexing solution was first deoxygenated by bubbling nitrogen for 15 min while the electrode in the glass bulb was kept in the solution. The bulb was then broken beneath the solution and the electrode was kept in solution for a certain time ($\tau_{dis.}$) in the presence of nitrogen. After the period $\tau_{dis.}$, the electrode was removed and $Q_{Ni}(\tau_{dis.})$ was determined spectrophotometrically as described above.

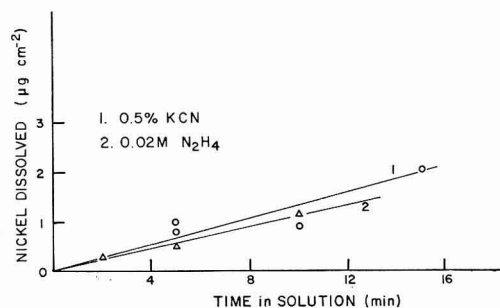


Fig. 5. Dissolution (corrosion) of metallic Ni in 0.5% aq. KCN and in 0.02 M N_2H_4 , at 22° .

Extent of reduction of higher-valent nickel oxides in a fast galvanostatic pulse

It is important to determine if higher valent nickel oxides are reduced to the Ni(II) state in fast galvanostatic reduction pulses (*cf.* ref. 12) and if hydrogen gas evolves on the lower-valent oxide ($Ni(OH)_2$) itself. A series of experiments were therefore carried out in which the electrode was polarized for 2 min at a certain potential in the usual manner and the reduction charge determined galvanostatically. After the pulse, the electrode was removed, the oxide stripped in 0.5% aq. KCN and the amount of nickel (from the oxide) complexed was determined spectrophotometrically. Another electrode was polarized at the same potential for 2 min in an identical manner but

TABLE 2

AMOUNT OF NICKEL IN THE OXIDE FILM AFTER CHARGING THE ELECTRODE, AND THAT REMAINING AFTER ELECTROCHEMICAL REDUCTION OF THE OXIDES

Polarization time (t_x)	Potential E_x vs. Hg/HgO (V) in 2 M KOH at 22°	Amount of electro- chemically reducible oxide ($\mu g \text{ atom } [O]$ cm^{-2})	Amount of Ni in oxide film after charge ($\mu g \text{ atom } \text{cm}^{-2}$)	Amount of Ni in oxide film after discharge ($\mu g \text{ atom } \text{cm}^{-2}$)	Stoichiometry of Ni oxide in the film*
0.2	0.004	0.462	—	—	$NiO_{1.01}$
0.2	0.004	—	0.465	—	$NiO_{1.01}$
0.5	0.031	0.245	—	—	$NiO_{1.13}$
0.5	0.035	—	0.181	—	$NiO_{1.19}$
0.8	0.119	0.325	—	—	$NiO_{1.37}$
0.8	0.098	—	0.256	—	$NiO_{1.38}$

* In this Table, and Tables 3 and 4, the nickel oxide is represented formally as NiO_x ; it is recognized, however, that an hydrated hydroxy-oxide of varying composition is involved.

without discharging it; the oxide was then stripped in 0.5% aq. KCN solution and the amount of nickel again determined. Experiments were carried out at three different potentials and the results are given in Table 2. It is seen that at all potentials the relative amount of nickel in the film (w.r.t. [O]) determined after charging is approximately equal to that determined after discharging. This proves that higher-valent nickel oxides are reduced only to Ni(II)-oxide (and not to metal) in a fast galvanostatic pulse. However, if cathodic hydrogen evolution is allowed to occur at the end of the cathodic pulse for some time, the Ni(II)-oxide becomes reduced to the metal, as in the first stage of the pre-treatment programme (Fig. 1). It was also found chemically that after the cathodic reduction, no higher oxide was left in an isolated condition as sometimes arises with bulk oxide material in sinters.

DISCUSSION AND SUMMARY OF ANALYTICAL RESULTS

In the first set of experiments, nickel wire electrodes were used as working electrodes, and 0.5% KCN solution was used as the complexing agent for dissolving the oxides from the electrode surface. The amounts of electrochemically active oxygen, and the corresponding amounts of nickel oxidized in the thin films of oxide are plotted in Fig. 6 as a function of electrode potential. In order to determine the stoichiometries of the oxides in the charged state of the electrode, the results are expressed in g atom units and the observed stoichiometries are calculated on the basis, demonstrated above, that higher oxides of nickel are reduced only to Ni(II)-oxide in fast reductive transients.

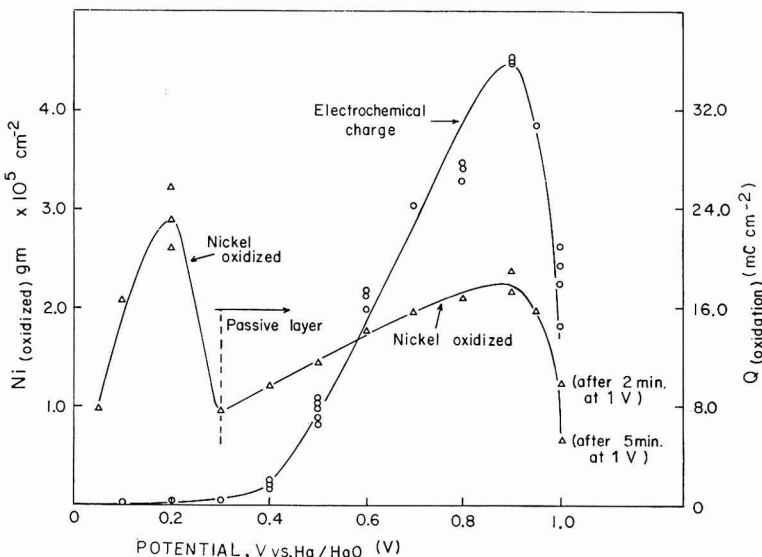


Fig. 6. Chemically determined Ni content (Ni oxidized) in anodic oxide films in comparison with electrochemically determined charge for oxide reduction (*i.e.*, [O]); both quantities are shown as a function of prior anode potential held potentiostatically for 120 sec (30°, 2 M KOH).

The results are shown in Table 3 for various potentials. A plot of the dependence of the ratio of active oxygen to nickel *vs.* electrode potential, which reflects the

stoichiometry of the nickel oxide in the thin film oxide layers as a function of electrode potential, has also been constructed (Fig. 7).

Although maxima are observed both in the $[O]$ (*i.e.*, charge for electrochemically reducible oxide) and the nickel content of the thin films (Fig. 6), the $[O]: Ni$ ratio plotted in Fig. 7 is a *continuously* increasing function of potential, so that the maxima in Fig. 6 simply reflect smaller film thicknesses at higher potentials ("tight", thin and probably more passive films). From Fig. 7, it is also evident that during the self-discharge process, nickel oxide in which the oxidation state of nickel exceeds +3, undergoes decomposition.

The maximum in the extent of oxide formation (*i.e.*, electrochemical charge for $[O]$) at *ca.* 0.9 V $E_{Hg/HgO}$ is reproducible and also corresponds to the inflections that are observed in the steady-state potentiostatic current–potential relations for O_2 evolution on oxide-film nickel electrodes (Part V¹⁴). It is evidently a real variation of

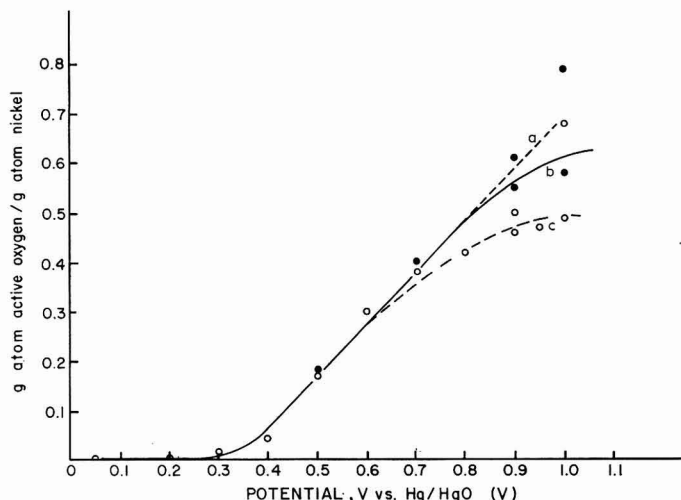


Fig. 7. $[O]: Ni$ ratio at 25° ($2 M$ aq. KOH) as a function of anodic electrode potential (data based on results in Table 3). (●) corrected values; (○) un-corrected values. (a) long time polarization; (b) after correction for loss of charge on open-circuit; (c) without correction.

the extent of nickel oxidation since a similar maximum occurs in the second curve ("nickel oxidized") in Fig. 6 for total nickel content in the chemically stripped film. Another maximum in stripped nickel also arises at low potentials and is a real effect (based on a number of independent points) and may correspond to a pre-passive, less consolidated film of the type also indicated by ellipsometry¹². Both from the electrochemical oxide reduction experiments and from chemical stripping, the apparent thicknesses of the films formed may be estimated as 20–40 layers (see below). The total reducible quantity of active oxygen developed depends, of course, on prior anodic polarisation time (see Fig. 8), which must be controlled in longer period experiments. Cathodic and anodic charge balance in cyclic potential scans was satisfactory between potentials of -0.695 and $+0.826$ V ($E_{Hg/HgO}$) but $Q_{red.}$ was slightly greater than $Q_{ox.}$ at higher sweep rates.

TABLE 3
APPARENT STOICHIOMETRIES AND STOICHIOMETRIES CORRECTED FOR SELF-DISCHARGE IN THIN FILM NICKEL OXIDE

Polarization time (min) t_x	Potential E_x vs. Hg/HgO (V) in 2 M KCl at 25°	Amount of Ni in oxide film ($\mu\text{g atom cm}^{-2}$)	Amount of electrochemically reducible oxide (active oxygen) ($\mu\text{g atom }[O] \text{ cm}^{-2}$)	Stoichiometry of Ni oxide in the film	Corr.* electrochem- ically reducible oxide ($\mu\text{g atom }[O] \text{ cm}^{-2}$)	Corr. sto- ichiometry of Ni oxide in the film
2	0.05	0.165	0.0003	NiO _{1.002}	NiO _{1.002}	NiO _{1.002}
2	0.20	0.546	0.0012	NiO _{1.002}	NiO _{1.002}	NiO _{1.002}
2	0.20	0.441	0.001	NiO _{1.002}	NiO _{1.012}	NiO _{1.012}
2	0.30	0.162	0.002	NiO _{1.012}	NiO _{1.012}	NiO _{1.012}
2	0.40	0.203	0.009	NiO _{1.044}	NiO _{1.044}	NiO _{1.044}
2	0.50	0.245	0.041	NiO _{1.17}	NiO _{1.17}	NiO _{1.17}
2	0.60	0.299	0.090	NiO _{1.30}	NiO _{1.30}	NiO _{1.30}
2	0.70	0.332	0.126	NiO _{1.38}	NiO _{1.38}	NiO _{1.38}
2	0.80	0.324	0.136	NiO _{1.42}	NiO _{1.42}	NiO _{1.42}
2	0.90	0.372	0.186	NiO _{1.50}	NiO _{1.50}	NiO _{1.50}
2	0.90	0.406	0.187	NiO _{1.46}	NiO _{1.46}	NiO _{1.46}
2	0.95	0.338	0.159	NiO _{1.47}	NiO _{1.47}	NiO _{1.47}
2	1.0	0.207	0.101	NiO _{1.49}	NiO _{1.49}	NiO _{1.49}
5	1.0	0.111	0.075	NiO _{1.68}	NiO _{0.88}	NiO _{1.79}

* Corrected for self-discharge during time, τ_G .

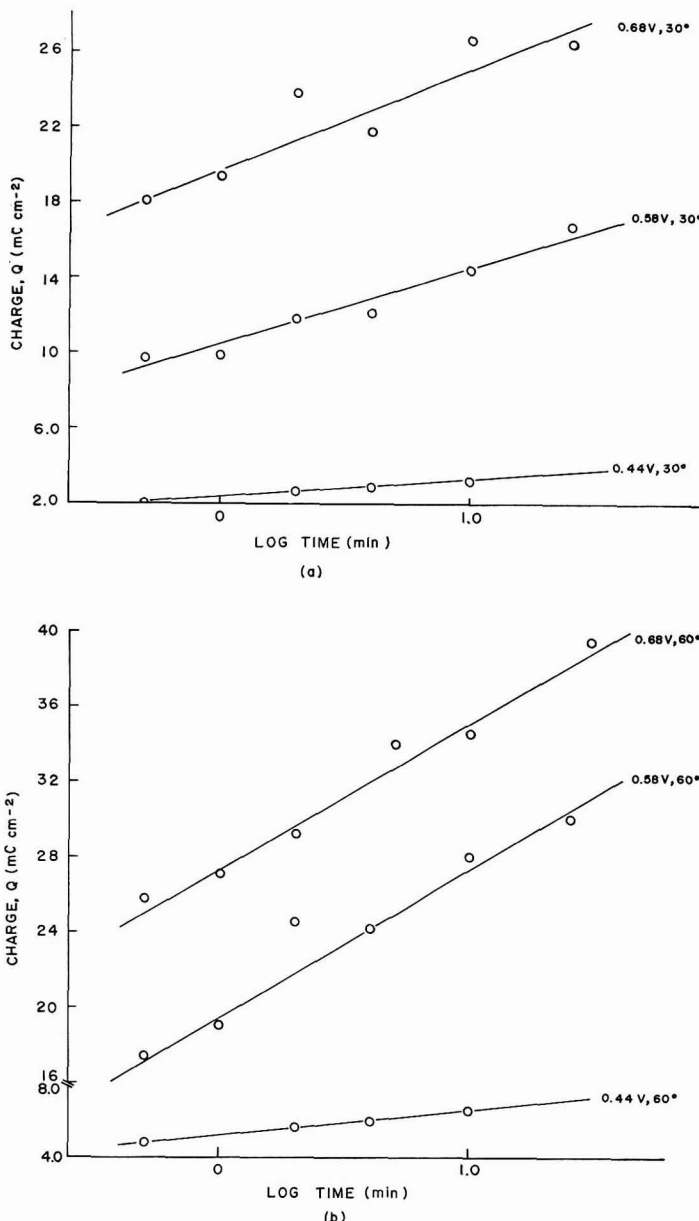


Fig. 8. Increase of active "O" at Ni (60° and 30° , 2 M KOH) based on galvanostatic reduction of the oxide potentiostatically formed at the indicated potentials (vs. Hg/HgO) as a function of the logarithm of time: (a), 30° ; (b), 60° .

In terms of the number of layers, n , of surface oxide involved, only an approximate estimate can be given since some of the available active oxygen determined in cathodic transients arises from a small slow increase of the $[O]:Ni$ ratio while the re-

mainder is associated with time-dependent thickening of the film. However, the latter process must have been the principal one leading to the observed active oxygen content developed in the formation time of 2 min (Table 3) since the maximum [O]: Ni ratio attained after long times is *ca.* 0.5 (*i.e.*, "Ni₂O₃"). The overall effect is as shown in Fig. 8. At nickel, *n* was found¹⁹ to vary from approximately 43/zR to 80/zR taking 275 z μC cm⁻² as the average charge for a *z*-electron oxidation of nickel in a surface monolayer and *R* as the initial real to apparent area factor. With *R* about 2 and *z* = 1[Ni(III) → Ni(II)] in the discharging peak*, *n* would be of the order of 20–40 layers, *i.e.*, somewhat greater than the figure obtained by WEININGER AND BREITER²⁰ but nearer to that obtained by BOCKRIS *et al.*¹² in acid but again greater than that obtained by SATO AND OKAMOTO²¹ for passive layers in acid. In the passivation work in acid, however, lower anodic potentials were involved so that quantitative comparisons are difficult to make. At silver, comparative experiments under similar conditions gave¹⁹ much larger apparent** layer thicknesses of the order of 1600/zR, or with *z* = 2 [Ag(II) → Ag(I) → Ag(O)] and *R* = 2, *n* = 400, based on 213z μC cm⁻² for a monolayer.

The highest formal oxidation state of nickel observed in the present work is in fair agreement with that found by us previously⁶ and by others (*e.g.*, refs. 5 and 8) using thicker oxide material. However, this degree of oxidation is only attained at the highest potentials*** *viz.*, *ca.* 1.0 V *E_{Hg/HgO}* (Table 3).

In the present experiments, the electrode was polarized potentiostatically for periods of only 2 min in which time only a fraction of the lower-valent oxide initially formed may have been converted to the higher-valent state; hence [O]: Ni ratios are observed which are lower than those found by other workers at corresponding potentials.

TABLE 4

STOICHIOMETRIES OF THIN FILM NICKEL OXIDE (IN 2 M KOH) AS A FUNCTION OF POLARISATION POTENTIAL* BASED ON CHEMICAL AND ELECTROCHEMICAL DETERMINATIONS

Polarization time (min)	Potential <i>E_x</i> vs. Hg/HgO (V) in 2 M KOH at 22°	Amount of Ni in oxide film (μg atom)	Amount of electro-chemically reducible surface oxide (μg atom [O])	Stoichiometry of Ni oxide in the film
5	0.1	0.169	0.044	NiO _{1.26}
5	0.2	0.213	0.054	NiO _{1.25}
5	0.3	0.304	0.063	NiO _{1.21}
5	0.4	0.188	0.082	NiO _{1.44}
5	0.45	0.149	0.138	NiO _{1.93} - - molecular O ₂ evolution

* Pre-treatment programme: 2 min at 0.5 V (*E_{Hg/HgO}*) followed by potential step to 0.0 V for 2 min; increase of potential to variable value, *E_x*, for time *t_x* (5 min) followed by cathodic galvanostatic pulse.

* A similar figure of *ca.* 1.1 F/g atom of Ni was deduced by BRIGGS AND WYNNE-JONES for thicker film nickel oxide electrodes^{5,10}.

** In cyclic potentiodynamic experiments, some roughening of the surface arises which may lead in part to the high values here. However, simultaneous H accommodation measurements for the real area determination at Ag are not possible as they are at Pt or Ir.

*** At potentials near the maximum in determined Ni and Q_{ox}. (Fig. 6) the Ni content of the film is 3.65 (± 0.1) · 10⁻⁷ g atoms cm⁻² and the charge for electroreduction is 3.6 · 10⁻⁷ F. It is thus reasonable to suppose that at the highest degree of oxidation, an average valence state of Ni(III) is involved which can be reduced to Ni(II) electrochemically, thus giving one reduction equiv./atom of Ni.

The data shown in Fig. 5 indicate that metallic nickel corrodes more easily in 0.5% KCN solution than in 0.02 M N₂H₄ solution. Therefore, hydrazine solution is thought to be a better complexing agent for nickel oxide at the electrode surface than potassium cyanide solution when the purpose is the estimation of the amount of nickel in the oxide film. The complexes formed are also stable.

A second set of experiments was therefore carried out using hydrazine as the complexing agent and nickel gauze as the electrode, and the stoichiometry of the oxide film was determined as a function of electrode potential. In this experiment, stoichiometries of the oxides at potentials above that for oxygen gas evolution were not investigated because at these potentials molecular oxygen is entrapped in the gauze and some is reduced during the galvanostatic pulse as mentioned above. Results are given in Table 4.

It was found in some experiments that as more time is allowed for formation of the higher oxide, a greater fraction of the lower-valent oxide is oxidized to the higher-valent state, and hence somewhat higher [O]: Ni stoichiometry tends to be attained. This result presumably requires that at any time the oxide species at the electrode surface is not homogeneous with respect to the valency state of nickel ions. Thus, it seems likely that a gradient of decreasing state of oxidation of nickel from the electrolyte/oxide interface [Ni(IV)] to the oxide/metal interface [Ni(II)] would be involved (see also refs. 19 and 22).

ACKNOWLEDGEMENT

Grateful acknowledgement is made to the Defence Research Board, Department of National Defence, Canada, for supporting this work on Grant No. 5480-12.

SUMMARY

Anodically-formed, thin film oxide layers at nickel in alkaline solutions have been studied in relation to the behaviour of bulk nickel oxide examined in previous work. The necessity for both chemical and electrochemical characterization is stressed. Analytical methods are developed for reductive stripping of the oxide which allow determination of the nickel content as the cyanide or hydrazine/ammonia complex. Stoichiometries of thin film layers are reported as a function of time and potential of prior polarization. Self-discharge effects are important and allowance must be made for loss of charge in galvanostatic reduction transients. In the latter, nickel oxide is reduced to the II-valent state. The apparent extent of oxidation of the nickel in the thin films, determined both chemically and electrochemically, passes through a maximum at *ca.* 0.9 V $E_{Hg/HgO}$, and this is believed to be connected with a change of the oxide layer to a more passive condition. The maximum in this curve can also be correlated with a self-passivation effect in the course of the oxygen evolution reaction at nickel.

REFERENCES

- 1 J. ZEDNER, *Z. Elektrochem.*, 11 (1905) 809; 12 (1906) 463; 13 (1907) 752.
- 2 F. FOERSTER, *Z. Elektrochem.*, 13 (1907) 414; 14 (1908) 17, 285.
- 3 O. GLEMSEY AND J. EINERHAND, *Z. Anorg. Allgem. Chem.*, 261 (1950) 43.

- 4 W. FEITKNECHT, H. R. CHRISTEN AND H. STUDER, *Z. Anorg. Allgem. Chem.*, 283 (1956) 88.
- 5 E. JONES AND W. F. K. WYNNE-JONES, *Trans. Faraday Soc.*, 52 (1956) 1260.
- 6 B. E. CONWAY AND P. L. BOURGAULT, *Can. J. Chem.*, 37 (1959) 292; 38 (1960) 1557; 40 (1962) 1690; B. E. CONWAY AND E. GILEADI, *Can. J. Chem.*, 40 (1962) 1933.
- 7 J. LABAT, Thesis, University of Bourdeaux; *Ann. Chim. (Paris)*, 9 (1964) 399; *J. Chim. Phys.*, 60 (1963) 1253.
- 8 M. A. AIA, *J. Electrochem. Soc.*, 114 (1967) 418.
- 9 P. L. BOURGAULT, Ph.D. Thesis, University of Ottawa, 1961.
- 10 G. W. D. BRIGGS AND W. F. K. WYNNE-JONES, *Trans. Faraday Soc.*, 52 (1956) 1272.
- 11 S. U. FALK, *J. Electrochem. Soc.*, 107 (1960) 661.
- 12 J. O'M. BOCKRIS, A. K. N. REDDY AND B. RAO, *J. Electrochem. Soc.*, 113 (1966) 1133.
- 13 F. P. KOBER, *J. Electrochem. Soc.*, 112 (1965) 1064; 114 (1967) 215.
- 14 M. A. SATTAR AND B. E. CONWAY, *Electrochim. Acta*, in press; B. E. CONWAY, M. A. SATTAR AND D. GILROY, *Electrochim. Acta*, in press.
- 15 E. J. CASEY, *Proceedings of the Meeting of the Advisory Group for Aerospace Research and Development, June 1967, Liège, Belgium*, edited by G. SHERMAN AND L. DEVOL, Dept. of the U.S. Air Force, Dayton, Ohio, 1968.
- 16 H. ANGERSTEIN-KOZLOWSKA AND B. E. CONWAY, *J. Electroanal. Chem.*, 7 (1964) 109; B. E. CONWAY AND M. DZIECIUCH, *Can. J. Chem.*, 41 (1963) 55; S. GILMAN, *J. Phys. Chem.*, 67 (1963) 1898.
- 17 B. D. BRUMMET AND R. M. HOLWEG, *Anal. Chem.*, 28 (1956) 887.
- 18 YU-MEI HUANG, N. P. KEIER AND S. Z. ROGINSKII, *Dokl. Akad. Nauk SSSR*, 133 (1960) 413.
- 19 B. E. CONWAY AND M. A. SATTAR, *Proceedings of the Meeting of the Advisory Group for Aerospace Research and Development, June 1967, Liège, Belgium*, edited by G. SHERMAN AND L. DEVOL, Dept. of the U. S. Air Force, Dayton, Ohio, 1968.
- 20 J. L. WEININGER AND M. W. BREITER, *J. Electrochem. Soc.*, 110 (1963) 484; 111 (1964) 707.
- 21 N. SATO AND G. OKAMOTO, *J. Electrochem. Soc.*, 110 (1963) 605.
- 22 P. D. LUKOVTSOV AND G. YA. SLAIDIN, *Russ. J. Phys. Chem. English Transl.*, 38 (1964) 299.

J. Electroanal. Chem., 19 (1968) 351-364

KINETICS OF THE Hg(I)/Hg ELECTRODE WITH CONSIDERATION OF SPECIFIC ADSORPTION

D. J. KOOIJMAN*

Department of Chemistry, New York University, New York, N. Y. 10003 (U.S.A.)

(Received May 27th, 1968)

INTRODUCTION

The kinetics of the $\text{Hg}_2^{2+}/\text{Hg}$ electrode reaction have been investigated by several authors^{1–5}. SLUYTERS-REHBACH AND SLUYTERS⁶, studying the reaction with the faradaic impedance method, observed that the double-layer capacitance increases rapidly in the potential region where the mercurous ion discharge occurs. The concept of coupling of double-layer charging with faradaic charge transfer, introduced by DELAHAY⁷, could explain this remarkable increase, by an accumulation of specific adsorbed mercurous ions at the interface at more anodic potentials. If, also, the electrode reaction is not entirely diffusion-controlled, an abnormal behaviour of the electrode impedance can be expected, *i.e.*, an impedance not consistent with an equivalent circuit of a double-layer capacitance shunted by the faradaic impedance, characterized by a charge transfer and mass-transfer impedance. SLUYTERS-REHBACH AND SLUYTERS⁶ did not observe any irreversibility, but measurements were performed at rather low frequencies, so that only a lower limit of $i_0 > 400 \text{ mA cm}^{-2}$ for 1 mM Hg_2^{2+} -ions in 1 M HClO_4 could be set. They pointed out that measurements at much higher frequencies are no longer meaningful since the ohmic resistance dominates the total cell impedance.

However, galvanostatic double pulse studies^{2,3,8}, in the 1–10 μsec range, showed some degree of irreversibility for the reaction, although the results obtained for the exchange current are suspicious and should probably be higher than reported⁸. Galvanostatic⁴ and coulostatic⁵ measurements, carried out in the microsecond range, also yielded finite exchange currents. In a recent paper⁹, the author has given a method for analyzing coulostatic and galvanostatic pulse data. With this method, the values of exchange current and double-layer capacitance can be obtained without any approximation of the theoretical equations for these methods. At the same time, one immediately observes a deviation of normal behaviour, which can be expected for the $\text{Hg}_2^{2+}/\text{Hg}$ -electrode reaction, if the exchange current is finite.

EXPERIMENTAL

The electrical set-up is given elsewhere¹⁰. Measurements were performed in the range, 0.5 μsec –10 msec. From the long-time experiments, the diffusion coefficient of the mercurous ion in 1 M HClO_4 at 25° could be obtained, the value of which is

* On leave from the State University of Utrecht, The Netherlands.

necessary for the analysis. Great care was given to the precision of the measurements. Time-base and vertical display of the oscilloscope were checked internally. Two identical hanging mercury drops¹² were used as cathode and anode. The impedance of the cell, corrected for the ohmic drop, behaved as a linear element up to at least 3 mV for all electrolysis times. Since impurities in the solution are not appreciably adsorbed at these high potentials, the same electrodes could be used for many experiments, which enhances the precision.

RESULTS FOLLOWING A CLASSICAL ANALYSIS

The diffusion coefficients, evaluated from the long-time experiments with the galvanostatic step method, are given in Table 1. Agreement with reported value is very good^{6,11}.

TABLE 1

$C^*_{Hg_2^{2+}}$ (mM)	$D_{Hg_2^{2-}}$ ($10^{-6} \text{ cm}^2 \text{ sec}^{-1}$)	i_0 (A cm^{-2})	$\left(\frac{\partial q}{\partial E}\right)_{c^*}$ ($\mu\text{F cm}^{-2}$)	$\frac{d(q + nFF_0)}{dE}$ ($\mu\text{F cm}^{-2}$)
0.152	8.9 ± 0.3	0.12 ± 0.05	~ 39	43.5 ± 2
0.303	9.1 ± 0.2	0.22 ± 0.1	~ 40	47 ± 2
0.653	9.0 ± 0.2	0.4 ± 0.15	44 ± 7	66 ± 5
1.12	9.3 ± 0.2	0.8 ± 0.3	41 ± 9	81 ± 8
1.98	9.1 ± 0.2	1.3 ± 0.4	48 ± 10	125 ± 10

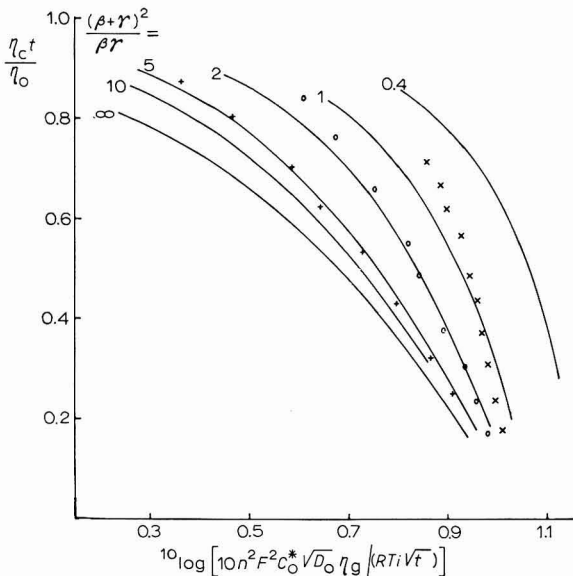


Fig. 1. Plots of data obtained from the coulostatic pulse method *vs.* those from the galvanostatic step method at several electrolysis times; (+), 0.15; (○), 0.65; (×), 2.0 mM Hg₂²⁺-ions. Solid lines, the prescribed curves to be found when the electrode reaction behaves in a classical way; $\beta + \gamma = i_0/(nFC_0^*/V^2)$ and $\beta\gamma = nFi_0/(RTC_0)$.

The data of the coulostatic and the galvanostatic pulse method at the shorter electrolysis times, $0.5 \mu\text{sec}$ – $100 \mu\text{sec}$, were plotted against each other as mentioned in an earlier paper⁹ (see Fig. 1). From this plot it can be seen that the mercurous ion discharge cannot be explained in a classical way, at least not for the higher concentrations. Other ways of plotting the data such as $t/\eta_g \cdot d\eta_g/dt$ vs. $aC_d \eta_g/i/t$ and determination of the double-layer capacity from the relation, $C_d = (idt/d\eta_g)(\eta_c(t)/\eta_0)$ indicate an increasingly abnormal behaviour at shorter electrolysis times (subscripts g and c pertain to the galvanostatic and the coulostatic step method, respectively and η_0 is the overvoltage resulting from the coulostatic charging of the double layer in a very short time). Frequency dispersion of the ohmic drop is not likely to occur with hanging mercury drops in a high conductive supporting electrolyte as $1 M \text{ HClO}_4$ ¹³. Experiments with large mercury drops hanging at a fine capillary, as done by TESSARI *et al.*¹⁴, gave the same results. Figure 1 indicates that the reaction is slightly irreversible and the values of the double-layer capacitance are excessively high, as was also observed by SLUYTERS-REHBACH AND SLUYTERS⁶. Therefore, it is likely that the data can be explained by the idea of coupling of double-layer charging with faradaic charge transfer, caused by specific adsorption of the mercurous ions at the interface. The equations for this particular case, a metal-ion/metal electrode perturbed by a galvanostatic single step current and a coulostatic charge injection, will be given below.

THEORY

The equations, to be solved, are given by DELAHAY⁷:

$$\frac{\partial C_o(x, t)}{\partial t} = D_o \frac{\partial^2 C_o(x, t)}{\partial x^2} \quad (1)$$

$$i = -nFD_o \left(\frac{\partial C_o(x, t)}{\partial x} \right)_{x=0} + \frac{d(q + nF\Gamma_o)}{dt} \quad (2)$$

$$i_0 \left[1 - \frac{C_o(0, t)}{C_o^*} + \frac{nF}{RT} \eta \right] = -nFD_o \left(\frac{\partial C_o(x, t)}{\partial x} \right)_{x=0} + nF \frac{d\Gamma_o}{dt} \quad (3)$$

with the initial conditions:

$$C_o(x, 0) = C_o(\infty, t) = C_o^* \quad (\text{the bulk concentration}) \quad (4)$$

The time derivatives of q and Γ_o can be expressed in the partial derivatives of the two independent variables, $C_o(0, t)$ and E .

$$\frac{dq}{dt} = q_C \frac{dC_o(0, t)}{dt} + q_E \frac{d\eta}{dt} \quad (5a)$$

$$\frac{d\Gamma_o}{dt} = \Gamma_C \frac{dC_o(0, t)}{dt} + \Gamma_E \frac{d\eta}{dt} \quad (5b)$$

in which

$$q_C = \left(\frac{\partial q}{\partial C_o} \right)_E, \quad q_E = \left(\frac{\partial q}{\partial E} \right)_{C_o^*}, \quad \Gamma_C = \left(\frac{\partial \Gamma_o}{\partial C_o} \right)_E \quad \text{and} \quad \Gamma_E = \left(\frac{\partial \Gamma_o}{\partial E} \right)_{C_o^*}$$

We shall first consider the galvanostatic single step case, the result of which can be easily transposed for the coulostatic pulse method. After Laplace transformation of eqns. (1)–(5) (see BERZINS AND DELAHAY¹⁵ for the simpler but related problem) and rearranging, one gets:

$$\bar{\eta}(s) = \frac{i}{s^{\frac{1}{2}}} \times \frac{D_0^{-\frac{1}{2}} \Gamma_C/s + s^{\frac{1}{2}} + i_0/(nFC_{\text{o}}^* \sqrt{D_0})}{D_0^{-\frac{1}{2}} (\Gamma_C q_E^* - \Gamma_E q_C^*) s^{\frac{1}{2}} + q_E s + (q_E^* + (nF/RT) C_{\text{o}}^* q_C^*) i_0 / (nFC_{\text{o}}^* \sqrt{D_0}) s^{\frac{1}{2}} + (nF/RT) i_0} \quad (6)$$

in which

$$q^* = q + nF\Gamma_{\text{o}}$$

Some remarks on eqn. (6): The low-frequency capacity, $q_E^* + (nF/RT)C_{\text{o}}^*q_C^*$, looks suspicious but is in agreement with thermodynamics. If i_0 or the electrolysis time is infinite, the low frequency capacity reduces, using the Nernst equation ($dC_{\text{o}} = nF/(RT)C_{\text{o}}^*dE$), to

$$\left(q_E^* + \frac{nF}{RT} C_{\text{o}}^* q_{\text{o}}^* \right)_{\substack{i_0=\infty \\ t \rightarrow \infty}} \rightarrow \frac{d(q + nF\Gamma_{\text{o}})}{dE}$$

The highest frequency capacity term can be written as:

$$\Gamma_C q_E^* - \Gamma_E q_C^* = \Gamma_C \left(\frac{\partial q^*}{\partial E} \right)_{\Gamma_{\text{o}}}$$

The latter conversion is implicitly given in TIMMER's¹⁶ treatment of the faradaic impedance of the reversible electrode with specific adsorption. SLUYTERS and co-workers found in their impedance study of specific adsorption of thallium^{17,18}, lead¹⁶ and indium¹⁹ ions that the value of Γ_C is negligible except in some extreme cases. For that reason we ignore Γ_C , occurring in eqn. (6), which simplifies the problem considerably, since also the factor $(q_E^* \Gamma_C - q_C^* \Gamma_E)$ can be neglected. It also means that either Γ_E or q_C^* is zero; obviously the choice is $q_C^* = 0$. Another reason for ignoring Γ_C and $q_E^* \Gamma_C - q_C^* \Gamma_E$ is the fact that the weight of these quantities in eqn. (6) is small, since measurements were done at relatively long times. With these simplifications, eqn. (6) becomes:

$$\bar{\eta}(s) = \frac{i}{s^{\frac{1}{2}}} \frac{s^{\frac{1}{2}} + i_0 / (nFC_{\text{o}}^* \sqrt{D_0})}{q_E s + i_0 / (nFC_{\text{o}}^* \sqrt{D_0}) (q_E + nF\Gamma_E) s^{\frac{1}{2}} + nF i_0 / RT} \quad (6a)$$

Back-transformation²⁰ gives:

$$\eta(t) = (i/q_E) / (b_2 - b_1) [\{(a - b_1)/b_1^2\} (\exp b_1^2 t \operatorname{erfc} b_1 \sqrt{t/\pi}) + 2b_1 \sqrt{(t/\pi)} - 1] - \{(a - b_2)/b_2^2\} (\exp b_2^2 t \operatorname{erfc} b_2 \sqrt{t/\pi}) + 2b_2 \sqrt{(t/\pi)} - 1] \quad (7)$$

in which

$$a = i_0 / (nFC_{\text{o}}^* \sqrt{D_0}) \quad (8a)$$

$$b_1 + b_2 = a (q_E + nF\Gamma_E) / q_E \quad (8b)$$

$$b_1 b_2 = (nF/RT) i_0 / q_E \quad (8c)$$

The corresponding equation for the coulostatic method can be obtained with the formula:

$$\eta_c(t)/\eta_0 = q_E d\eta_g(t)/idt,$$

so that

$$\eta_c(t) = \eta_0 (b_2 - b_1)^{-1} [(a - b_1) \exp b_1^2 t \operatorname{erfc} b_1 \sqrt{t} - (a - b_2) \exp b_2^2 t \operatorname{erfc} b_2 \sqrt{t}] \quad (9)$$

ANALYSIS OF THE DATA, BASED ON EQNS. (7) AND (9)

Equation (7) can be expanded for long electrolysis times, giving:

$$\eta(t) = \frac{RT}{nF} \frac{i}{i_0} - \left(\frac{RT}{n^2 F^2} \right)^2 \frac{i}{(C_{O^*} \sqrt{D_O})^2} (q_E + nF\Gamma_E) + \frac{2}{\sqrt{\pi}} \frac{RT}{n^2 F^2} \frac{i}{C_{O^*} \sqrt{D_O}} \quad (10)$$

From this approximation, the values of $C_{O^*} \sqrt{D_O}$ and $(q_E + nF\Gamma_E)$ could be obtained and a reasonable estimate of i_0 could be made. These values were used to analyze all data with eqn. (7) in which now only the value of q_E is unknown. Analysis was performed with a computer (CDC 6600). A good curve-fit could be produced by varying only q_E . Both the two double-layer parameters and the exchange current were then varied giving only minor changes. The theoretical and experimental curves fit within 1% over the whole time range that was examined. The accuracy of the computed data was determined on the basis that experiments had a mean precision of at least 2% for the longer-time region, and within 2–6% for the shorter times because of uncertainty due to the ohmic drop. Analyses of the data could be performed only after the preparation of a sub-routine program which evaluates the $\exp \lambda^2 \operatorname{erfc} \lambda$ for both real and complex argument, which is not available as a standard library program. This program is given elsewhere²¹.

RESULTS AND DISCUSSION

The results are given in Table I.

The values of i_0 in Table I are higher by at least a factor of three than the values reported previously^{1–5}. This is partly due to the fact that in this paper the overvoltage-time curve at short times is analyzed by means of another formula than the one used previously.

The anodic transfer coefficient calculated from the reported exchange current densities, is close to unity. This is rather strange, although BARKER²² also found many electrode reactions with extreme transfer coefficients. Moreover, measurements were performed at potentials far away from the standard potential. It is also possible that the electrode reaction takes place *via* the specific adsorbed mercurous ions only and we shall show below that there is an indication that the amount of specific adsorbed mercurous ions is proportional to the concentration. MOHILNER AND DELAHAY²³ have indicated that the apparent charge transfer coefficient can behave strangely in such a case.

The reported values of the low frequency capacitances, $d(q + nF\Gamma_O)/dE$, are in good agreement with the values given by SLUYTERS⁶ and coworkers, except for the highest concentration. The values of q_E are reasonable if the irreversible C_d -values

at more cathodic potentials may be extrapolated to the potential region where the mercury-ion discharge occurs.

If the same assumptions are made as those by TIMMER *et al.*^{16,19} for the specific adsorption of In and Pb electroactive species, the amount of specific adsorbed mercurous ions can be calculated. The arguments are: neglect of non-specific adsorption; a linear adsorption isotherm with a proportionality factor almost independent of E , or for that matter, q . The assumptions are reasonable for low concentrations and a small potential span.

Thus

$$\Gamma_0 = kC_0$$

$$nF \frac{d\Gamma_0}{dE} = nFk \frac{dC_0}{dE} = \frac{n^2 F^2}{RT} kC_0$$

From Fig. 2 it can be seen that eqn. (11) holds reasonably, giving an amount of specific adsorbed mercurous ions of *ca.* $1 \mu\text{C cm}^{-2}$ in the case of the highest concentration (1.98 mM).

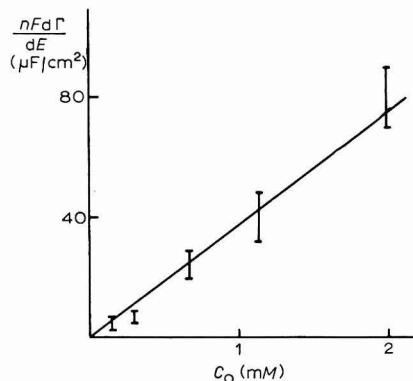


Fig. 2. Plot of difference between the lower and higher frequency double-layer parameter *vs.* bulk concn. of mercurous ions.

Data obtained with the coulostatic pulse method could not be analyzed according to eqn. (9) since there are at least two capacitances involved. Equation (9) can be applied only if the charge injection is accomplished in such a short time that the influence of the low frequency capacitance is negligible, which was not the case with these experiments.

ACKNOWLEDGEMENT

This work was supported by the Office of Naval Research. The initial experimental work was supported by the Netherlands Organization for Scientific Research (ZWO). The author wishes to thank Professor P. DELAHAY for valuable comments and kind interest in this work.

SUMMARY

The kinetics of the Hg(I)/Hg electrode reaction in 1 M HClO_4 are re-examined with the galvanostatic and coulostatic pulse methods. Results are interpreted on the basis of coupling between double-layer charging and faradaic charge transfer. Such a coupling is clearly established. Adsorption of mercurous ions is tentatively explained by a linear adsorption isotherm.

REFERENCES

- 1 H. GERISCHER AND K. STAUBACH, *Z. Physik. Chem. (Frankfurt)*, 6 (1956) 118.
- 2 H. GERISCHER AND M. KRAUSE, *Z. Physik. Chem. (Frankfurt)*, 14 (1952) 184.
- 3 H. MATSUDA, S. OKA AND P. DELAHAY, *J. Am. Chem. Soc.*, 81 (1959) 5077.
- 4 R. L. BIRKE AND D. K. ROE, *Anal. Chem.*, 37 (1965) 450, 455.
- 5 W. D. WEIR AND C. G. ENKE, *J. Phys. Chem.*, 71 (1967) 280.
- 6 M. SLUYTERS-REHBACH AND J. H. SLUYTERS, *Rec. Trav. Chim.*, 83 (1964) 967, 983.
- 7 P. DELAHAY, *J. Phys. Chem.*, 70 (1966) 2373.
- 8 D. J. KOOIJMAN AND J. H. SLUYTERS, *J. Electroanal. Chem.*, 13 (1967) 152.
- 9 D. J. KOOIJMAN, *J. Electroanal. Chem.*, 18 (1968) 81.
- 10 D. J. KOOIJMAN AND J. H. SLUYTERS, *Electrochim. Acta*, II (1966) 1147.
- 11 E. LEVART AND E. POIRIER D'ANGE D'ORSAY, *J. Electroanal. Chem.*, 12 (1966) 277.
- 12 D. J. KOOIJMAN, M. SLUYTERS-REHBACH AND J. H. SLUYTERS, *Electrochim. Acta*, II (1966) 1197.
- 13 G. G. SUSBIELLES, *J. Electroanal. Chem.*, 12 (1966) 230.
- 14 G. TESSARI, P. DELAHAY AND K. HOLUB, *J. Electroanal. Chem.*, 17 (1968) 69.
- 15 T. BERZINS AND P. DELAHAY, *J. Am. Chem. Soc.*, 77 (1955) 6448.
- 16 B. TIMMER, M. SLUYTERS-REHBACH AND J. H. SLUYTERS, *J. Electroanal. Chem.*, 19 (1968) 73.
- 17 M. SLUYTERS-REHBACH, B. TIMMER AND J. H. SLUYTERS, *Rec. Trav. Chim.*, 82 (1963) 553.
- 18 B. TIMMER, Thesis, Utrecht, 1968.
- 19 B. TIMMER, M. SLUYTERS-REHBACH AND J. H. SLUYTERS, *J. Electroanal. Chem.*, 18 (1968) 93.
- 20 R. KAUFMAN, *Table of Laplace Transforms*, Saunders, London, 1966.
- 21 D. J. KOOIJMAN, *J. Electroanal. Chem.*, 19 (1968) 443.
- 22 G. C. BARKER, *Trans. Symposium on Electrode Processes*, edited by E. YEAGER, Wiley, New York, 1959, p. 325.
- 23 D. MOHILNER AND P. DELAHAY, *J. Phys. Chem.*, 67 (1963) 588.

J. Electroanal. Chem., 19 (1968) 365-371

ON THE ANODIC OXIDATION OF MERCURY IN KCl SOLUTIONS

BARBARA BEHR AND JOANNA TARASZEWSKA

Laboratory of Physico-Chemical Analytical Methods, Institute of Physical Chemistry of the Polish Academy of Sciences, Warsaw (Poland)

(Received April 17th, 1968)

The system, $\text{Hg} | (\text{Hg}_2\text{Cl}_2)_{\text{solid}} + (\text{Hg(I)} + \text{Hg(II)} + \text{Cl}^-)_{\text{solution}}$, has been extensively investigated. Equilibria in solutions of ionic strength, 0.5 M , have been determined by SILLÉN¹. According to his data, the total equilibrium concentration of soluble mercury compounds in dilute KCl solutions is *ca.* 10^{-6} M (practically constant over several orders of magnitude of $[\text{Cl}^-]$), the main component being HgCl_2 .

At $[\text{Cl}^-] > 0.1 \text{ M}$, the total concentration of mercury compounds increases, reaching *ca.* 10^{-4} M in 1 M KCl (*cf.* Fig. 3). The equilibrium is shifted towards HgCl_3^- and HgCl_4^{2-} ions.

The formation of Hg_2Cl_2 on Hg and the behaviour of calomel electrodes prepared by various methods has been studied in detail by IVES *et al.*²⁻⁴ using chiefly the galvanostatic technique and microscopic observations of the electrode. Their measurements covered a wide range of current densities and $[\text{Cl}^-]$ -values. They suggest that a change in the mechanism of Hg oxidation takes place with decreasing current density or increasing $[\text{Cl}^-]$ owing to the increasing role of the soluble chloromercuric complexes.

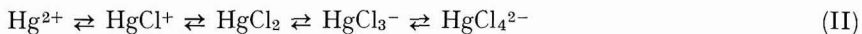
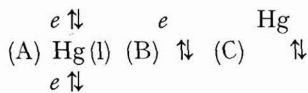
Two papers^{5,6} dealing with the first stage of anodic oxidation of Hg in the absence of calomel, consider the diffusion problem quantitatively. ARMSTRONG *et al.*⁶ presented experimental evidence to show that in concentrated HCl solutions, the electrode process at equilibrium potential is purely diffusion-controlled. They conclude that the rate constant of the electrode reaction, $\text{Hg} + 4 \text{ Cl}^- \rightleftharpoons \text{HgCl}_4^{2-} + 2 e$, is higher than 1.5 cm sec^{-1} . However, an exact comparison of their results with theoretical values was not made because of the unknown equilibrium concentrations of chloromercuric compounds in the solutions investigated. Also, their conclusions cannot be unambiguously extended to more positive potentials and to galvanostatic conditions. BOCKRIS *et al.*⁵ have studied ellipsometrically the anodic oxidation of Hg under galvanostatic conditions. They did not compare their results with equilibrium data and this led them to propose a slow chemical step*—this hypothesis is not justified by their results.

The purpose of the present work was to obtain new information on the initial stage of Hg oxidation in KCl solutions, and to consider more exactly the role of diffusion in this process.

* The theory presented by these authors does not explain the lowering of the experimental $i\tau_t^{\frac{1}{2}}$ -values at low current densities. The $i\tau_t^{\frac{1}{2}}$ -value could only increase if a slow chemical step were present. Equation (1) in the paper under discussion has been re-derived by GALUS who has found an error of sign on the last term of this equation.

GENERAL CONSIDERATIONS

The equilibria in the system investigated may be represented diagrammatically as follows:



The components present in the form of a separate phase are indicated. The equilibrium between systems I and II can be achieved in three ways, A and B being electrode reactions and C, a disproportionation reaction. It is known from the literature that the reaction, $2\text{Hg} \rightleftharpoons \text{Hg}_2^{2+} + 2e^-$, in the absence of chloride ions, is fast⁷. Also, at high $[\text{Cl}^-]$, at the equilibrium potential of the calomel electrode ($E_{\text{cal}}^{\text{eq}}$), the electrode process following the overall reaction, $\text{Hg} + 4\text{Cl}^- \rightleftharpoons \text{HgCl}_4^{2-} + 2e^-$, is purely diffusion-controlled⁶. This suggests the quick setting up of equilibrium within the whole of system II, or, at least, between the higher complexes. The disproportionation reaction, $\text{I} \rightarrow \text{II} + \text{Hg}$, is rapid only if the process does not involve the formation of a new phase of Hg metal, *i.e.*, at the surface of the mercury electrode, or if the resulting Hg concentrations do not exceed the solubility of Hg in the solution (*ca.* $3 \cdot 10^{-7}\text{M}$)⁸.

It may be concluded that, if times of the order of a millisecond, or longer, are involved in the measurements, the electrode is at equilibrium with all soluble products of the electrode reactions, the potential being a measure of their concentrations. It appears that the only slow steps are crystallization or disproportionation of solid Hg_2Cl_2 . We will further regard the deviation of the electrode potential from that of ($E_{\text{cal}}^{\text{eq}}$) as a measure of supersaturation with respect to the Hg_2Cl_2 , provided the electrode is not coated extensively with the calomel layer.

On the basis of these assumptions, several steps could be distinguished in the process of anodic oxidation of Hg in chloride solutions. This is shown in Table I.

TABLE I

<i>Non-passive electrode, relatively low overvoltage</i>	<i>Passive electrode, relatively high overvoltage</i>
Formation of soluble products	Formation of the calomel film and of soluble products
→ 0	→ q_{t_1}

This scheme may be more generally valid in all cases where the electrode reaction leading to soluble products is a rapid one. The charge consumed in particular stages depends on the mode of polarization, on the equilibrium concentrations of the soluble products, and on the rate of crystallization. Blocking of the electrode is accompanied by a steep rise of potential due to the inhibition of the electrode reaction by the Hg_2Cl_2 film. The time elapsed before blocking will be called the transition time, τ , by analogy with ordinary chronopotentiometric curves, although

in the usual case the potential rise is due to the concentration polarization. In the case of blocking, the surface concentrations at the transition time cannot be easily determined and therefore $\tau-i$ relationships known from the theory of chronopotentiometry cannot be applied. The behaviour of the passive electrode is described elsewhere^{9,10}.

The charge used during Hg oxidation is consumed for:

1. Charging the double layer, q_e . This process probably needs less than 50 $\mu\text{C}/\text{cm}^2$.

2. Formation of soluble products, q_{sol} .

3. Formation of the Hg_2Cl_2 film, q_t . The first step in diluted solutions is "chloromercury" postulated by HILLS AND IVES¹¹, corresponding to a charge of 80–100 $\mu\text{C}/\text{cm}^2$.*

In order to estimate q_t , the charge, q_{sol} , should be known. This may be approximated by the integrated linear diffusion equation:

$$q_{\text{sol}} = nF \sum_i D_i \left(\frac{\partial c_i}{\partial x} \right)_{x=0} dt \quad (1)$$

Assuming equal diffusion coefficients, D , and an equilibrium between all soluble mercury compounds, the equation becomes

$$q_{\text{sol}} = nF \int_0^t D \left(\frac{\partial c}{\partial x} \right)_{x=0} dt \quad (2)$$

where c is the total concentration of soluble (mercurous + mercuric) species:

$$c = \sum_i c_i^{\text{eq}} \cdot \exp \{ (RT/nF) \eta \} \quad \text{with } \eta = E - E_{\text{cal}}^{\text{eq}} \quad (3)$$

The solutions of the diffusion problem are well known in two cases, which may be useful in further discussion:

(a) *Constant gradient* ($\partial c/\partial x|_{x=0}$)—this is realized under galvanostatic conditions, before the formation of the film begins, *i.e.*, at $q < q_{t_1}$ (*cf.* Table 1); q_{sol} is then equal to the total charge, $q_{\text{sol}} = it$, and the surface concentration increases according to (assuming zero initial concentration)

$$c^0 = 2it^{1/2}/(\pi D)^{1/2}nF \quad (4)$$

The electrode potential then follows the equation

$$E = E_0 + (RT/nF) \ln (2it^{1/2}/nF(\pi D)^{1/2}) \quad (5)$$

in which we neglect the change in $[\text{Cl}^-]$ which is insignificant, and the charging process which can considerably alter this relation in the case of high current densities and short times. The $E-t$ relationship does not tend to any characteristic point, because of the constant activity of the substrate. Therefore, for analysing the experimental $E-t$ curves we shall use a chosen value of t_η *i.e.*, the time at which the electrode achieves the overvoltage, η . Taking, for example, $\eta = 20$ mV, eqn (5) may be transformed into:

$$\eta (\text{mV}) = 20 + (59/2n) \lg (t/t_{\eta=20}) \quad (6)$$

The theoretical value of $it_{\eta=20}^{1/2}$ can be calculated from (4) and (3). The $c^0-t^{1/2}$ relationships calculated from (4) using $D = 7 \cdot 10^{-6} \text{ cm}^2 \text{ sec}^{-1}$ for different current densities

* The formation of chloromercury can be distinguished also by numerous other methods (*e.g.* as the polarographic adsorption prewave¹² corresponding to *ca.* 80 $\mu\text{C}/\text{cm}^2$).

are shown in Fig. 1. The equilibrium total mercury concentrations at various KCl concentrations are indicated.

(b) *Constant potential*, equivalent to a constant surface concentration:

$$q_{\text{sol}} = 2nFD^{\frac{1}{2}}C^0t^{\frac{1}{2}}/\pi^{\frac{1}{2}} \quad (7)$$

The theoretical $q_{\text{sol}}-t^{\frac{1}{2}}$ curves at ($E_{\text{cal}}^{\text{eq}}$) in different KCl concentrations are shown in

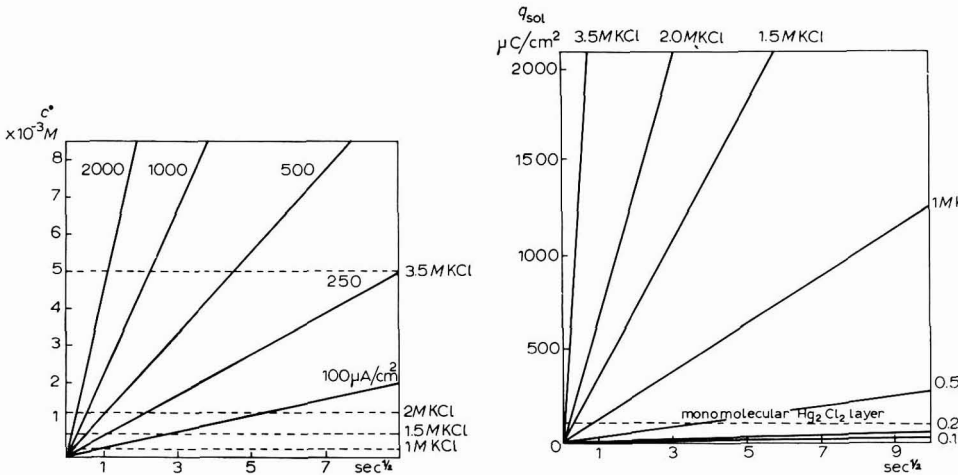


Fig. 1. $c-t^{\frac{1}{2}}$ relationships calc'd. for different current densities according to eqn. (4). The equilibrium total mercury concn. at various $[\text{Cl}^-]$ are indicated.

Fig. 2. Theoretical $q_{\text{sol}}-t^{\frac{1}{2}}$ curves at $E_{\text{cal}}^{\text{eq}}$ at various $[\text{Cl}^-]$ according to eqn. (7). The charge consumed for monomolecular calomel layer formation (ca. $100 \mu\text{C cm}^{-2}$) is indicated.

Fig. 2. We have used the total concentration of mercury complexes from the data of SILLÉN¹ for $C_{\text{Cl}^-} < 1 M$ and from our own measurements for $C_{\text{Cl}^-} \geq 1 M$. It is seen that in the case of concentrated KCl solutions, the formation of soluble mercuric complexes consumes considerable amounts of charge in relatively short times. For comparison, the charge needed for a monomolecular calomel layer (ca. $100 \mu\text{C cm}^{-2}$) is indicated.

EXPERIMENTAL

The hanging mercury drop electrode (HMDE) previously described¹³ with a surface area of $(0.02 \pm 0.002)\text{cm}^2$, was used. The calomel electrode with the same concentration of Cl^- ions as in the electrolytic cell was used as external reference electrode. Measurements were performed at a temperature of $25^\circ \pm 0.5^\circ$. All solutions were de-aerated with electrolytic hydrogen. Solutions of KCl and HCl were prepared from analytically pure reagents and twice-distilled water.

In order to test for the effects of impurities on the "fine structure" of the $E-t$ curves, solutions were prepared from HCl purified by isopiestic distillation and from thrice-distilled water. The third distillation was carried out in a quartz still. Tests were also made on the HMDE when the capillary was not treated with silicone and the mercury

had no contact with piceine wax. In every case, the shape of the $E-t$ curves was exactly reproduced, and only slight differences in the shape of the "pre-peak" could be observed.

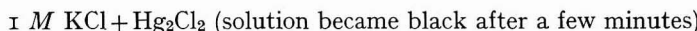
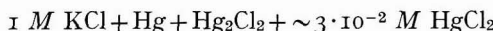
The galvanostatic technique was used. A battery of 100 V with a set of high resistances was employed as the source of constant current. The $E-t$ curves were photographed from the screen of a Tektronix oscilloscope, type 532.

RESULTS AND DISCUSSION

Determination of the equilibrium mercury concentration

To fill the gap in the existing data we have determined quantitatively the concentrations of mercury compounds in equilibrium with solid Hg_2Cl_2 and Hg metal in concentrated KCl solutions.

The following solutions were prepared:



The solutions were shaken for 24 h to allow the system to attain equilibrium and then the polarographic waves of mercury were recorded. The concentrations were found by comparison with the wave height measured for the known concentration of $HgCl_2$ in 1 M KCl. A comparison with the Cd(II) wave recorded from $2 \cdot 10^{-4}$ M $CdSO_4$ in 1 M KCl demonstrated the equality of the diffusion coefficients of Cd(II) and Hg(II) so that we could assume $D_{Hg(II)} = 7 \cdot 10^{-6} \text{ cm}^2 \text{ sec}^{-1}$. The results for all four solutions were in agreement to within 10%—the total mercury concentration being $(2 \pm 0.2) \cdot 10^{-4} \text{ M}$. This value did not change after repeated shaking.

Similar experiments were performed in saturated KCl solutions. In this case the total equilibrium concentration of mercury was $(5.2 \pm 0.2) \cdot 10^{-3} \text{ M}$. Our results and the literature values are shown in Fig. 3.

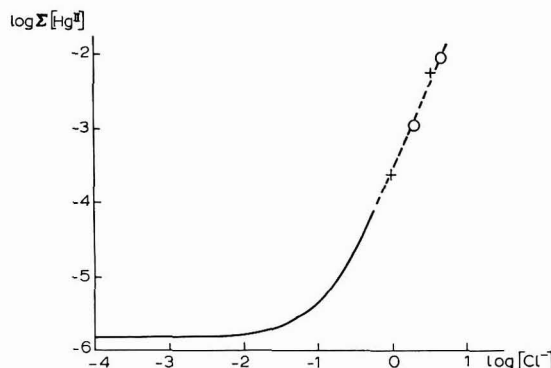


Fig. 3. Total mercury concn. in equilibrium with Hg and Hg_2Cl_2 vs. $\log [Cl^-]$, (—) according to SILLÉN¹; (+), determined polarographically (this paper); (○), calcd. by ARMSTRONG *et al.*⁶ from the Warburg impedance.

Chronopotentiometric measurements

A series of the $E-t$ curves for different KCl concentrations and current densities was measured (Fig. 4). The characteristic "fine structure" of these curves, similar to that observed by IVES *et al.* in 0.1 M KCl or HCl³, is seen only in the case of 0.2 M KCl. The character of the curves is changed in 0.5 M KCl (no "pre-peak"), although the two peaks are still observed. The curves recorded in 1 and 1.5 M KCl are smooth and differ only slightly in shape from the curves characteristic of the formation of soluble products. For 1 M KCl, the measurements were made also at higher current densities, up to 9600 $\mu\text{A}/\text{cm}^2$. At the highest current density, a sort of second peak is observed but the character of the curve is still different from that in more dilute solutions.

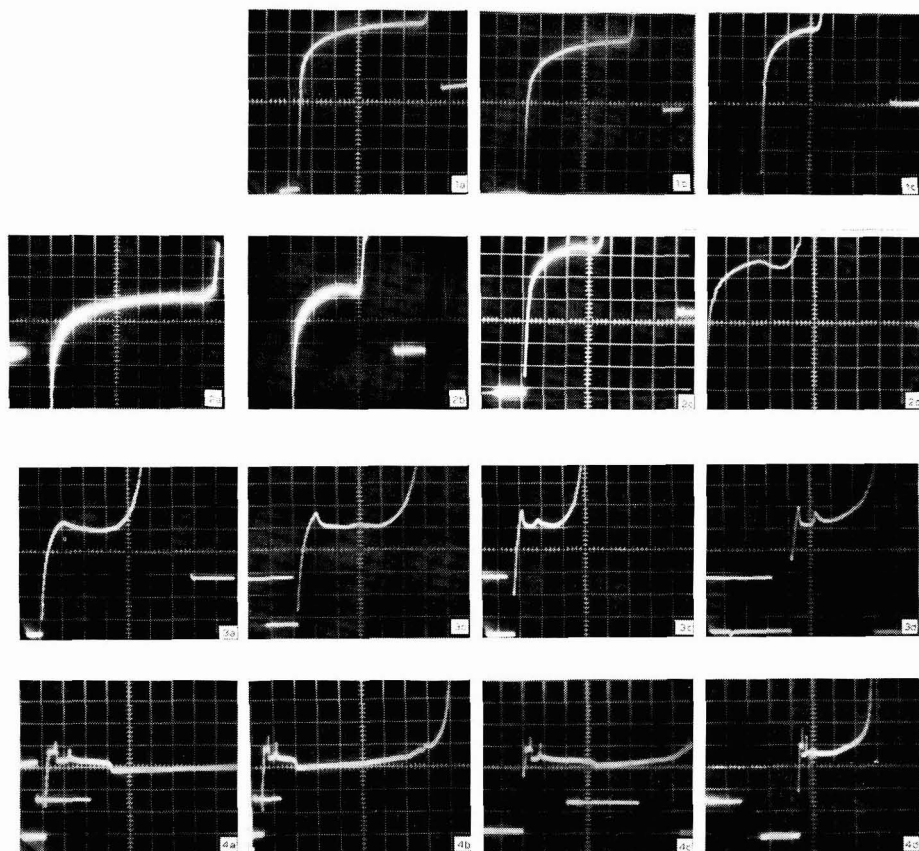


Fig. 4. Dependence of character of $E-t$ curves on KCl concn. and current density. All curves recorded at sensitivity 8.3 mV/cm. (1a, b, c), 1.5; (2a, b, c, d), 1; (3a, b, c, d), 0.5; (4a, b, c, d), 0.2 M KCl.

(1a) 237 $\mu\text{A}/\text{cm}^2$, 4.5 sec cm^{-1} ; (1b) 475 $\mu\text{A}/\text{cm}^2$, 1.8 sec cm^{-1} ; (1c) 1000 $\mu\text{A}/\text{cm}^2$; (2a) 95 $\mu\text{A}/\text{cm}^2$, 5 sec cm^{-1} ; (2b) 240 $\mu\text{A}/\text{cm}^2$, 2 sec cm^{-1} ; (2c) 480 $\mu\text{A}/\text{cm}^2$, 0.9 sec cm^{-1} ; (2d) 960 $\mu\text{A}/\text{cm}^2$, 0.18 sec cm^{-1} ; (3a) 121 $\mu\text{A}/\text{cm}^2$, 0.9 sec cm^{-1} ; (3b) 235 $\mu\text{A}/\text{cm}^2$, 0.45 sec cm^{-1} ; (3c) 464 $\mu\text{A}/\text{cm}^2$, 0.45 sec cm^{-1} ; (3d) 928 $\mu\text{A}/\text{cm}^2$, 0.18 sec cm^{-1} ; (4a) 122 $\mu\text{A}/\text{cm}^2$, 0.9 sec cm^{-1} ; (4b) 235 $\mu\text{A}/\text{cm}^2$, 0.9 sec cm^{-1} ; (4c) 465 $\mu\text{A}/\text{cm}^2$, 0.45 sec cm^{-1} ; (4d) 928 $\mu\text{A}/\text{cm}^2$, 0.45 sec cm^{-1} . Zero potential is registered at the end of each curve.

The characteristic structure of the $E-t$ curves in the case of dilute solutions and low current densities has been studied by IVES *et al.* A few details may now be added to their observations. Figure 5 presents the $E-t$ curves recorded in 0.2 M KCl at low current densities.

At $3 \mu\text{A cm}^{-2}$ (curve a) a smooth curve is registered. At a slightly increased current density ($5.5 \mu\text{A cm}^{-2}$, curve b) a plateau is observed with subsequent stepwise lowering of potential. The plateau corresponds probably to the formation of "chloromercury", and the further crystallization of calomel probably requires a somewhat

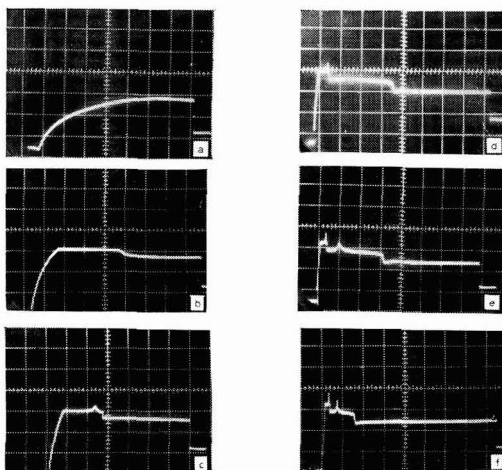


Fig. 5. Effect of current density on formation of "fine structure" of $E-t$ curves recorded in 0.2 M KCl. Time base, 4.5 sec cm^{-1} ; sensitivity 5 mV cm^{-1} . (a) 3, (b) 5.5, (c) 8.8, (d) 19.5, (e) 27.5, (f) $36.5 \mu\text{A cm}^{-2}$.

lower overvoltage, hence the step. At $8.8 \mu\text{A cm}^{-2}$ (curve c), a small peak is observed just before the end of the "chloromercury" formation and the step is much steeper. At $19.5 \mu\text{A cm}^{-2}$ (curve d), all the effects described above may still be observed during the first period of polarization (*ca.* 3.5 sec) and after a longer time a second step is formed and, consequently, at $27.5 \mu\text{A cm}^{-2}$ (curve e), a second small peak, while the first becomes higher and sharper. Further increase of current density does not change this picture qualitatively until $928 \mu\text{A cm}^{-2}$ (curve 4d, Fig. 4) when the second step disappears. The second peak corresponds probably to the "hump" observed by IVES *et al.* in 0.1 M KCl, but here its nature does not seem to differ from that of the first peak.

Figure 6 presents the behaviour of the electrode after the circuit is opened. At $i=3 \mu\text{A cm}^{-2}$ (curve a), the potential decreases slowly as if the process were diffusion-controlled. The decay curves (Fig. 6, b and c) after switching off the current before the second step (even after the second peak or "the hump"—Fig. 6e) showed two potential arrests: the first at a few millivolts below the potential just before opening the circuit, and the second near $E_{\text{cal}}^{\text{eq}}$.

The potential tended to $E_{\text{cal}}^{\text{eq}}$ immediately, only if the current was switched off after passing the second step (Fig. 6, d and f)—and not the "hump" as observed in 0.1 M KCl by IVES *et al.* These results suggest that before the second step is reach-

ed, there exists at the electrode surface a crystalline form of calomel of higher solubility. This form dissolves after opening the circuit, while the mercuric complexes diffuse away from the electrode, and thus keeps the electrode potential at a more positive value than $E_{\text{cal}}^{\text{eq}}$. The reason why the less stable crystals are formed is obviously their higher crystallization rate. The crystallization takes place with a very low activation energy, as the potentials during the current flow and after opening the circuit are similar. The more active form should recrystallize with the formation of the more stable equilibrium form of calomel. The second step is probably formed after the recrystallization process is completed. From that time, the crystallization of the equilibrium calomel form is rapid enough to keep the electrode potential low enough to prevent the formation of the more active form.

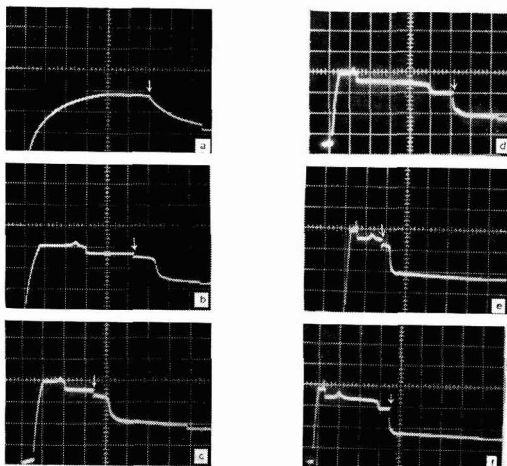


Fig. 6. $E-t$ curves in 0.2 M KCl recorded after disconnecting the circuit (arrow) at various stages of anodization; time base, 4.5 sec cm^{-1} ; sensitivity, 5 mV cm^{-1} . (a) 3, (b) 8.8, (c) 13.5, (d) 13.5, (e) 27.5, (f) 27.5 $\mu\text{A} \text{ cm}^{-2}$.

Our views concerning dilute KCl solutions may be summarized as follows. The first peak corresponds to the beginning of crystallization of the more active form of calomel and the second peak to the beginning of crystallization of the equilibrium calomel form. The condition for the electrode attaining $E_{\text{cal}}^{\text{eq}}$ is not only the existence of the equilibrium calomel form but also the absence of the more soluble form, which recrystallizes until it disappears completely when the second step is reached. If the current was switched off before the second step, the electrode attained the $E_{\text{cal}}^{\text{eq}}$ after a period of time (Fig. 6, b,c and e). Probably, the process of recrystallization was completed also in the absence of current flow, producing a sufficient amount of the equilibrium form of calomel. This is due to the slow process of diffusion of soluble products away from the electrode in dilute KCl solutions (*cf.* Fig. 2).

The role of diffusion and the thickness of the blocking film

To estimate the role of diffusion, we determined the total charge needed for blocking the electrode, q , (Table 2). This charge does not change appreciably with current density in dilute solutions and diminishes strongly with increasing current

TABLE 2

DEPENDENCE OF q CONSUMED, ON PASSIVATION OF MERCURY AND OF $q_{\text{sol}}^{\text{max}}$ ON CHLORIDE ION CONCENTRATIONIn 0.1 and 0.2 M KCl, $q_{\text{sol}}^{\text{max}}$ was calcd. for $\eta = 20$ mV

KCl conc.	i ($\mu\text{A cm}^{-2}$)	τ_p (sec)	q ($\mu\text{C cm}^{-2}$)	$q_{\text{sol}}^{\text{max}}$ ($\mu\text{C cm}^{-2}$)
0.1	30	110	3300	500
	90	36	3240	300
0.2	19.5	128	2500	1125
	122	18	2200	500
	235	7.6	1790	315
	465	3.4	1590	210
	928	1.5	1400	135
0.5	121	3.8	460	210
	235	2.2	520	174
	464	1.3	600	135
	928	0.61	560	115
	2500	0.14	360	~ 70
1.0	33	>600	>20000	
	63.5	120	7600	
	135	17	2300	
	240	6.7	1600	
	480	2.9	1150	
	960	0.75	720	
	2400	~ 0.27	~ 650	
	4800	~ 0.1	~ 430	
	9600	~ 0.04	~ 380	
1.5	237	24.5	5800	
	475	8.5	4050	
	1000	2.2	2200	
	2150	0.60	1290	
	4300	0.27	1160	
	8600	~ 0.1	~ 860	

density in concentrated KCl solutions. In 0.1 and 0.2 M KCl the surface concentrations of mercury compounds during the anodization are not known because the $E-t$ curves (Fig. 4) indicate the presence of crystallization phenomena from the very beginning of the current flow. However, these concentrations cannot be higher than those corresponding to supersaturation, $c/c_{\text{eq}} = 10^{\eta/29}$ at 25° . To estimate the upper limit of q_{sol} , we have assumed a constant value of $\eta = 20$ mV, corresponding to the highest potential plateau (Fig. 4). Thus, using $c^0 = 5c_{\text{eq}}$ and the equilibrium data (cf. Fig. 2) we have found the $q_{\text{sol}}^{\text{max}}$ -values shown in Table 2. It follows that the contribution of diffusion to the anodic process is, in dilute solutions, insignificant, amounting to less than 20% of the total charge. Therefore, we can regard the total charge as a measure of the thickness of the calomel film.

In 1 and 1.5 M KCl (Fig. 4) the curves pass a maximum which can be regarded as a remainder of the "fine structure" and is probably related to the crystallization phenomena. At current densities $> 200 \mu\text{A cm}^{-2}$, the maximum was formed always at $\eta > 20$ mV. To determine whether the process is initially purely diffusion-controlled, we analyzed initial sections of the $E-t$ curves ($t \leq t_{\eta=20}$) by: (i) plotting η vs. $\log(t/t_{\eta=20})$ —straight lines with nearly theoretical slopes were obtained; (ii) comparison

TABLE 3

VALUES OF $it_{\eta=20}^{\frac{1}{2}}$ FOR DIFFERENT CURRENT DENSITIES IN 1 M KCl.The theoretical value of $it_{\eta=20}^{\frac{1}{2}}$ is $4.95 \cdot 10^{-4}$, calcd. with $D = 7 \cdot 10^{-6} \text{ cm}^2 \text{ sec}^{-1}$

$i(\mu A \text{ cm}^{-2})$	$t_{\eta=20} \text{ (sec)}$	$it_{\eta=20}^{\frac{1}{2}} \cdot 10^4$
63.5	45.8	4.2
95.0	22.2	4.5
	26.5	4.9
120	10.4	3.9
	11.5	4.1
	10.5	3.9
240	2.6	3.9
	2.4	3.7
	2.8	4.0
480	0.7	4.1
	0.75	4.6
	0.7	4.1
	0.95	4.8
960	0.24	4.7
2400	0.048	5.1
4800	0.014	5.7

of the $it_{\eta=20}^{\frac{1}{2}}$ -values with the theoretical value for a diffusion-controlled process (Table 3). The results are in agreement with our assumption that the electrode is in an equilibrium with all soluble products, although the solution is strongly supersaturated with respect to solid Hg_2Cl_2 . The discrepancies of the $it_{\eta=20}^{\frac{1}{2}}$ -values can be explained by an error in potential determination of *ca.* 1.5 mV. The $it_{\eta=20}^{\frac{1}{2}}$ -value at the highest current density is the least exact one. The total charge at $t_{\eta=20}$ decreased in this case to *ca.* $70 \mu\text{C cm}^{-2}$. This value is comparable with the charge of the double layer and the process of charging can increase the results significantly. The other source of error (of opposite sign) in the case of high current densities can be the ohmic drop in the solution.

Crystallization probably sets in near the maximum on the $E-t$ curves. The maximum is formed if the rate of crystallization exceeds that of the generation of mercury compounds which is limited by the pre-set current. To maintain the equilibrium between Hg(II) and Hg(I) compounds, the reaction opposite to disproportionation (reaction C) should occur at the electrode surface and the sign of the gradient $(\partial c_{\text{Hg(III)}} / \partial x)_{x=0}$, should be reversed. Thus, soluble mercury compounds should be supplied to the electrode surface by the reversed diffusion from the solution, until the sign of the gradient changes again. This process stabilizes the electrode potential and therefore no sharp peaks on the $E-t$ curves similar to those observed in the case of 0.1 and 0.2 M KCl can be formed. It is obvious that the process of the reversed diffusion of Hg(II) complexes from the solution can take place also if the electric circuit is disconnected after crystallization has set in (growth of the calomel layer after opening the circuit has been observed by several authors).

It is rather difficult to estimate the instantaneous thickness of the growing calomel layer in concentrated KCl solutions in view of an abundant source of mercury

in the solution surrounding the electrode (*cf.* Fig. 1—the equilibrium values should be multiplied by *ca.* 5 owing to *ca.* 5-fold supersaturation). However, a comparison of the blocking films in dilute and concentrated KCl solutions is possible. It is seen from Table 2 that in 0.1 and 0.2 M KCl where diffusion effects are negligibly small, the total charge, q_t , amounts to 2000–3000 $\mu\text{C cm}^{-2}$ corresponding to an average thickness of 20–30 molecular layers. In the case of 0.5 M KCl, where the contribution of diffusion is still not very pronounced, q_t is several times smaller. This charge corresponds to 3–4 molecular layers at high current densities, when diffusion becomes insignificant. The comparison of these figures suggests a change in the structure of Hg_2Cl_2 films with increasing KCl concentration. The structure may be related to the formation or the absence of "chloromercury" in the initial stage of Hg oxidation: the shape of the $E-t$ curves in the case of 0.5 M KCl does not show the characteristic plateau observed in more dilute solutions due to the formation of "chloromercury" (*cf.* Fig. 4).

q_t increases again in 1 and 1.5 M KCl at low current densities. However, at high current densities, q_t becomes as small as in 0.5 M KCl. This indicates good blocking properties of the Hg_2Cl_2 films formed in concentrated solutions. It is possible that the increase in q_t with decreasing current density is due to the increasing role of the diffusion process only, while the thickness of the blocking film remains unchanged.

Comparison of galvanostatic and potentiostatic conditions may result in different reaction paths (*cf.* CORNISH *et al.*³ and ARMSTRONG *et al.*⁶). Galvanostatic measurements involve control of reactions A and B (*cf.* diagram). Therefore, if the equilibrium between systems I and II is significantly disturbed owing to the crystallization of Hg_2Cl_2 , reaction C sets in. On the contrary, there is no reason for this reaction to occur under potentiostatic conditions. In this case there are no restrictions for the current flow and any quantity of Hg(I) needed for Hg_2Cl_2 formation as well as of Hg(I) and Hg(II) species diffusing away from the electrode, can be supplied by the electrode reactions A.

SUMMARY

The initial stage of electrooxidation of mercury in KCl solutions of various concentrations has been investigated. From the analysis of the $E-t$ curves at constant current densities, the following conclusions can be drawn.

1. The free surface of the mercury electrode is in equilibrium with all soluble Hg(I) and Hg(II) compounds.
2. The process of oxidation at $[\text{Cl}^-] > 0.5 \text{ M}$ is diffusion-controlled until the solution is strongly supersaturated in respect to calomel and crystallization sets in.
3. The thickness of the blocking film is much higher in dilute KCl solutions (~ 10 –20 molecular) than in concentrated ones, where it is as thin as about 3-molecular.

REFERENCES

- 1 L. G. SILLÉN, *Acta Chem. Scand.*, 3 (1949) 539.
- 2 H. P. DIBBS, D. J. G. IVES AND R. W. PITTMAN, *J. Chem. Soc.*, (1957) 3370.
- 3 D. C. CURNISH, D. J. G. IVES AND R. W. PITTMAN, *J. Chem. Soc.*, (1966) 111, 116.

- 4 S. N. DAS AND D. J. G. IVES, *J. Chem. Soc.*, (1962) 1619.
- 5 J. O'M. BOCKRIS, M. A. V. DEVANATHAN AND A. K. N. REDDY, *Proc. Roy. Soc. London*, A279 (1964) 327.
- 6 R. D. ARMSTRONG, M. FLEISCHMANN AND R. M. THIRSK, *Trans. Faraday Soc.*, 61 (1965) 2238.
- 7 H. TANAKA AND R. TAMAMUSHI, *Electrochim. Acta*, 9 (1964) 963.
- 8 H. C. MOSER AND A. F. VOIGT, *J. Am. Chem. Soc.*, 79 (1957) 1837.
- 9 W. KEMULA, Z. KUBLIK AND J. TARASZEWSKA, *Bull. Acad. Polon. Sci. Ser. Sci. Chim.*, 8 (1960) 269.
- 10 W. KEMULA AND J. TARASZEWSKA, *Rev. Chim. Min.*, 5 (1968) 535.
- 11 G. J. HILLS AND D. J. G. IVES, *J. Chem. Soc.*, (1951) 311.
- 12 A. A. VLČEK, *Collection Czech. Chem. Commun.*, 19 (1954) 221.
- 13 W. KEMULA AND Z. KUBLIK, *Anal. Chim. Acta*, 18 (1958) 104.

J. Electroanal. Chem., 19 (1968) 373-384

E.M.F. MEASUREMENTS ON THE NICKEL–NICKEL(II) COUPLE IN MOLTEN FLUORIDES*†

H. W. JENKINS AND GLEB MAMANTOV

Department of Chemistry, University of Tennessee, Knoxville, Tenn. 37916 (U.S.A.)

D. L. MANNING

Analytical Chemistry Division, Oak Ridge National Laboratory, Oak Ridge, Tenn. 37830 (U.S.A.)

(Received March 21st, 1968; in revised form, May 21st, 1968)

INTRODUCTION

Interest in molten fluorides has been stimulated by the Molten Salt Reactor Experiment at Oak Ridge National Laboratory; in this reactor, fluoride salts are used as fuel solvent and reactor coolant. Electroanalytical methods offer promise for *in situ* analysis of corrosion products (iron, nickel, and chromium), some fission products, and uranium present in these salts. A simple and stable reference electrode should be very useful for thermodynamic studies in molten fluorides, such as the determination of the e.m.f. series in these solvents, in addition to being of general utility for electroanalytical measurements in molten fluorides^{1–8}.

Although several reference electrodes have been used in molten fluorides^{9–12}, they are either too complex in design, or cannot be separated readily from the rest of the melt. The latter factor presents a serious disadvantage in electroanalytical studies.

The Ni–Ni(II) couple was employed originally by GRJOTHEIM¹³ for potential measurements in molten NaF–KF (40–60 mole %). Alumina rod that was wet by the solvent was employed as the salt bridge, resulting in some solubility of alumina in the solvent and the presence of undesired oxide ions**. We decided to use boron nitride as the salt bridge material, since it was observed in earlier work³ that boron nitride is penetrated by molten fluorides. During the course of this work, a paper by WINAND AND CHAUDRON¹⁴ appeared, also describing the use of boron nitride as the container material for the reference electrode compartment, but employing a sodium borate plug for ionic contact. This design adds to the complexity of the electrode and is not necessary in view of our results. In addition, the use of oxide-containing materials is to be avoided as much as possible. This is usually not completely feasible, since most commercial grades of BN have a small amount of some oxygen-containing material, presumably used as a binder.

* Presented partially at the Symposium on Electrochemical Processes, 153d Meeting of the American Chemical Society, April 1967, Miami Beach, Fl.

† Research sponsored by the U.S. Atomic Energy Commission under contract with the Union Carbide Corporation, and Contract AT-(40-1)-3518.

** A similar arrangement was used by SENDEROFF *et al.*¹⁵ as a reference electrode for chronopotentiometric measurements in molten LiF–NaF–KF eutectic.

EXPERIMENTAL

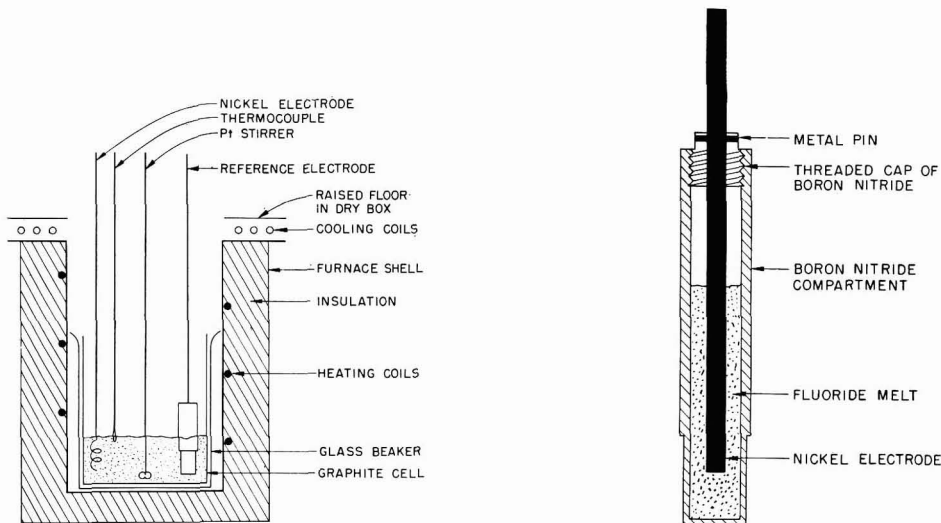
Materials

Two fluoride salt mixtures were used in this investigation: (i) LiF-NaF-KF (42.0-11.5-46.5 mole%) and (ii) LiF-BeF₂-ZrF₄ (65.6-29.4-5.0 mole%). These salts and the anhydrous nickel fluoride were obtained from the Reactor Chemistry Division of the Oak Ridge National Laboratory¹⁵. Boron nitride (Grade A or HP, Carborundum Co.) was used for construction of electrode sheaths. The Ni(II) concentration in the melt was determined spectrophotometrically on a salt sample taken after each e.m.f. measurement.

Apparatus

A dry box-furnace combination, which provides an inert atmosphere while allowing some freedom in the manipulation of electrodes and addition of reagents to the melt, was used. A pot type furnace, approximately 5 kW heating capacity, is connected to the bottom of the dry box. The bottom of the dry box is covered with water-cooled coils; the cooling coils are covered with a raised floor. The helium cover gas in the box was continuously circulated through a moisture trap (3 in. diam. and 10 in. high) containing 13X molecular sieve. A moisture content (measured with a Beckman Hygromite, Model-97) of less than 20 p.p.m. was obtained before the salt was melted. All e.m.f. measurements were made with a Moseley Autograph X-Y recorder, Model 2D-2A (input impedance 1 MΩ). The temperature was measured with a platinum-platinum/10% rhodium thermocouple and controlled to within $\pm 2^\circ$.

The cell assembly, Fig. 1, consisted of a graphite cup (3½ in. i.d. and 5 in. high) contained in a one-liter borosilicate beaker to insulate it from the furnace. The half-



Furnace and Cell Assembly.

Nickel Electrode in Boron Nitride.

Fig. 1. The cell assembly and Ni/Ni(II) reference electrode for e.m.f. measurements in molten fluorides.

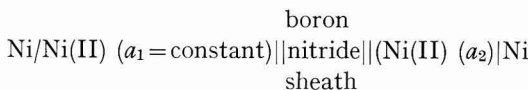
cell opposite the reference electrode consisted of a high purity nickel wire immersed in ~ 400 g of salt. The Ni(II) concentration in the bulk of the melt was varied through additions of anhydrous nickel fluoride.

RESULTS AND DISCUSSION

The reference electrode design used in this study is also shown in Fig. 1. It consists of the Ni/Ni(II) couple in a fluoride melt, contained in a boron nitride sheath. The boron nitride sheath, which is $\frac{1}{2}$ in. o.d. and ~ 3 in. long, is $1/32$ in. thick in the lower portion, and $3/32$ in. thick in the upper portion. Although boron nitride has a resistivity of about $2.3 \cdot 10^{10} \Omega\text{-cm}$ at 500°C , its electrical conductivity decreases as it becomes impregnated with the molten salt, thus providing good electrical contact between the two half-cells while limiting diffusion between them.

In a few cases, however, diffusion of the solute species into the reference electrode compartment was observed to occur upon long exposure (> 2 weeks) of the boron nitride sheath to the fluoride melts. The extent of diffusion appears to be related to the free oxide content of the fluoride melts as well as the previous history of the boron nitride, *i.e.*, grade of BN utilized and amount of exposure to atmospheric moisture during machining, etc. Provided wetting could be achieved in a reasonable period of time, a thicker BN membrane may be advantageous.

Using the described reference electrode, the applicability of the Nernst equation to the Ni/Ni(II) couple in the two salt mixtures was investigated using the following concentration cell:



The Ni(II) concentration in the boron nitride sheath was constant. The e.m.f. of the cell is represented by

$$E_{\text{cell}} = (RT/nF) \ln \alpha_2/\alpha_1 + E_{\text{junction}} \quad (1)$$

where E_{junction} is the junction potential between the two half-cells. Assuming the junction potential at any temperature and the activity coefficient over the concentration range studied (approximately 10^{-4} – 10^{-3} mole fraction) to be constant, the cell e.m.f. is represented by

$$E_{\text{cell}} = (RT/nF) \ln X_2 + \text{constant} \quad (2)$$

where X_2 is the mole fraction of Ni(II) in the bulk of the melt.

Thus, a plot of E_{cell} vs. $\ln X_2$ should yield a straight line of slope RT/nF . In Fig. 2 are shown representative plots of the data recorded in molten LiF–BeF₂–ZrF₄ and LiF–NaF–KF. Good agreement with the theoretical slope is observed for the nickel couple in both solvents.

The junction potential of the cell using the LiF–BeF₂–ZrF₄ salt mixture was found to be quite dependent on temperature (or resistance since the resistance between the half-cells varied greatly with temperature, decreasing as temperature increased). For example, at 499° the measured resistance with a conductance bridge was found

to be 19,600 Ω ; at 551° the value was 266 Ω . A value of the junction potential measured at 500° with the resistance of the reference electrode greater than 20,000 Ω was 25 mV. Owing to this variation of junction potential with temperature, the cell e.m.f. did not show the dependence of e.m.f. on temperature as predicted by the Nernst equation. No such measurements have yet been made in LiF-NaF-KF.

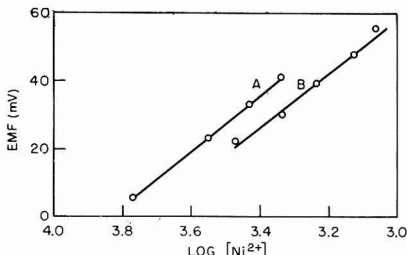


Fig. 2. Nernstian log plots for the Ni/Ni(II) couple in molten fluorides. (A), LiF-NaF-KF (517°) slope 0.080, theory 0.078; (B), LiF-BeF₂-ZrF₄ (507°) slope 0.081, theory 0.077.

The wetting of the boron nitride by the two melts was found to be quite different. The LiF-NaF-KF melt wets the reference electrode fairly rapidly; the resistance is lowered to less than 1,000 Ω in approximately 24–48 h at 500°; in LiF-BeF₂-ZrF₄, 10–14 days are required to lower the resistance to 10,000 Ω at 550°. The difference in wetting ability of the two solvents apparently depends on the free oxide concentration of the melts. This is supported by the fact that the melt, LiF-BeF₂ (66.0–34.0 mole%), wets the boron nitride at about the same rate as the LiF-NaF-KF. The LiF-BeF₂ differs from the LiF-BeF₂-ZrF₄ melt by the 5.0 mole% ZrF₄ which is added to precipitate free oxide as insoluble ZrO₂.

The e.m.f. of the concentration cells at constant composition was observed to be reasonably stable. In the LiF-BeF₂-ZrF₄ melt at 492°, the e.m.f. was constant to within ± 6 mV over a 12-day period; in the LiF-NaF-KF melt at 505°, the e.m.f. was constant to within ± 3 mV over an 11-day period. Another reference electrode was in continuous use for over 4½ months in the LiF-BeF₂-ZrF₄ solvent, containing U(IV).

The choice of the Ni/Ni(II) couple as a reference electrode for fluoride melts appears to be a good one. The couple shows Nernstian reversibility, and fairly large exchange currents¹⁷. Ni(II) is the most noble of common impurities in most fluoride salts. The standard potential of the Ni/Ni(II) couple is essentially in the middle of the potential scale in molten fluorides.

SUMMARY

E.m.f. measurements on the concentration cells Ni/Ni(II) ($a_1 = \text{constant}$) || BN sheath || Ni(II) (a_2) | Ni in molten LiF-NaF-KF (42.0–11.5–46.5 mole%) and LiF-BeF₂-ZrF₄ (65.6–29.4–5.0 mole%) at $\sim 500^\circ$ result in linear plots of e.m.f. vs. $\log X_2$ (the mole fraction of Ni(II) in the bulk of the melt), and the slopes predicted from the Nernst equation. The measured e.m.f. values are stable. The Ni/Ni(II) couple, contained in a boron nitride sheath, is a useful reference electrode for fluoride melts.

REFERENCES

- 1 D. L. MANNING, *J. Electroanal. Chem.*, 6 (1963) 227.
- 2 D. L. MANNING AND G. MAMANTOV, *J. Electroanal. Chem.*, 6 (1963) 328.
- 3 D. L. MANNING AND G. MAMANTOV, *J. Electroanal. Chem.*, 7 (1964) 102.
- 4 D. L. MANNING, *J. Electroanal. Chem.*, 7 (1964) 302.
- 5 D. L. MANNING, J. M. DALE AND G. MAMANTOV, *Polarography 1964*, Vol. 2, edited by G. J. HILLS, Macmillan, London, 1966, p. 1143.
- 6 G. MAMANTOV AND D. L. MANNING, *Anal. Chem.*, 38 (1966) 1494.
- 7 D. L. MANNING AND G. MAMANTOV, *J. Electroanal. Chem.*, 18 (1968) 137.
- 8 G. MAMANTOV AND D. L. MANNING, *J. Electroanal. Chem.*, 18 (1968) 309.
- 9 H. CORIOU, J. DIRIAN AND J. HURE, *J. Chim. Phys.*, 52 (1955) 479.
- 10 A. F. ALABYSHEV, M. F. LANTRATOV AND A. G. MORACHEVSKII, *Reference Electrodes for Fused Salts*, Sigma Press, Washington, D.C., 1965, pp. 164-167.
- 11 G. DIRIAN, K. A. ROMBERGER AND C. F. BAES, JR., U.S. At. Energy Comm. Rept., ORNL-3789, 76 (1965).
- 12 S. PIZZINTI AND R. MORLOTTI, *Electrochim. Acta*, 10 (1965) 1033.
- 13 K. GRJOTHEIM, *Z. Physik. Chem. N.F.*, 11 (1957) 150.
- 14 R. WINAND AND G. CHAUDRON, *Compt. Rend.*, 264C (1967) 649.
- 15 W. R. GRIMES, *Chemical Aspects of Molten-Fluoride-Salt Reactor Fuels in Fluid Fuel Reactors*, edited by J. A. LANE, H. G. MACPHERSON AND FRANK MOSLAN, Addison-Wesley, Reading, Mass., 1958, p. 584.
- 16 K. M. TAYLOR, *Ind. Eng. Chem.*, 47 (1955) 2506.
- 17 G. MAMANTOV, H. W. JENKINS AND D. L. MANNING, *Preprints*, Division of Fuel Chemistry, Am. Chem. Soc., 11(1) (1967) 147.
- 18 S. SENDEROFF, G. W. MELLORS AND W. J. REINHART, *J. Electrochem. Soc.*, 112 (1965) 840.

J. Electroanal. Chem., 19 (1968) 385-389

ZUR REDUKTION DER HYPOCHLORSÄURE UND IHRES ANIONS AN PLATIN-ELEKTRODEN

O. SCHWARZER UND R. LANDSBERG*

Institut für physikalische Chemie, TH für Chemie "Carl Schorlemmer", Merseburg (DDR)

(Eingegangen am 15 Mai 1968)

I. EINLEITUNG

Elektrodenkinetische Untersuchungen über das Redoxverhalten des Hypochlorits an Platin-Elektroden wurden in neuerer Zeit von FLIS UND WOROBJEW¹ mit dem Ziel durchgeführt, aus den anodischen und kathodischen Durchtrittsreaktionen zur pH-Abhängigkeit des Potentials der stromlosen Elektrode, die in der Bleichmittelindustrie interessiert, zu gelangen. Auf Grund stationärer Strom-Spannungs-Kurven schlossen sie, dass sich an Platin in diesem System ein Mischpotential ausbildet. Es soll sich auf folgende Prozesse zurückführen lassen: Die kathodische Hypochlorsäurereduktion und anodischerseits entweder deren Oxydation bei niederen pH-Werten oder die anodische Sauerstoffbildung bei höheren pH-Werten. Obwohl die sich an Platin einstellenden Potentiale keine Gleichgewichtspotentiale darstellen, eignen sie sich zur pH-Indikation an diesem System, wie NIKOLSKII UND FLIS² fanden.

JAKOWLEWA *u.a.*³ zeigten an Hand eines Polarogramms, dass Hypochlorit, Chlorit und Chlorid nebeneinander anodisch an rotierenden Platindrähtelektroden nachgewiesen werden könnten. Die Chloritstufe ist der Oxydation $\text{ClO}_2^- \rightleftharpoons \text{ClO}_2 + e$ zuzuschreiben⁴.

LANDOLT UND IBL haben die Kinetik der Chloratbildung bei der NaCl-Elektrolyse untersucht und dabei das anodische Verhalten des Hypochlorits eingehend charakterisiert⁵.

Die Hypochlorit reduktion wurde meist unter Bedingungen wie sie in der Chloratzelle herrschen, in der die Reaktion störend auftritt, untersucht^{6,7}.

In der Arbeit von FLIS UND BINAJEWA⁸ wird versucht, aus der pH-Abhängigkeit der Geschwindigkeit der Chloratbildung zu schliessen, welcher der beiden Stoffe das Oxydationsmittel ist. Sie finden, dass beide beteiligt sein können.

Die elektrochemische Reduktion des Hypochlorits am Quecksilbertropfen untersuchte JENKINS⁹, wobei er sich hauptsächlich mit der Wirkung des sich in chemischer Reaktion bildenden Kalomels bzw. Quecksilberoxids befasste.

Unsere Arbeit hatte das Ziel, die Kinetik der kathodischen Reduktion des Hypochlorits bzw. der Hypochlorsäure in Abhängigkeit vom pH-Wert an glatten Platin-Elektroden unter besonderer Berücksichtigung des Oberflächenzustandes zu untersuchen.

* Gegenwärtige Anschrift: Physikalisch-Chemisches Institut der Humboldt-Universität, 108 Berlin (DDR).

2. EXPERIMENTELLES

Das Versuchsprogramm umfasste sowohl stationäre Messungen, die ausschliesslich mit einer rotierenden Scheibenelektrode ausgeführt wurden, als auch nicht-stationäre Messungen mit konstanter Stromdichte.

Die Fläche der Scheibenelektrode wurde mit 0.26 cm^2 vorteilhaft gross gewählt. Zur Herstellung einer entsprechenden Graphitelektrode vgl. die Literatur⁴.

Zur punktweisen Aufnahme von Strom-Spannungs-Kurven wurde eine einfache Schaltung mit Polarisationsstrom- und Kompensations-kreis verwendet. Für eine kontinuierliche Aufnahme der kathodischen Strom-Spannungs-Kurven stand ein einfacher, nach einem Vorschlag von WILL¹⁰ bereits früher¹¹ aufgebauter Potentiostat zur Verfügung. Eine kontinuierliche Aufnahme der Strom-Spannungs-Kurven war für die Reproduzierbarkeit der Messungen gegebenenfalls günstiger.

Die Potentiale wurden gewöhnlich gegen die gesättigte Kalomelektrode gemessen, die über eine Haber-Lugginkapillare möglichst nahe an das Zentrum der rotierenden Scheibenelektrode herangeführt wurde.

Die chronopotentiometrischen Messungen wurden in der bekannten Schaltung mit oszillographischer Anzeige des Potential-Zeitverlaufs ausgeführt.

Die für die Messungen verwendeten Hypochloritlösungen wurden aus Chlor und Natronlauge nach einer Vorschrift von SAN JOURCHE UND GARDENT¹² hergestellt. Die bei der Synthese gewonnenen $\text{NaClO} \cdot 5\text{H}_2\text{O}$ -Kristalle wurden in verdünnter Natronlauge gelöst und als etwa 1 M Stammlösung bei Temperaturen um 0° aufbewahrt. Die Versuchslösungen wurden aus der Stammlösung durch Verdünnung mit dem Grundelektrolyten, der auch das Puffersystem enthielt, in den gewünschten Konzentrationen gewonnen. Als Grundelektrolyt diente fast ausnahmslos 0.5 M Natriumsulfatlösung unter Zusatz von Phosphaten als Pufferstoffen (Puffersystem nach Sörensen). Wenn nicht anders angegeben, war die Pufferkonzentration der Lösungen $6.6 \cdot 10^{-2} \text{ M}$. Die Versuchstemperatur betrug 20° .

3. ERGEBNISSE

3.1 Stationäre Messungen

An der rotierenden Platscheibenelektrode tritt in genügend alkalischen Lösungen die diffusionsbedingte Reduktionsstufe des Hypochlorits, in genügend sauren Lösungen die diffusionsbedingte Stufe der Reduktion der Hypochlorsäure, im pH-Bereich zwischen 5.3 und 9.3 treten in Gegenwart eines geeigneten Puffersystems beide Reduktionsstufen nebeneinander auf. Die Grenzstromdichte der Hypochloritreduktion ist der Wurzel aus der Umdrehungszahl der Scheibenelektrode stets proportional, die der Säurereduktion nur, wenn die Pufferkonzentration nicht zu hoch gewählt wird (bei Phosphatpuffer kleiner 0.1 M).

Abbildung 1 zeigt beide Stufen in gepufferter Lösung bei drei pH-Werten und drei Rührgeschwindigkeiten. Bei $\text{pH}=5.3$ ist in der Säurereduktionsstufe ein Wendepunkt angedeutet, der der Reduktion von Oberflächenverbindungen zuzuschreiben ist, wodurch eine geringfügige Oberflächenblockierung aufgehoben wird (vgl. auch Abb. 8 und 9 und deren Diskussion). In gepufferter Lösung entsprechen die Verhältnisse aus den einzelnen Grenzströmen und dem Gesamtgrenzstrom den aus der Dissoziationskonstante (nach FLIS¹³ $K_D=4.35 \cdot 10^{-8} \text{ M}$ bei 20°) berechneten Kon-

zentrationsverhältnissen aus Säure- bzw. Säureanionkonzentration und der Gesamtkonzentration (Abb. 2). Das zeigt, dass die Diffusionskoeffizienten von Säure und Anion näherungsweise gleich sind.

In ungepufferten Lösungen ist die Stufe der Säurereduktion im Vergleich zu gepufferten Lösungen bei gleichem pH-Wert kleiner. Daraus folgt, dass bei der Säurereduktion Wasserstoffionen verbraucht werden. Vergrößert man das Angebot an Wasserstoffionen durch Erhöhung der Pufferkonzentration z.B. auf das 40-fache, so trägt auch die Rekombination der Anionen mit den Wasserstoffionen zum Stromfluss bei, und die Säurestufe ist erhöht: Abb. 3. Die Strom-Spannungs-Kurve bei

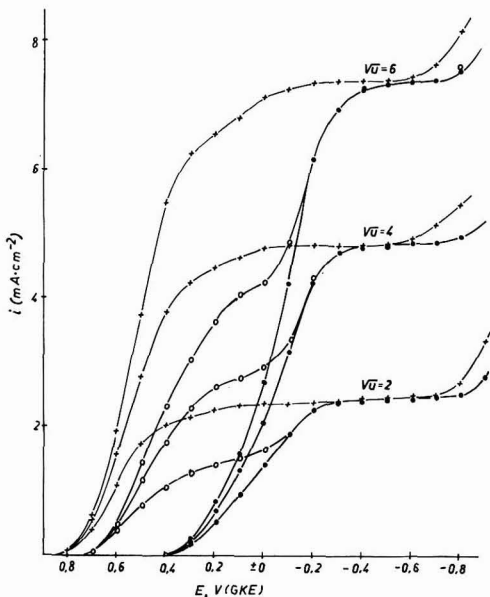


Abb. 1. Stationäre Strom-Spannungs-Kurve der Hypochlorit- bzw. Hypochlorsäurereduktion bei den pH-Werten 5.3 (+), 7.5 (○) und 10.0 (●) und Umdrehungsgeschwindigkeiten der Platin-scheibenelektrode, 4, 16 und 36 U/sec; Grundeletrolyt 0.5 M Natriumsulfat, $6.6 \cdot 10^{-2}$ M Phosphat als Puffer; Hypochlorit- bzw. Hypochlorsäurekonzentration, ca. $5 \cdot 10^{-3}$ M.

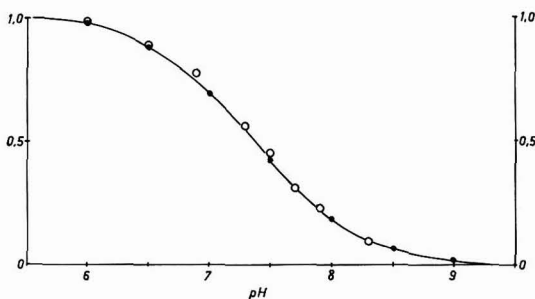


Abb. 2. Abhängigkeit des Konzentrationsverhältnisses (●) $c_{\text{HClO}}/c_{\text{gesamt}}$ (mit $K_D = 4.35 \cdot 10^{-8}$ M berechnet) und des Grenzstromverhältnisses (○) $i_{\text{gr}, \text{HClO}}/i_{\text{gr}, \text{gesamt}}$ (gemessen bei Phosphatpufferkonzentration $6.6 \cdot 10^{-2}$ M) vom pH-Wert. Gesamtkonzentration der Depolarisatoren, ca. $5 \cdot 10^3$ M.

36 U/sec zeigt den die Hypochlorsäurereduktion fördernden Einfluss von sauerstoffhaltigen Oberflächenschichten: Bei Aufnahme der Strom-Spannungs-Kurve in anodischer Richtung tritt ein Minimum auf, da die Oberflächenschicht zunächst noch nicht vorhanden ist (Abb. 3). Diese Erscheinung ist von MÜLLER¹⁴ ausführlich untersucht und diskutiert worden, so dass wir auf die Beschreibung weiterer Beobachtungen hierzu, die mit seiner Deutung im Einklang stehen, verzichten können.

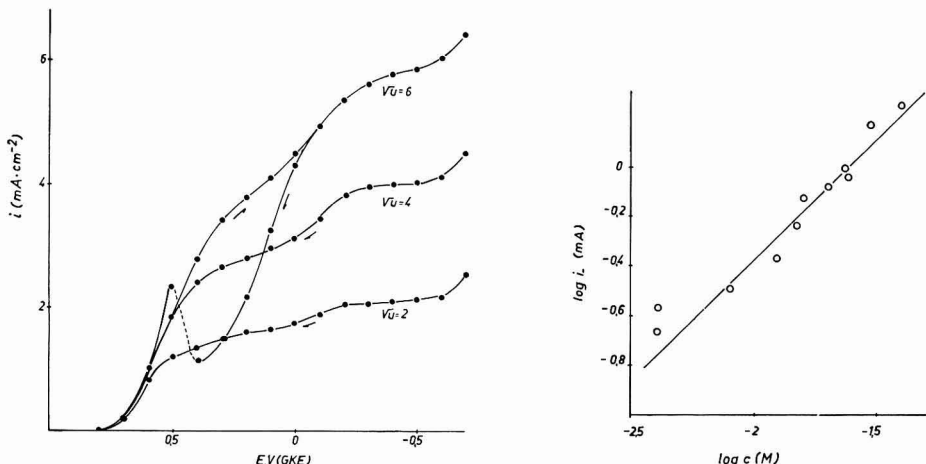


Abb. 3. Stationäre Strom-Spannungs-Kurve der HClO_- und ClO_- -Reduktion an Platin; Gesamt-konzentration der Depolarisatoren, ca. $5 \cdot 10^{-3} M$; Phosphatpufferkonzentration (gleichzeitig Grundelektrolyt) $0.25 M$; pH = 7.5; (Pfeile bezeichnen die Änderungsrichtung des Potentials).

Abb. 4. Abhängigkeit der Durchtrittsstrome von der HClO -Konzentration (logarithmisch) bei konstantem Potential: 300 mV negativer als das streuende Ruhépotential, das aber von Säurekonzentration nicht abhängt (vgl. Abb. 10). pH = 5.9, Phosphatpufferkonzentration $6.6 \cdot 10^{-2} M$; Grundelektrolyt $0.5 M$ Natriumsulfat.

Es wurde der Versuch gemacht, die elektrochemischen Reaktionsordnungen bei der Reduktion der Säure und des Anions mit der für die Scheibenelektrode üblichen Methode zu bestimmen (FRUMKIN UND TEDORADSE¹⁵). Es wurde die Rührabhängigkeit der Stromdichte, i , bei konstantem Potential gemessen und die reziproke Stromdichte gegen die reziproke Wurzel aus der Umdrehungszahl ($U^{-\frac{1}{2}}$) aufgetragen. Die Konzentrationsabhängigkeit der auf unendliche Rührgeschwindigkeit extrapolierte Durchtrittsstromdichte ergab die Reaktionsordnung eins, sowohl bezüglich der Reduktion der Säure als auch des Anions. Besonders bei der Reduktion des Anions machte sich der veränderliche Oberflächenzustand stark bemerkbar und führte zu beträchtlichen Streuungen der Messwerte. Abbildung 4 zeigt die Konzentrations-abhängigkeit der Durchtrittsstromdichte der Hypochlorsäurereduktion. Der Wert des Durchtrittsfaktors betrug 0.35 ± 0.03 . Der veränderliche, besonders vom pH-Wert abhängige Oberflächenzustand gestattet keine genaue Angabe bezüglich der Reaktionsordnung für die Wasserstoffionen, die nach unseren Ergebnissen zwischen 0.2 und 0.5 liegen müsste. Am Gold ist das Halbstufenpotential der Hypochlorsäurereduktion um 0.25 V, an Graphitelektroden um 0.75 V negativer. Wir fanden am Platin, dass sich das Halbstufenpotential der Hypochlorsäurereduktion um etwa

35 mV/pH und das der Reduktion des Anions um etwa 60 mV/pH mit fallendem pH-Wert zu positiveren Potentialen verschiebt.

3.2 Galvanostatische Messungen

Den Potentialverlauf bei konstanter Stromdichte und pH = 7.0 zeigt Abb. 5. Es treten drei Stufen auf, wobei, wie noch gezeigt werden wird, die erste der Reduk-

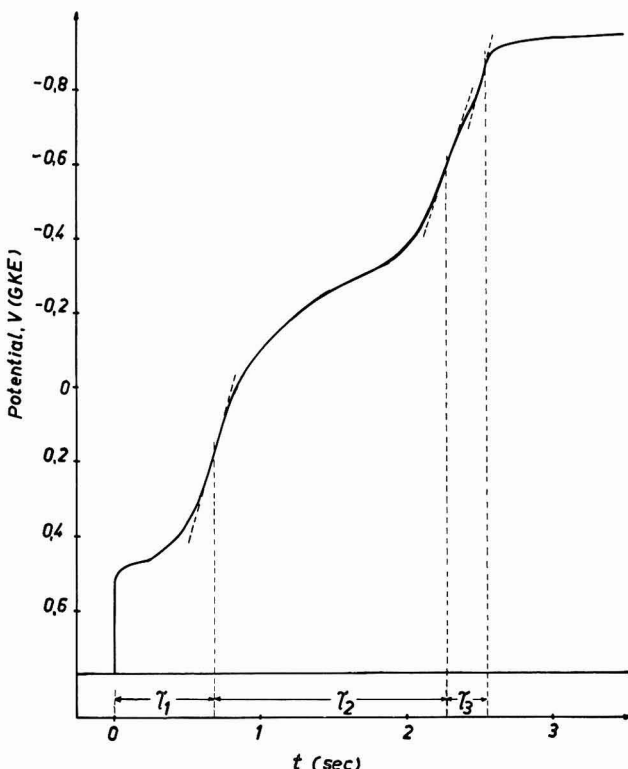


Abb. 5. Potential Zeitkurve der Reduktion des Hypochlorits und der Hypochlorsäure an Platin; Gesamtkonzentration der Depolarisatoren $2 \cdot 10^{-2} M$; pH = 7.0, Phosphatpufferkonzentration $6.6 \cdot 10^{-2} M$; $i = 9.25 \text{ mA cm}^{-2}$; Grundeletrolyt $0.5 M$ Natriumsulfat.

tion der Säure, die zweite vor allem der des Anions und die dritte der von Oberflächenoxydationsprodukten entspricht. Für die erste Reduktionsstufe gilt die Beziehung von SAND¹⁶ mit

$$i\tau_1^{\frac{1}{2}} = \frac{1}{2}n_1 F(\pi D_1)^{\frac{1}{2}} C_1 x=0 \quad (1)$$

für die zweite, bei der neben dem Anion die Säure immer noch in dem Masse reduziert wird, wie sie durch Diffusion nachgeliefert wird, gilt¹⁷

$$i\{(\tau_1 + \tau_2)^{\frac{1}{2}} - \tau_1^{\frac{1}{2}}\} = \frac{1}{2}n_2 F(\pi D_2)^{\frac{1}{2}} C_2 x=0 \quad (2)$$

Es bedeuten

τ_i = Transitionszeiten

n_1, n_2 = die Zahl der beim ersten bzw. zweiten Vorgang ausgetauschten Elektronen

D_i = Diffusionskoeffizienten der beiden Depolarisatoren

C_i = Konzentrationen der beiden Depolarisatoren

i = Stromdichte

Abbildung 6 zeigt in welchem Grade die beiden genannten Beziehungen erfüllt sind. Der Anstieg der Geraden für die zweite Stufe ist auf die Mitreduktion von Oberflächenverbindungen zurückzuführen, die durch Einwirkung des Hypochlorsäuresystems auf die Platinoberfläche entstehen.

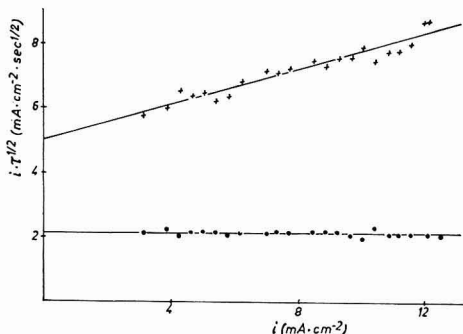


Abb. 6. $i\tau^{\frac{1}{2}}-i$ -Beziehungen für die Hypochlorsäure- ($i\tau_1^{\frac{1}{2}}$, ●) und die Hypochlorit-Oxidschicht-reduktion ($i[(\tau_1 + \tau_2)^{\frac{1}{2}} - \tau_1^{\frac{1}{2}}]$, +) an Platin; pH = 7.9, Phosphatpufferkonzentration $6.6 \cdot 10^{-2} M$; Gesamtkonzentration der Depolarisatoren $1 \cdot 10^{-2} M$; Grundelektrolyt $0.5 M$ Natriumsulfat.

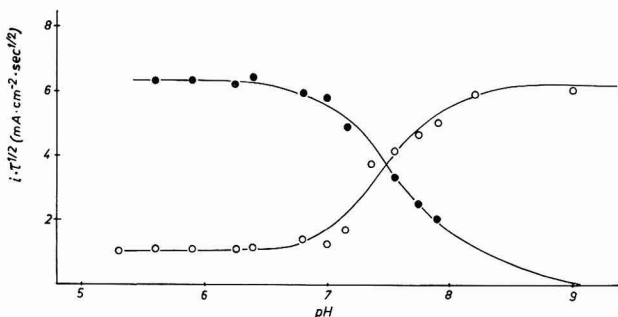


Abb. 7. $i\tau_1^{\frac{1}{2}}$ und $(i\tau_2^{\frac{1}{2}})_{i=0}$ (●) bzw. $\{i[(\tau_1 + \tau_2)^{\frac{1}{2}} - \tau_1^{\frac{1}{2}}]\}_{i=0}$ (○) in Abhängigkeit vom pH-Wert; Gesamtkonzentration der Depolarisatoren $1 \cdot 10^{-2} M$; Phosphatpufferkonzentration $6.6 \cdot 10^{-2} M$; Grundelektrolyt $0.5 M$ Natriumsulfat.

Diese Deutung wird schon durch Abb. 7 gestützt, in der die pH-Abhängigkeit der beiden Transitionszeiten dargestellt ist. Es wurden die auf die Stromdichte Null extrapolierten Ordinatenabschnitte aufgetragen. Im Einklang mit der gegebenen Deutung entspricht die pH-Abhängigkeit der Transitionszeiten den in Abb. 2 dargestellten Gleichgewichtskonzentrationen der Säure und des Anions mit einer auch in saurer sauerstofffreier Lösung verbleibenden zweiten Reduktionsstufe, die den Oberflächenverbindungen zuzuschreiben ist.

Die Abhängigkeit der Transitionszeiten (auf Stromlosigkeit extrapoliert) von der Konzentration des jeweiligen Depolarisators bei den pH-Werten 10 ($\tau_1=0$) und 5.3 ist in den Abb. 8 und 9 dargestellt und entspricht gleichfalls der gegebenen Deutung.

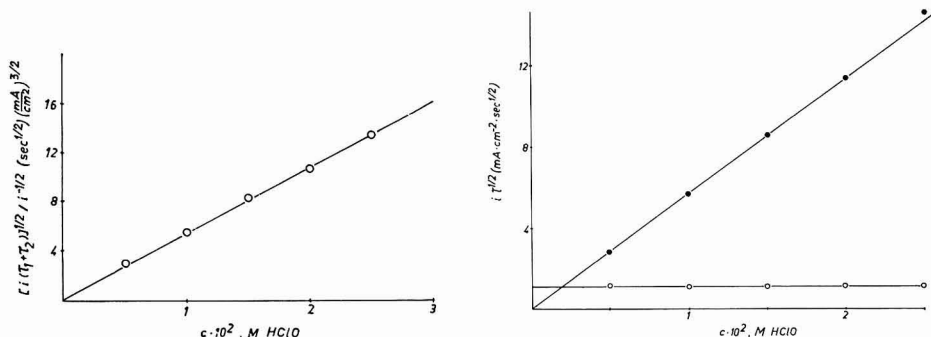


Abb. 8. $(i\tau_2^{1/2})_{i=0}$ in Abhängigkeit von der Hypochloritkonzentration; pH = 10.0, Phosphatpufferkonzentration $6.6 \cdot 10^{-2}$ M; Grundelektrolyt 0.5 M Natriumsulfat.

Abb. 9. $i\tau_1^{1/2}$ (●) und $i[(\tau_1 + \tau_2)^{1/2} - \tau_1^{1/2}]_{i=0}$ (○) in Abhängigkeit von der Hypochlorsäurekonzentration; pH = 5.3, Phosphatpufferkonzentration $6.6 \cdot 10^{-2}$ M; Grundelektrolyt 0.5 M Natriumsulfat.

3.3 Ruhepotentiale

Unsere Beobachtungen zum Ruhepotential an Platin in diesem System mit 1 N NaNO₃ als Leitelektrolyt bestätigten in vielen Punkten die Ergebnisse von FLIS und Mitarbeitern^{1,2}.

Platin eignet sich in diesen Lösungen mehr oder weniger zur pH-Indikation bzw. zur potentiometrischen Titration, obwohl sich vom Oberflächenzustand abhängige Mischpotentiale ausbilden (vgl. Abb. 10). Ihre absoluten Werte stimmten mit den in Lit. 1, nicht jedoch mit den in Lit. 2 angegebenen überein. Sie änderten sich langsam, im alkalischen Gebiet konnten keine wirklich stationären Potentiale erhalten werden. Der Knick im Potential-pH-Diagramm lag bei etwas niedrigeren pH-Werten

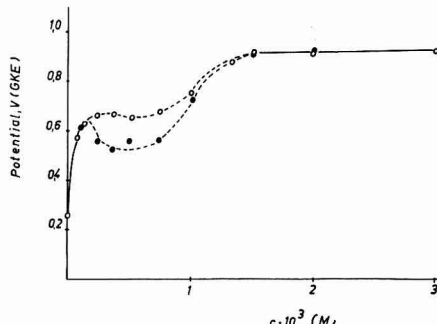


Abb. 10. Abhängigkeit des Oxydationspotentials der Hypochlorsäure an Platin von ihrer Konzentration; pH = 6, Phosphatpuffer. (○) Potential gleich gem.; (●) Potential nach 4–5 Minuten nach Erhöhung der Hypochlorsäurekonzentration gemessen.

als in der Arbeit von FLIS² angegeben ist. Die Neigung betrug 70 mV/pH im Gebiet, in dem die Hypochlorsäure überwiegt, und 120 mV/pH im Bereich, in dem das Anion vorherrscht. Chlorid hatte kaum einen Einfluss auf das Potential. Hypochlorsäurezugabe erhöhte das Potential zunächst sehr ausgeprägt, bei höheren Konzentrationen dann schwächer als dem Gleichgewicht $\text{Cl}^- + \text{H}_2\text{O} \rightleftharpoons \text{HClO} + \text{H}^+ + e^-$ entspricht, vgl. Abb. 10. Im alkalischen Bereich hatte das Anion einen stärkeren Einfluss auf das Potential als die Säure im sauren Gebiet. Besonders bei kleinen Hypochlorsäurekonzentrationen beobachtet man einen zeitlichen Potentialabfall (Abb. 10). Die von FLIS und Mitarbeitern¹ gegebene Deutung des Mischpotentials ist zu einfach: Eine wesentliche Rolle spielt der Oberflächenzustand der Elektrode.

Graphit und Goldelektroden eignen sich in diesem System nicht zur pH-Indikation.

4. DISKUSSION DER ERGEBNISSE

4.1 Stationäre Messungen

Unter den hier beschriebenen Bedingungen wurde weder bei stationären noch bei galvanostatischen Messungen eine Überhöhung der diffusionsbedingten Säure-reduktionsstufe beobachtet, obwohl denkbar ist, dass ein Anteil auf die Rekombination des Anions mit Protonen aus dem Puffersystem oder dem Lösungsmittel zurückgeführt werden könnte.

Nach NÜRNBERG *u.a.*¹⁹ beträgt die Dissoziationsgeschwindigkeitskonstante von H_2PO_4^- , $6 \cdot 10^4 \text{ sec}^{-1}$, während die von HPO_4^{2-} vernachlässigbar ist. Mit zunehmendem pH-Wert nimmt nun sowohl die HClO -Konzentration wie die H_2PO_4^- -Konzentration in dem Gleichgewichtssystem der Lösung ab, so dass bei konstanter Pufferkonzentration die Rekombination nicht begünstigt wird.

Nach ALBERY²⁰ könnte eine Nachlieferung von Protonen aus dem Lösungsmittel nur dann eine Rolle spielen, wenn der pK -Wert der Puffersäure grösser als 9 bzw. wenn ihre Konzentration kleiner als 10^{-4} M ist. Der pK -Wert für den Phosphatpuffer beträgt 6.92, und die Pufferkonzentration war stets grösser als 10^{-2} M .

Diese Überlegungen machen verständlich, dass keine Überhöhung der Säure-reduktionsstufe beobachtet werden konnte.

Abbildung 3 zeigt ein Beispiel für die Erhöhung der Säurereduktionsstufe, wenn die Pufferkonzentration wesentlich gesteigert wird. Eine Steigerung der Pufferkonzentration über 0.25 M bringt keine weitere Erhöhung, d.h. nicht die Dissoziation der Puffersäure, sondern die Rekombination ist geschwindigkeitsbestimmend. Die Messwerte sind nicht sehr genau und gestatten nur die Rekombinationsgeschwindigkeitskonstante auf 10^9 – $10^{10} \text{ l/Mole sec}$ zu schätzen. Unter galvanostatischen Bedingungen macht der auch bei der Hypochlorsäurereduktion bemerkbare Abbau von Oberflächenschichten die Messung der Rekombinationsgeschwindigkeit unmöglich: Die Oxidschichten führen zu ansteigenden Geraden in der $i\tau^i$ gegen i Auftragung — ein geringer Anstieg ist tatsächlich meist zu beobachten — die vorgelagerte Rekombinationsreaktion müsste zu einem linearen Abfall führen.

Für den kathodischen Durchtrittsfaktor wurde unter stationären Bedingungen gemessen

(1) für das Anion bei verschiedenen Konzentrationen und pH-Werten: 0.32 ± 0.03 ;

(2) für die Säurereduktion: 0.35 ± 0.03 .

Aus galvanostatischen Messungen wurden die Durchtrittsfaktoren nach einer methode von DELAHAY UND BERZINS²¹ bestimmt, sie waren mit 0.25 niedriger als unter stationären Bedingungen. Das ist zweifellos dem unter den jeweiligen Versuchsbedingungen unterschiedlichen Oberflächenzustand zuzuschreiben. Dieser unterschiedliche Oberflächenzustand kommt auch in den aus den Messwerten berechneten Diffusionskoeffizienten zum Ausdruck. Die stationären Grenzströme ergeben (Gleichung von Lewitsch) für die Diffusionskoeffizienten von Säure und Anion innerhalb der Fehlergrenze die gleichen Werte:

$$D_{\text{HClO}} = (0.82 \pm 0.05) \cdot 10^{-5} \text{ cm}^2 \text{ sec}^{-1}$$

$$D_{\text{ClO}^-} = (0.85 \pm 0.05) \cdot 10^{-5} \text{ cm}^2 \text{ sec}^{-1}$$

Mit Hilfe der Sandschen Gleichung errechnen sich aus dem von der Stromdichte unabhängigen Produkt (galvanostatische Versuche) $i\tau_1^{\frac{1}{2}}$

$$D_{\text{HClO}} = (1.10 \pm 0.05) \cdot 10^{-5} \text{ cm}^2 \text{ sec}^{-1}$$

bzw. aus dem auf $i=0$ extrapolierten Produkt $i\tau_2^{\frac{1}{2}}$

$$D_{\text{ClO}^-} = (1.12 \pm 0.05) \cdot 10^{-5} \text{ cm}^2 \text{ sec}^{-1}$$

Die aus galvanostatischen Messungen berechneten Diffusionskoeffizienten werden etwas kleiner, wenn zur Ermittlung der Transitionszeiten nicht die Wendepunkte im Potential-Zeit-Oszillogramm, sondern die Schnittpunkte der Tangenten herangezogen werden. Die daraus errechneten Diffusionskoeffizienten für Säure und Anion liegen zwischen $0.95 \cdot 10^{-5}$ und $1.0 \cdot 10^{-5} \text{ cm}^2 \text{ sec}^{-1}$. Die Werte aus den stationären Messungen sind aber immer noch kleiner. Wir führen das auf Blockierungs- bzw. Oberflächeneffekte zurück (evtl. Vergrößerung der Transitionszeit durch Mitreduktion der Oberflächenverbindung).

4.2 Galvanostatische Messungen

Weitere Information über die entstandenen Oberflächenverbindungen ist den galvanostatischen Messungen zu entnehmen.

In saurer Lösung findet erst die Reduktion der Säure und dann bei negativerem Potential die Reduktion der Oberflächenverbindung statt. Hierbei wird Hypochlorsäure gleichzeitig mitreduziert. Sie stammt aus der in das Innere wachsenden Diffusionsschicht und bestreitet einen mit $t^{-\frac{1}{2}}$ (t -Zeit) abnehmenden Anteil am konstanten Gesamtreduktionsstrom. Für die Transitionszeit gilt eine von LORENZ²² aufgestellte Beziehung (2. Lorenzsche Näherung)

$$(i\tau)^{\frac{1}{2}} = (nFA_0)^{\frac{1}{2}} + \frac{1}{2}nF(\pi D)^{\frac{1}{2}}C i^{-\frac{1}{2}}$$

A_0 — adsorbierte Stoffmenge.

Abbildung 11 zeigt die nach dieser Beziehung ausgewerteten Messergebnisse. Die Neigung der erhaltenen Geraden ist der Säurekonzentration proportional, wie die nächste Abb. 12 zeigt. Der daraus ermittelte Diffusionskoeffizient von $1.04 \cdot 10^{-5} \text{ cm}^2 \text{ sec}^{-1}$ befindet sich in guter Übereinstimmung mit dem für die Säure aus der Sandschen Beziehung ermittelten. Der Ordinatenabschnitt ist ein Mass für die in der Oberflächenschicht gespeicherte reduzierbare Substanzmenge, die von etwa 1 mC cm^{-2} bei $0.5 \cdot 10^{-2} M \text{ HClO}$ auf ca. 1.6 mC cm^{-2} in $0.025 M \text{ HClO}$ ansteigt. Diese Werte sind von der Größenordnung, wie sie vielfach an Platin durch chemische oder

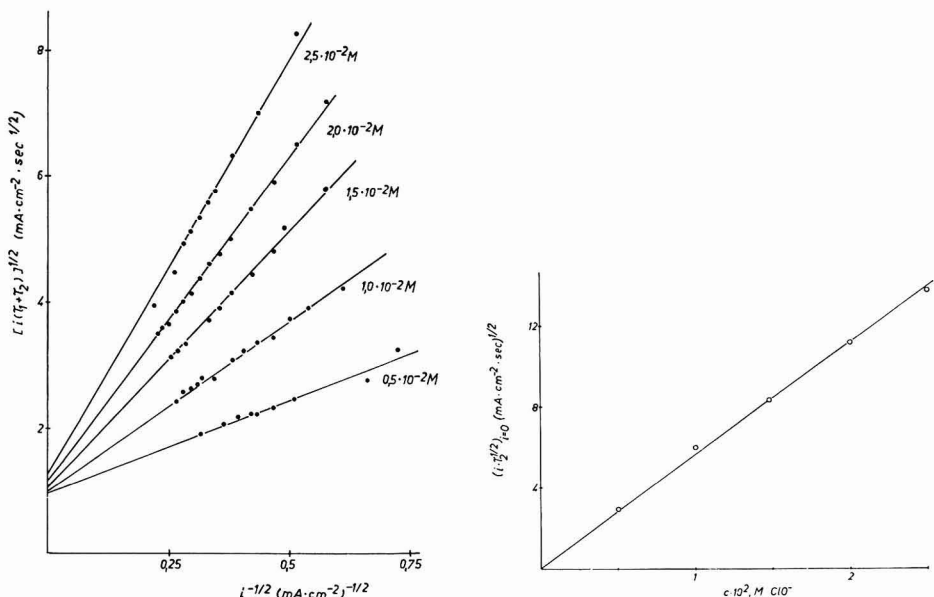


Abb. 11. 2. Näherung nach LORENZ: Ermittlung der für die Reduktion der Oberflächenschicht benötigten Strommenge in Abhängigkeit von der HClO-Konzentration an Platin; pH = 5.3, Phosphatpufferkonzentration $6.6 \cdot 10^{-2} M$; Grundelektrolyt $0.5 M$ Natriumsulfat.

Abb. 12. Konzentrationsabhängigkeit der Neigungen der Geraden auf Abb. 15.

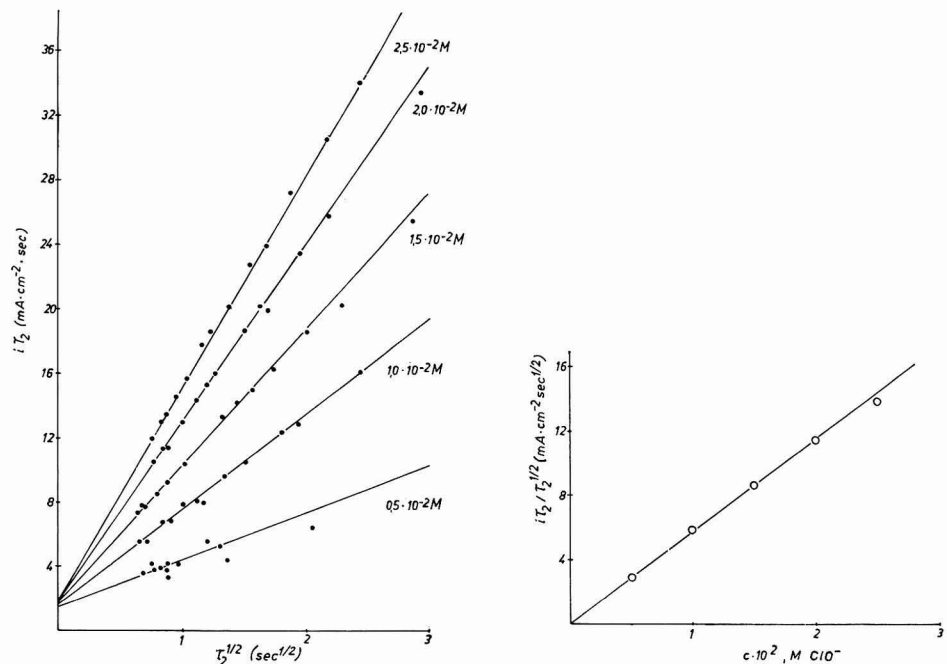


Abb. 13. 3. Näherung nach LORENZ: Ermittlung der für die Reduktion der Oberflächenschicht benötigten Strommenge in Abhängigkeit von der ClO₄⁻-Konzentration an Platin; pH = 10.0, Phosphatpufferkonzentration $6.6 \cdot 10^{-2} M$; Grundelektrolyt $0.5 M$ Natriumsulfat.

Abb. 14. Konzentrationsabhängigkeit der Neigungen der Geraden auf Abb. 13.

elektrochemische Oxydation gefunden wurden. Sie werden einer monomolekularen Chemisorptionsschicht zugeschrieben. Die pH-Abhängigkeit der Anionenreduktionsstufe (Abb. 7) zeigt, dass gleichzeitig mit dem Anion eine Oberflächenverbindung reduziert wird.

Für die gleichzeitige Entladung einer Adsorptionsschicht und einer Diffusionsschicht, die gleichbleibende Anteile des Gesamtstromes verbrauchen, gibt LORENZ²² folgende Näherungsgleichung an (3. Lorenzsche Näherung):

$$i\tau = nFA_0 + \frac{1}{2}nF(\pi D)^{\frac{1}{2}}\tau^{\frac{1}{2}}$$

Abbildung 13 zeigt die Auswertung der Versuche zur Anionenreduktion nach dieser Gleichung. Die Konzentrationsabhängigkeit der Neigung der Geraden ist in Abb. 14 dargestellt. Die Neigung in Abb. 14 ergibt für den Koeffizienten

$$D_{\text{ClO}^-} = (1.15 \pm 0.05) \cdot 10^{-5} \text{ cm}^2 \text{ sec}^{-1}$$

Der Ordinatenabschnitt in Abb. 13 ist ein Mass der für die gleichzeitige Reduktion der Oberflächenverbindung benötigten Strommenge. Sie liegt zwischen 1.5 und 1.9 mC cm⁻² im Konzentrationsbereich von 0.5 M–2.5 · 10⁻² M ClO⁻ und stimmt in etwa mit den in saurer Lösung gefundenen Werten überein.

Die dritte Reduktionsstufe im galvanostatischen Potential-Zeit-Oszillogramm ist offensichtlich keinem diffusionsbestimmten Vorgang zuzuschreiben, sondern der Reduktion einer Oberflächenverbindung nachdem die Diffusionsschicht bereits entladen ist und weiter in das Lösunginnere wächst.

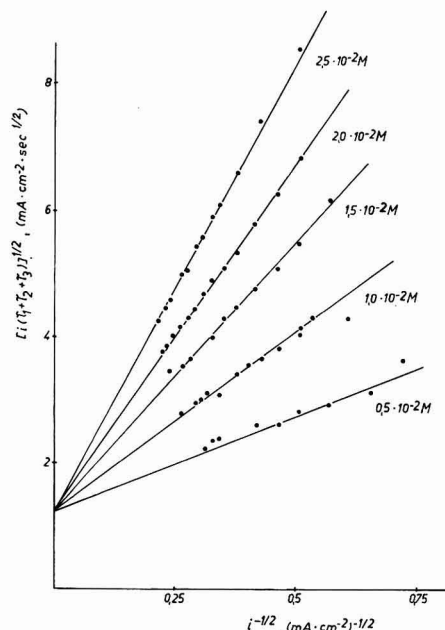


Abb. 15. Auswertung der dritten Potentialstufe nach der 2. Näherung von Lorenz: Ermittlung der für die Reduktion der Oberflächenschicht benötigten Strommenge in Abhängigkeit von der HClO-Konzentration an Platin; pH = 5.3, Phosphatpufferkonzentration 6.6 · 10⁻² M; Grundelektrolyt 0.5 M Natriumsulfat.

Die Auswertung für $\text{pH} = 5.3$ erfolgte also nach der 2. Lorenzschen Näherung²²: Abb. 15. Das Ergebnis scheint die Anwendung zu rechtfertigen; aus der Darstellung errechnet sich der Diffusionskoeffizient, $D_{\text{HClO}} = 1.13 \cdot 10^{-5} \text{ cm}^2 \text{ sec}^{-1}$ und die in der Schicht gespeicherte Strommenge zu ca. 1.5 mC cm^{-2} (konzentrationsunabhängig).

Die Schicht besteht aus zwei Anteilen, in denen das Platin evtl. eine unterschiedliche Wertigkeit besitzt. Der schwerer reduzierbare Anteil ist bei niedrigerer Depolarisatorkonzentration etwas grösser, was auch im Einklang mit dem Befund steht, dass das Ruhepotential mit zunehmender Hypochloritkonzentration steigt.

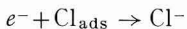
4.3 Betrachtungen zu den Reaktionsmechanismen

Der starke Potential- und zeitabhängige Oberflächenzustand bei den hier untersuchten Reduktionsreaktionen erschwert eine Diskussion der Reaktionsmechanismen.

Unsere Versuche zur HClO-Reduktion stützen die Vorstellung von MÜLLER, dass die Chemisorptionsschicht am Platin eine der Säurereduktion vorgelagerte heterogene chemische Reaktion erleichtert:



Dementsprechend könnte an der reduzierten Platinoberfläche folgender Mechanismus vorgeschlagen werden



wobei die Reaktionsordnung bezüglich der Wasserstoffionen wegen der Katalyse nach (Ic) kleiner als eins erscheint. (Ic) wird bei höheren pH-Werten durch die Chemisorptionsschichten begünstigt.

Die Anionenreduktion wird im Gegensatz dazu durch die Oberflächenbedeckung erschwert. Da das Hypochlorit und die Oberflächenschicht im gleichen Potentialintervall reduziert werden, ändert sich mit zunehmender Stromdichte, d.h. negativer werdendem Potential, die Struktur der Elektrodenoberfläche. In welcher Weise sich die Reduktion des Anions und die der Oberflächenschicht beeinflussen, zeigen die folgenden Versuche bei $\text{pH} = 13.6$ und einer Hypochloritkonzentration von $1 \cdot 10^{-2} \text{ M}$.

Um den Einfluss der Rührgeschwindigkeit, d.h. Konzentrationspolarisation, mit zu berücksichtigen und dabei einen annähernd gleichen Ausgangszustand der Elektrodenoberfläche zu erreichen, wurden die Strom-Spannungs-Kurven nebeneinander aufgenommen. Dazu wurde bei jeweils konstanter Stromdichte und konstanter Rührgeschwindigkeit das Potential nach 3–4 Minuten gemessen, das sich dann kaum noch änderte. Bei zunächst konstant bleibender Stromdichte wurde die Rührgeschwindigkeit stufenweise erhöht und das sich einstellende Potential gemessen. Danach wurde die Stromdichte um einen Schritt erhöht und wiederum die Rührgeschwindigkeit von 4 U/sec beginnend über 9.16 auf 25 U/sec vergrössert usw.: Abb. 16. Das annähernd stationäre Potential wird zunächst negativer, bei weiterer Stromsteigerung aber sinkt die Überspannung der Anionenreduktion, um schliesslich

bei erreichtem Grenzstrom sich sprunghaft zu vergrössern. Einen normalen Verlauf zeigt die Strom-Spannungs-Kurve bei der Drehzahl 4 sec^{-1} der Scheibenelektrode.

Durch die steigende Stromdichte, die durch die Diffusionspolarisation verminderte Depolarisatorkonzentration an der Elektrode und das negativere Elek-

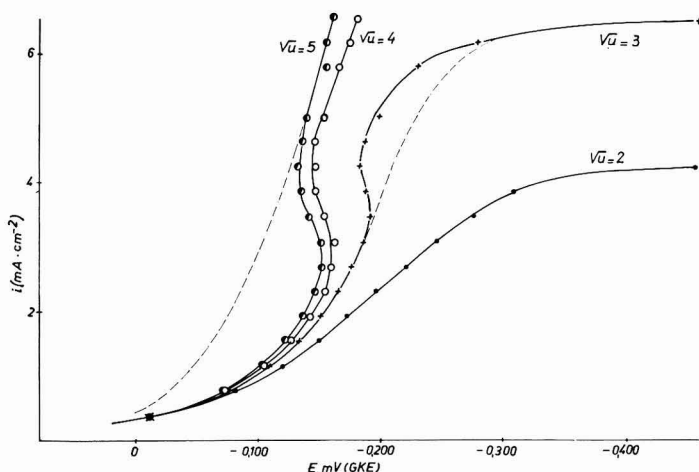


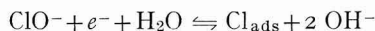
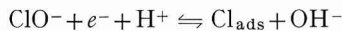
Abb. 16. Strom-Spannungs-Kurve der ClO^- -Reduktion in alkalischer Lösung an Platin bei unterschiedlichen Drehzahlen der Scheibenelektrode; Hypochloritkonzentration $1 \cdot 10^{-2} M$; pH = 13.6; Messverfahren vgl. Text.

trodenpotential überwiegt letztlich der Abbau der Oberflächenschicht, so dass sich trotz grösserer Stromdichte die Überspannung der Anionenreduktion verringert. Das Potential wird positiver. Die Oberflächenschicht wird wegen der nun zu geringen Hypochloritkonzentration nicht oder nicht vollständig erneuert. Es lässt sich hieraus der Schluss ziehen, dass elektrochemischer Abbau und chemischer Aufbau konkurrieren, wobei mit steigender Stromdichte der Abbau begünstigt wird.

Die fallende Kennlinie kommt dadurch zustande, dass mit zunehmender Stromdichte und sonst gleichbleibenden Bedingungen die die Überspannung erhöhende Schicht abgebaut wird, die Anionenreduktion wird durch sie im Gegensatz zur Säurereduktion erschwert.

Bei kleineren Rührgeschwindigkeiten dominiert die Diffusionsüberspannung, und die Gesamtüberspannung steigt monoton mit der Stromdichte an.

Schliesslich könnte man im Einklang mit unseren Ergebnissen für die Durchtrittsreaktion der Anionenreduktion in schwach sauren bzw. alkalischen Lösungen formulieren:



ZUSAMMENFASSUNG

Das Verhältnis der stationären Grenzströme für die Reduktion der Hypo-

chlorsäure und ihres Anions entspricht mit Einschränkungen der Dissoziationskonstante der Säure. Eine Überhöhung des Säurereduktionsgrenzstromes auf Grund der Säurenachbildung durch Rekombination tritt bei höchsten Pufferkonzentrationen auf. Unter galvanostatischen Bedingungen lässt sich ein Strommengenanteil erfassen, der auf die Reduktion der oxydierten Elektrodenoberfläche zurückgeführt werden kann. Ein mit zunehmender Substratkonzentration steigender Bruchteil dieser Oberflächenschicht wird gemeinsam mit dem Anion, die Restmenge (konzentrationsunabhängig) bei negativeren Potentialen reduziert. Aus stationären Messungen folgt, dass die Oberflächenschicht die Säurereduktion fördert, die Anionenreduktion hemmt.

SUMMARY

The relative size of the limiting currents observed for the reduction of hypochlorous acid and its anion, respectively, correspond to the dissociation constant of the acid. In solutions with the highest buffer concentration, recombination between protons and chlorite anions raises the limiting current of acid reduction. A portion of the charge measured chronopotentiometrically is due to the reduction of the oxidised surface layer. One part of this layer is reduced together with the anion (increasing with increasing concentration of depolariser), the rest (independent of concentration) is reduced at more negative potentials. Stationary experiments show that this surface layer catalyses acid reduction but inhibits anion reduction.

LITERATUR

- 1 I. E. FLIS UND I. M. WOROBJEW, *Zh. Fiz. Khim.*, 37 (1963) 1805.
- 2 B. NIKOLSKII UND I. E. FLIS, *Zh. Obshch. Khim.*, 22 (1952) 1298.
- 3 E. J. JAKOWLEWA, K. J. ROSENTHAL UND T. S. FILIPPOW, *Zh. Fiz. Khim.*, 30 (1956) 937.
- 4 O. SCHWARZER UND R. LANDSBERG, *J. Electroanal. Chem.*, 14 (1967) 339.
- 5 D. LANDOLT UND N. IBL, *Chem. Ing. Tech.*, 39 (1967) 706.
- 6 L. HAMMAR UND G. WRANGLEN, *Electrochim. Acta*, 9 (1964) 1.
- 7 T. NAGAI UND T. TAKEI, *J. Electrochem. Soc. Japan*, 24 (1956) 557; 25 (1957) 373.
- 8 I. E. FLIS UND M. K. BINJAJEWA, *Zh. Fiz. Khim.*, 35 (1961) 1003.
- 9 E. N. JENKINS, *J. Chem. Soc., London*, (1951) 2627.
- 10 F. G. WILL, *Z. Elektrochem.*, 63 (1959) 484.
- 11 O. SCHWARZER, Diplomarbeit, TH Chemie Leuna-Merseburg, 1961.
- 12 SAN JOURCHE UND L. GARDET, *Bull. Soc. Chim. France*, 35 (1924) 1089.
- 13 I. E. FLIS, *Zh. Obshch. Khim.*, 31 (1958) 1194.
- 14 L. MÜLLER, *Elektrokhimiya*, 4 (1968) 199.
- 15 A. FRUMKIN UND G. TEDORADSE, *Z. Elektrochem.*, 62 (1958) 251.
- 16 H. J. B. SAND, *Z. Phys. Chem.*, 35 (1900) 641; *Phil. Mag.*, 1 (1900) 45.
- 17 T. BERZINS UND P. DELAHAY, *J. Am. Chem. Soc.*, 75 (1953) 4205.
- 18 K. J. VETTER, *Z. Elektrochem.*, 66 (1962) 577.
- 19 H. W. NÜRNBERG, G. VAN RIESENBECK UND M. VON STACKELBERG, *Z. Elektrochem.*, 64 (1960) 130.
- 20 W. J. ALBERY, *Trans. Faraday Soc.*, 62 (1966) 1575.
- 21 P. DELAHAY UND T. BERZINS, *J. Am. Chem. Soc.*, 75 (1953) 2486.
- 22 W. LORENZ, *Z. Elektrochem.*, 59 (1955) 730.

THE ELECTROCHEMICAL OXIDATION OF HYDROXYLAMINE AT PLATINUM AND GOLD ELECTRODES IN DIMETHYLSULFOXIDE

ALVIN D. GOOLSBY AND DONALD T. SAWYER

Department of Chemistry, University of California, Riverside, California 92502 (U.S.A.)

(Received February 27th, 1968)

The electrochemical properties of hydroxylamine in aqueous solutions and the dependence of these properties on pH, electrode material, electrode pre-conditioning and type of electrochemical experiment, have been discussed previously¹⁻³. By selection of proper conditions and potentials, hydroxylamine may be oxidized by a one-, two-, four-, or six-electron process to N₂, N₂O, HNO₂ or NO₃⁻ at a platinum electrode. Although complete oxidation of hydroxylamine to nitrate ion is hindered by deactivation of the electrode during the experiment, chronopotentiometric studies at a reduced platinum electrode indicate a six-electron oxidation in acidic aqueous solution². A recent study⁴ of the electrochemical reduction of nitrous acid at a mercury electrode has established that hydroxylamine is a major product. This result has prompted additional study of the electrochemistry of the various oxidation states of nitrogen.

The present paper summarizes the results of an investigation of the electrochemical oxidation of hydroxylamine in dimethylsulfoxide. The system has been investigated by chronopotentiometry, controlled-potential coulometry, and cyclic voltammetry using platinum and gold electrodes. The idealized conditions for chronopotentiometric analysis of hydroxylamine have been established and its diffusion coefficient has been determined. Mechanisms for the oxidation process have been postulated and are consistent with the electrochemical data and the products of the reaction.

EXPERIMENTAL

A combination potentiostat–amperostat⁵ with a Sargent Model SR strip-chart recorder and a Tektronix Model 564 oscilloscope was used for all of the electrochemical operations and measurements. Most of the chronopotentiometric measurements were made with a Leeds and Northrup coulometric cell (No. 7961), and the coulometric measurements were made with a sealed gas-tight glass cell. A three-electrode system was incorporated into each cell, with provision for either gold or platinum working electrodes. The areas of these electrodes were determined by chronopotentiometric reduction of ferricyanide ion. An aqueous Ag–AgCl reference electrode was used which has been described previously⁶; its potential was 0.000 V vs. SCE.

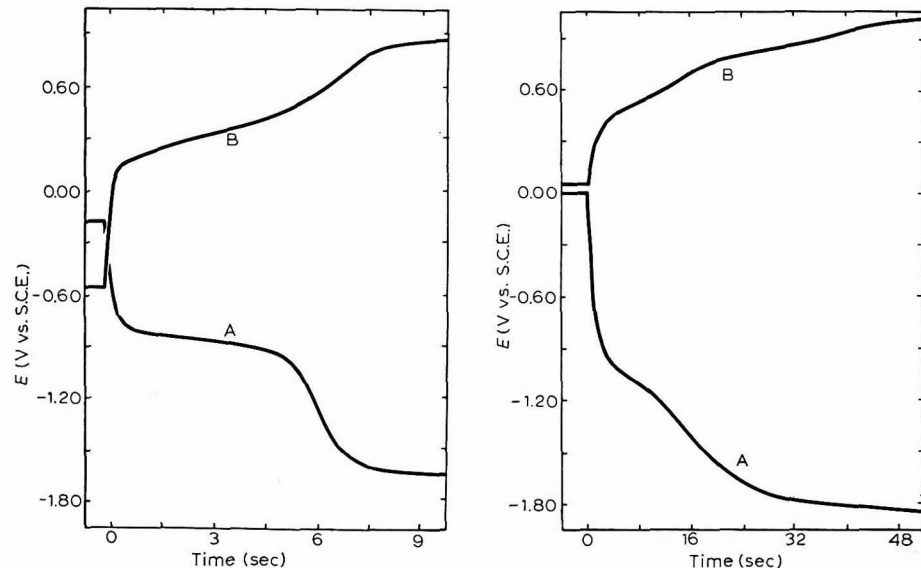
Solution acidity was determined with a Leeds and Northrup expanded scale pH-meter. The gas chromatographic analyses were made with a six-foot Poropak-Q column at room temperature and a Carle Model 100 Micro-Detector.

Dimethylsulfoxide (J. T. Baker analyzed reagent-grade) was obtained in pint bottles to minimize water contamination; the reported water content was 0.03%. A 0.349 F solution of NaOH in water was prepared from reagent-grade base; a 25% aqueous solution of Et₄NOH (analyzed to be 1.72 F) was supplied by Matheson, Coleman and Bell. Reagent-grade hydroxylamine hydrochloride ([NH₃OH]Cl) and hydroxylamine sulfate ([NH₃OH]₂SO₄) were obtained from Matheson, Coleman and Bell. Compressed pre-purified nitrogen gas was supplied by the Air Reduction Company. All other materials were reagent-grade.

Solutions of (NH₃OH)Cl and of (NH₃OH)₂SO₄ in DMSO containing 0.20 F LiClO₄ were prepared by introduction of weighed amounts of the dry compounds into known volumes of the solvent.

RESULTS

The chronopotentiometric reduction waves for (NH₃OH)⁺, and oxidation waves for (NH₂OH) at gold and platinum electrodes are illustrated by Figs. 1 and 2. The reduction waves have average $E_{\frac{1}{2}}$ -values of -0.84 V vs. SCE at platinum and -1.18 V vs. SCE at gold in the nitrogen-saturated solutions. Many acids in DMSO exhibit reduction waves in this potential range⁷. The value of $i\tau^{\frac{1}{2}}$ for this reduction wave⁸ at both electrodes decreases stoichiometrically to zero with the addition of a standardized 25% Et₄NOH solution. These two observations establish that the reduction wave is due to the acidic proton of the hydroxylamine cation.



Figs. 1-2. Chronopotentiometric reduction of (NH₃OH)⁺ (A) and oxidation of neutral NH₂OH (B) in DMSO containing 0.20 F LiClO₄. (1) Pt electrode (2.14 cm²), current, 400 μA; (2) Au electrode (0.214 cm²); current, 40 μA. Hydroxylamine derived from (NH₃OH)Cl, 2.88 · 10⁻³ F.

Platinum

At a platinum electrode an oxidation wave is not obtained for $(\text{NH}_3\text{OH})\text{Cl}$, until part of the HCl has been neutralized by NaOH or Et_4NOH . As NaOH is added, the value for $i\tau^{1/2}$ for the anodic wave ($E_{\frac{1}{2}}$, $+0.27 \pm 0.02$ V vs. SCE) increases until 3 moles of base have been added per mole of $(\text{NH}_3\text{OH})\text{Cl}$; this is illustrated by Fig. 3. A reverse chronopotentiometric wave due to the oxidation products is not observed. Anodic chronopotentiometry of $(\text{NH}_3\text{OH})_2\text{SO}_4$ at a platinum electrode is similar to $(\text{NH}_3\text{OH})\text{Cl}$, except that a shortened oxidation wave is obtained ($E_{\frac{1}{2}}$, $+0.27$ vs. SCE) before the addition of any NaOH (because of its oxidation at $+0.75$ V vs. SCE; Et_4NOH has not been used for anodic studies).⁹

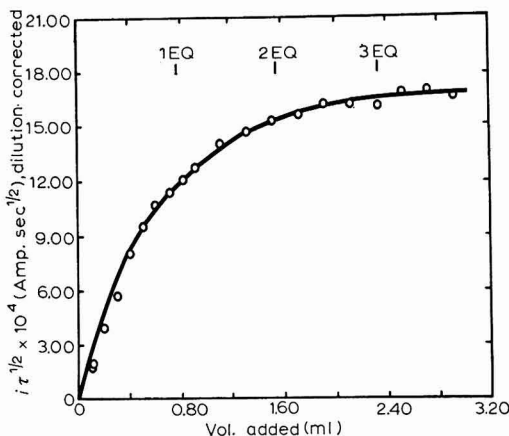


Fig. 3. Growth of the chronopotentiometric oxidation wave for $(\text{NH}_3\text{OH})\text{Cl}$ in DMSO as a function of added base. Solution, $4.86 \cdot 10^{-3}$ F $(\text{NH}_3\text{OH})\text{Cl}$ + 0.20 F LiClO_4 ; titrant, 0.349 F NaOH; electrode, Pt (2.14 cm²); $E_{\frac{1}{2}}$, +0.27 V vs. SCE.

Controlled-potential coulometric oxidation of hydroxylamine with a platinum foil electrode at +0.50 V vs. SCE has been carried out with varying amounts of hydroxide ion added to the solution. For solutions with one, two, three and four moles of OH^- ion added initially per mole of $(\text{NH}_3\text{OH})^+$, coulometric electrolysis n -values (number of electrons removed per hydroxylamine) of 0.62, 0.88, 1.14 and 1.2,

TABLE I

CONTROLLED POTENTIAL COULOMETRIC OXIDATION OF HYDROXYLAMINE IN DMSO CONTROLLED TO pH 10.0 ± 1.5

E , +0.50 V vs. SCE; 0.20 F LiClO_4

	n	$\text{OH}^-/(\text{NH}_3\text{OH})^+$	N_2O yields (%)
A. Platinum			
$(\text{NH}_3\text{OH})\text{Cl}$	1.98 ± 0.08	3.0 ± 0.1	78 ± 15
$(\text{NH}_3\text{OH})_2\text{SO}_4$	1.99 ± 0.04	3.0 ± 0.1	71 ± 15
B. Gold			
$(\text{NH}_3\text{OH})\text{Cl}$	2.00 ± 0.20	3.0 ± 0.1	87 ± 15
$(\text{NH}_3\text{OH})_2\text{SO}_4$	1.98 ± 0.04	2.9 ± 0.1	—

respectively, are obtained. The maximum and most consistent values for n are achieved by first neutralizing the $(\text{NH}_3\text{OH})^+$ species to NH_2OH , and then performing coulometry while keeping the solution "neutral". Solution neutrality has been controlled by periodically measuring the pH during the experiment and adding sufficient hydroxide ion to maintain the acidity at $\text{pH } 10.0 \pm 1.5$. Table 1 summarizes the n -values for several coulometric oxidation experiments and includes values of the total amount of hydroxide ion consumed. Similar n -values have been obtained by "buffering" the DMSO solution with excess solid LiOH , which dissolves only enough to neutralize generated acidity, thus maintaining the solution at $\text{pH } 10$. The mass of the platinum electrode remains unchanged during the controlled-potential electrolysis experiments.

The major product of the controlled-potential oxidation of hydroxylamine in DMSO is nitrous oxide (N_2O) on the basis of gas chromatographic analyses. This has been established by performing the NH_2OH oxidation in a sealed coulometry cell so that the products are trapped in the solution and the gas space above the solution. Analysis for total N_2O requires calibration of the gas chromatograph with pure N_2O , knowledge of the gas and liquid volumes as well as the temperature and pressure, and knowledge of the solubility of N_2O in DMSO (determined to be $0.055 \pm 0.005 \text{ F}$ at 1 atm pressure and 24° for 0.2 F LiClO_4 in DMSO). The yields of N_2O obtained for various conditions are summarized in Table 1 (100% would represent complete conversion of NH_2OH to N_2O). If the solution pH is controlled more basic than $\text{pH } \approx 13$, N_2 gas becomes a significant product, and the coulometric n -value obtained is less than 2.00.

Chronopotentiometric studies have also been made of hydroxylamine at a platinum electrode with solution conditions selected to give the maximum value for n and $i\tau^{1/2}/AC$. This occurs when three moles of hydroxide ion are added per mole of $(\text{NH}_3\text{OH})^+$. For such a condition the average value of $i\tau^{1/2}/AC$ for the oxidation wave of $(\text{NH}_3\text{OH})\text{Cl}$ in DMSO containing 0.20 F LiClO_4 ($E_{\frac{1}{2}}$, $+0.27 \text{ V vs. SCE}$) is $225 \pm 52 \text{ A sec}^{1/2} \text{ cm/mole}$ from $0.86 \cdot 10^{-3}$ to $4.67 \cdot 10^{-3} \text{ F}$ hydroxylamine. Consistent values of $i\tau^{1/2}$ are not obtained at a given hydroxylamine concentration if the platinum electrode is pre-reduced, but are obtained if it is pre-oxidized. In a typical case, $i\tau^{1/2}$ for hydroxylamine oxidation under the conditions described varies $\pm 4.1\%$ over a 25-fold range in τ .

For irreversible chronopotentiometric systems an expression has been developed for evaluating the kinetic parameters for oxidation processes⁸

$$E = \frac{-2.3 RT}{(1-\alpha) n_a F} \log \frac{nFAC^0 k_{b,h}^0}{i} - \frac{2.3 RT}{(1-\alpha) n_a F} \log [1 - (t/\tau)^{\frac{1}{2}}] \quad (1)$$

where E is the potential of the working electrode *vs.* the normal hydrogen electrode (NHE), $(1-\alpha)$ the anodic transfer coefficient, n_a the number of electrons involved in the rate-determining charge transfer step, A the electrode area, F the faraday, R the gas constant, T the absolute temperature, C^0 the bulk concentration of electroactive species, τ the transition time, t the time of electrolysis, $k_{b,h}^0$ the heterogeneous rate constant and i the current.

Plots of E_t *vs.* $\log[1 - (t/\tau)^{\frac{1}{2}}]$ for typical anodic chronopotentiograms of hydroxylamine in DMSO give straight lines which indicate an irreversible process. However, the slopes yield a low value of 0.17 for $(1-\alpha)n_a$. The galvanostatic method⁸,

which involves plotting values of $E_{t=0}$ (obtained by extrapolation of the linear portion of the chronopotentiometric wave to $t=0$) vs. $\log i$ for several currents, gives a higher value of 0.26 for $(1-\alpha)n_a$ for $(\text{NH}_3\text{OH})^+$ neutralized with 3 hydroxide ions; the value is 0.48 for $(\text{NH}_3\text{OH})_2\text{SO}_4$ with no added hydroxide ion. A plot of $E_{t=0}$ vs. $\log (i/[\text{OH}^-])$ for a DMSO solution containing $(\text{NH}_3\text{OH})^+$ to which hydroxide ion is being added gives a comparable value of 0.47 for $(1-\alpha)n_a$, which indicates that hydroxide ion probably is involved in the rate-determining step.

Gold

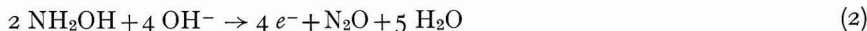
The chronopotentiometric oxidation of NH_2OH at gold gives almost the same results as those obtained with a platinum electrode. For $(\text{NH}_3\text{OH})_2\text{SO}_4$ in DMSO containing 0.20 F LiClO_4 , the value of $E_{\frac{1}{2}}$ is $+0.46 \pm 0.02$ V vs. SCE; reverse waves due to oxidation products are not observed. Under these same conditions two oxidation waves are observed for $(\text{NH}_3\text{OH})\text{Cl}$ at gold (see Fig. 2). The first occurs at an $E_{\frac{1}{2}}$ -value of $+0.47 \pm 0.02$ V vs. SCE, and is similar to that obtained for $(\text{NH}_3\text{OH})_2\text{SO}_4$. The second wave has an $E_{\frac{1}{2}}$ -value of $+0.84 \pm 0.03$ V vs. SCE, and is approximately 50% longer than the first wave. With DMSO containing 0.20 F LiClO_4 and a small quantity of chloride ion, anodic chronopotentiometry at a platinum electrode which has been coated thinly with metallic gold gives two oxidation waves. These waves, which have $E_{\frac{1}{2}}$ -values of $+0.45 \pm 0.02$ and $+0.76 \pm 0.02$ V vs. SCE, appear to be due to the formation of Au(I) and Au(III) chloride complexes.

Both $(\text{NH}_3\text{OH})\text{Cl}$ and $(\text{NH}_3\text{OH})_2\text{SO}_4$ have been oxidized by controlled-potential coulometry with a gold foil electrode at $+0.50$ V vs. SCE. As with platinum, the most consistent results are obtained by first neutralizing $(\text{NH}_3\text{OH})^+$ to NH_2OH with hydroxide ion, and then controlling the pH of the solution to 10.0 ± 1.5 during the oxidation. The results of the coulometry experiments with a gold electrode are summarized in Table I. The weight of the gold electrode remains constant during coulometric oxidation of $(\text{NH}_3\text{OH})_2\text{SO}_4$; in contrast, the oxidation of $2.39 \cdot 10^{-4}$ mole of $(\text{NH}_3\text{OH})\text{Cl}$ is accompanied by a loss in weight of the electrode equivalent to $2.21 \cdot 10^{-4}$ mole of gold. In addition, finely divided gold particles are formed in the solution.

The average value of $i\tau^{\frac{1}{2}}/AC$ for the $(\text{NH}_3\text{OH})_2\text{SO}_4$ oxidation wave at a gold electrode ($E_{\frac{1}{2}}$, $+0.46$ V vs. SCE) has not been determined owing to the low solubility of the sulfate in DMSO. The value of $i\tau^{\frac{1}{2}}/AC$ for the oxidation of $(\text{NH}_3\text{OH})\text{Cl}$ is not meaningful because of the simultaneous oxidation of the gold electrode in the presence of chloride ion. Plots of E_t vs. $\log [1 - (t/\tau)^{\frac{1}{2}}]$ for the oxidation of $(\text{NH}_3\text{OH})_2\text{SO}_4$ to which 3 hydroxide ions have been added per $(\text{NH}_3\text{OH})^+$ give a value of 0.41 for $(1-\alpha)n_a$; galvanostatic studies yield linear curves for plots of $E_{t=0}$ vs. $\log i$ and give a value of 0.48 for $(1-\alpha)n_a$.

DISCUSSION AND CONCLUSIONS

The results in Table I indicate that oxidation at $+0.50$ V vs. SCE of neutralized $(\text{NH}_3\text{OH})\text{Cl}$ or $(\text{NH}_3\text{OH})_2\text{SO}_4$ in DMSO is represented by the overall reaction:



With an excess of hydroxide ion present in the solution, the reaction yields N_2 in addition to N_2O and H_2O . In the case of the oxidation of neutralized $(\text{NH}_3\text{OH})\text{Cl}$

with a gold electrode, the presence of metallic gold in solution and the fact that gold undergoes a one-electron oxidation at +0.45 V vs. SCE in DMSO containing chloride ion, confirms that a portion of the electrolysis current oxidizes metallic gold to Au(I). The latter is reduced by NH₂OH to give finely divided metallic gold and the products in reaction (2).

From the chronopotentiometric data obtained for the oxidation of (NH₃OH)Cl at a platinum electrode, and (NH₃OH)₂SO₄ at platinum and gold electrodes, the electrode process is concluded to be diffusion-controlled and irreversible. The average diffusion coefficient, D , for NH₂OH derived from the addition of 3 moles of OH⁻ ion per mole of (NH₃OH)Cl in DMSO containing 0.20 F LiClO₄, is $1.7 \pm 0.7 \cdot 10^{-6}$ cm²/sec, assuming an overall two-electron process. The values for $(1-\alpha)n_a$ indicate that the electrochemical rate-determining step is a one-electron process which requires one hydroxide ion per NH₂OH molecule. A mechanism which is consistent with the electrochemical data and the known decomposition of the HNO species^{4,10} is represented by the equations:



The values of K are not known for NH₂OH in DMSO, but the equilibrium presumably is rapid because the value of $i\tau^\frac{1}{2}$ is independent of i over a wide range of currents¹¹. The chemical steps following the electrochemical oxidation are sufficiently rapid that the intermediate species cannot be observed with multi-scan cyclic voltammetry (Pt electrode, $v=4$ V/sec). This also prevents calculation of a rate constant for the electrochemical step. In the proposed mechanism, NH₂OH is regenerated by reaction (5) and cycled back to reaction (3) to give an overall stoichiometry of two electrons and two hydroxide ions per neutral NH₂OH.

ACKNOWLEDGEMENT

This work was supported by the National Science Foundation under Grant No. GP-7201.

SUMMARY

The electrochemistry of hydroxylamine has been studied at gold and platinum electrodes in dimethylsulfoxide containing 0.20 F LiClO₄ using chronopotentiometry, controlled-potential coulometry, cyclic voltammetry and gas chromatography. The electroactive species is NH₂OH which is oxidized irreversibly by a diffusion-controlled two-electron process. The major products are H₂O, H⁺ and N₂O. Mechanisms consistent with the results are proposed; the rate-controlling step is a one-electron process which follows a pre-chemical reaction of a hydroxide ion with NH₂OH.

REFERENCES

- 1 J. J. LINGANE AND S. JONES, *Anal. Chem.*, 23 (1951) 1804.
- 2 D. G. DAVIS, *Anal. Chem.*, 35 (1963) 764.
- 3 T. MOELLER, *Inorganic Chemistry*, J. Wiley and Sons, Inc., New York, 1954, p. 580.
- 4 D. L. EHMAN AND D. T. SAWYER, *J. Electroanal. Chem.*, 16 (1968) 541.
- 5 A. D. GOOLSBY AND D. T. SAWYER, *Anal. Chem.*, 39 (1967) 411.
- 6 D. T. SAWYER AND J. L. ROBERTS, JR., *J. Electroanal. Chem.*, 12 (1966) 90.
- 7 T. B. REDDY, *Electrochemical and Acid-Base Studies in Dimethylsulfoxide*, Ph.D. Thesis, University of Minnesota, 1960, Univ. Microfilms No. 60-5606.
- 8 P. DELAHAY, *New Instrumental Methods in Electrochemistry*, Interscience Publishers Inc., New York, 1954, pp. 179-216.
- 9 A. D. GOOLSBY AND D. T. SAWYER, *Anal. Chem.*, 40 (1968) 83.
- 10 M. C. SNEED AND R. C. BRASTED, *Comprehensive Inorganic Chemistry*, Vol. 5, D. Van Nostrand Co., Inc., New York, p. 39.
- 11 M. PAUNOVIC, *J. Electroanal. Chem.*, 14 (1967) 447.

J. Electroanal. Chem., 19 (1968) 405-411

DETERMINATION OF TRACES OF ZINC AND MANGANESE IN COBALT BY PULSE POLAROGRAPHY

A. LAGROU AND F. VERBEEK

Laboratory for Analytical Chemistry, University of Ghent (Belgium)

(Received April 20th, 1968)

Zinc and manganese, together with nickel and iron, are in nature often found in association with cobalt and these elements are, therefore, usually present as impurities in cobalt and its compounds. Thus, a purity control of cobalt always involves the determination of traces of zinc and manganese.

Zinc is determined in cobalt by colorimetry¹ and classical polarography²⁻⁴; SPEECKE AND MAES⁵ applied activation analysis. Most of the few techniques for manganese reported are photometric procedures after oxidation to permanganate^{4,6,7}, emission spectrography⁸⁻¹⁰, and activation analysis⁵. Except for the last technique, there have been no determinations below concentrations of 50 p.p.m.

This investigation deals with the determination of traces of zinc and manganese in cobalt by pulse polarography. This very sensitive polarographic technique, developed by BARKER and coworkers¹¹, has already been used for bismuth¹² and nickel¹³ in cobalt.

The reduction waves of zinc(II) and manganese(II) were used in the polarographic analysis and as these elements are reduced at nearly the same, or at a more negative, potential than cobalt(II), prior separation from the cobalt matrix was necessary. The separation was carried out on a synthetic anion-exchange resin, using ⁶⁵Zn and ⁵⁴Mn radioactive tracers for checking the yield.

Pulse polarographic methods for determining traces of copper, lead, cadmium and indium in cobalt were also developed and will be published shortly.

EXPERIMENTAL

1. Apparatus and reagents

Pulse polarograph, Southern type A 1700 Mark II. The potentialities, measurement of peak heights, and working conditions of this instrument were described in a previous paper¹⁴.

Scaler, ACEC type ANC 660 with a NaI(Tl) well-type crystal.

Dowex 1 X800, 100–200 mesh anion-exchange resin.

⁶⁵Zn solution: 0.5 ml with a specific activity of 0.387 mC/mg and a concentration of 13.4 mg/ml was obtained by neutron irradiation in the BR-1 reactor. A stock solution was prepared by appropriate dilution with 1 M hydrochloric acid (γ -energy: 0.511 and 1.114 MeV; $T_{\frac{1}{2}} = 245$ d).

^{54}Mn solution: 1 mC of carrier free ^{54}Mn (γ -energy: 0.840 MeV; $T_{\frac{1}{2}} = 324$ d) in 0.1 M hydrochloric acid was obtained from U.K.A.E.A. (Amersham, England). A stock solution was prepared by diluting 0.100 ml to 100 ml with 6 M hydrochloric acid. The activity of this solution was approximately $2.5 \cdot 10^5$ counts/min ml.

Zinc stock solution: prepared by dissolving analytical-grade metallic zinc in hydrochloric acid, evaporating to dryness and redissolving in twice-distilled water. The stock solution was standardised electrolytically. Dilute solutions were freshly prepared by appropriate dilution and stored in glass flasks.

Manganese stock solution: prepared by dissolving analytical-grade $\text{MnSO}_4 \cdot 1 \text{ H}_2\text{O}$. The stock solution was standardised gravimetrically by the ammonium phosphate procedure. Dilutions were prepared as for zinc.

Acetic acid, analytical-grade, was twice distilled in a quartz apparatus.

Very pure ammonium acetate was obtained by a 24-h electrolysis of the 6 M solution on a mercury cathode, at a controlled potential of -1.5 V vs. a saturated calomel electrode (SCE); the electrolysis was performed in separate electrode compartments under a nitrogen atmosphere.

All other reagents were analytical-grade purified to reduce the zinc and manganese content as described previously^{14,15}.

2. Polarographic data

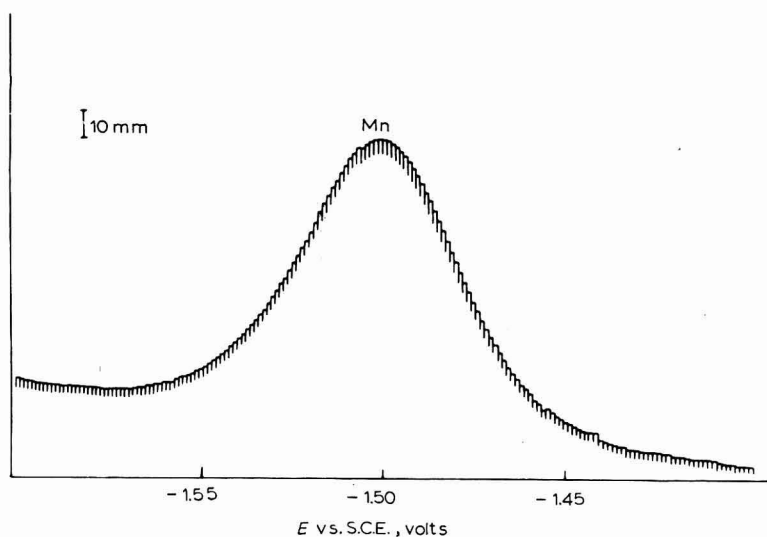
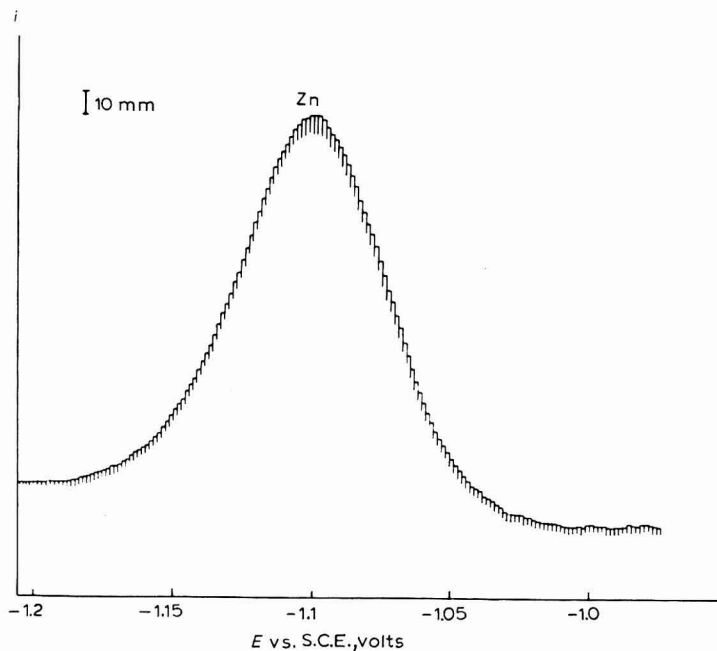
(a) Zinc. The favourable polarographic characteristics of zinc in various supporting electrolytes show well-defined waves corresponding to a two-electron reduction. The determination must be performed in slightly acidic (pH = 5–6), neutral or alkaline solution, because at lower pH-values the neighbouring reduction wave of the hydrogen ion ($E_{\frac{1}{2}} = -1.58$ V vs. SCE) tends to distort the zinc peak.

In most supporting electrolytes the half-wave potentials are insufficiently separated from that of cobalt to allow the direct polarographic determination of traces of zinc in a cobalt matrix without prior separation of cobalt. Electrolytes that are more or less suitable from this point of view cannot be used because of the slight solubility of cobalt in these media (oxalate, malonate, citrate). A prior separation is therefore necessary.

The determination in 1 M ammonia – 1 M ammonium chloride after a previous separation did not give satisfactory results for low zinc concentrations. At such a high sensitivity of the apparatus the polarogram shows a peak coinciding with the zinc peak and having a comparable shape, which cannot, however, be attributed unambiguously to zinc as its height was irreproducible and increased on longer de-aeration with nitrogen. Electrolysis at a controlled cathode potential and the substitution of nitrogen by argon gave no improvement. Finally, 0.1 M ammonium acetate and 0.1 M acetic acid – 0.1 M ammonium acetate were chosen as supporting electrolytes. The half-wave potentials of zinc and cobalt are -1.10 V and -1.19 V vs. SCE, respectively. Because of this difference in the half-wave potentials, interference from cobalt can be eliminated to a certain extent after an incomplete separation. In an acetate buffer, zinc can be determined up to a molar concentration ratio, Zn/Co:1/250. A typical derivative pulse polarogram of zinc in acetate medium is represented in Fig. 1.

The interference from other ions such as iron, manganese and nickel (impurities commonly present in cobalt) was then investigated. Only nickel interferes, as the reduction peaks of nickel and zinc coincide in an acetate buffer. The polarographic behav-

our of nickel is very irreversible and less sensitive. The separation technique applied, however, gave simultaneously a cobalt-zinc and a nickel-zinc separation and nickel did not interfere. A thiocyanate-acetate mixture can also be used for the simultaneous determination of nickel, zinc, cobalt and manganese^{16,17}.



Figs. 1-2. Pulse polarogram of: (1) $2.50 \cdot 10^{-6} M$ Zn in $0.1 M$ NH₄Ac, (2) $1.80 \cdot 10^{-6} M$ Mn in $0.1 M$ LiCl. Conditions: sensitivity $1/10$, 35 mV, 9 integrations, 60 min/V, recorder 1 in./min.

The last traces of peroxide, which could not be removed, gave an interfering reduction wave at high sensitivity of the polarograph. This peroxide arises from the reduction of the dissolved oxygen on the mercury anode. Satisfactory results were obtained after de-aerating with nitrogen for 15 min before adding the mercury for the pool anode. Good results could probably also be obtained with a cell with an external reference electrode, as proposed by PEKER *et al.*¹⁸.

The linear relationship between concentration and peak height and the reproducibility of the pulse polarographic determination in acetate medium were verified by a calibration curve (10^{-4} – $10^{-7} M$). All determinations were carried out by the standard addition method.

(b) *Manganese*. For the polarographic determination of manganese, two types of procedure can be considered depending on whether a reduction or an oxidation wave is used. When the polarographic determination is carried out in electrolytes such as potassium or lithium chloride, ammonia–ammonium chloride, potassium cyanide, and others, the diffusion current corresponds to the reduction of manganese(II) to the metallic state. The manganese peak can only be satisfactorily measured in the absence of excess cobalt, nickel, iron and zinc. Attempts have been made to suppress interfering waves, but the determination was only successful after a chemical separation of extraneous metals. Most of these procedures are based on the reduction of, or oxidation to, manganese(III); the method, however, suffers from many disadvantages owing to the interference of the cobalt matrix or the impurities present. A manganese–cobalt separation was therefore used after which manganese was determined by using the classical reduction wave of manganese(II). A neutral electrolyte is necessary, however, as in acidic medium the hydrogen wave tends to distort the manganese wave.

A lithium chloride supporting electrolyte, already recommended by several authors^{19–21}, seemed to be most suitable for determining manganese after the cobalt–zinc separation. Manganese produces a well-defined wave at -1.5 V *vs.* SCE in $0.1 M$ lithium chloride. A typical derivative pulse polarogram of manganese in $0.1 M$ lithium chloride is given in Fig. 2. The manganese peak is fully separated from the rising base-line due to the discharge of the lithium ions. In other supporting electrolytes such as ammonia–ammonium chloride, the position of the manganese peak with respect to the reduction current of the ammonium ions is less favourable and the greater resolution capacity of the polarograph that is required excludes the use of the 35-mV pulse amplitude for very low concentrations, resulting in a loss of sensitivity.

The $E_{\frac{1}{2}}$ -values of nickel and zinc in $0.1 M$ lithium chloride are -1.1 V and -1.0 V *vs.* SCE, respectively. As these elements are present as impurities in cobalt, the difference between the $E_{\frac{1}{2}}$ potentials is sufficient for eliminating any mutual interference. However, the interference due to cobalt ($E_{\frac{1}{2}} = -1.2$ V *vs.* SCE) and iron ($E_{\frac{1}{2}} = -1.3$ V *vs.* SCE) is not negligible; it was difficult to evaluate the reduction peak of manganese when more than a hundred-fold excess of one of both elements was present. In all the determinations there was no interference from cobalt or iron after the separation.

The stability of the dilute manganese solutions in $0.1 M$ lithium chloride was checked by keeping a $10^{-6} M$ solution for several days in a glass flask. After a week there was no change in the reduction wave, proving that there was no sorption of manganese(II) on the glass.

Cobalt compounds can contain iron(III) which in neutral medium easily hydrolyses to iron(III) hydroxide; consequently, the possibility of coprecipitation of

manganese had to be considered. After one weeks storage, a mixture of $2 \cdot 10^{-6} M$ manganese and $10^{-4} M$ iron(III) showed the same peak height for manganese although a considerable amount of iron(III) hydroxide had precipitated. In all cobalt analyses no precipitate of iron(III) hydroxide was ever noticed in the final solution.

More dilute supporting electrolytes may be used instead of $0.1 M$ lithium chloride. This is one of the advantages of derivative pulse polarography over square wave polarography.

To verify the reproducibility and the linear relationship between concentration and peak height, a calibration curve was established. The standard addition method was applied for all determinations.

3. Separation techniques

(a) *Zinc*. Various methods were considered for separating zinc from a cobalt matrix: controlled-potential electrolysis²², selective sulphide precipitation²³⁻²⁶ or precipitation of cobalt with α -nitroso- β -naphthol³, extraction^{3,27-29} and column separation^{2,30,31}. Finally, the separation was done on an anion-exchange resin, a method already successfully applied by CARSON² for determining as little as 0.02% of zinc in cobalt. It has been shown by KRAUS AND MOORE^{30,31} that the divalent transition metals (Mn---Zn) can be separated by anion exchange of their chloro-complexes. The different anion exchange behaviour is caused by the large difference in the stability of their negatively charged complexes. Cobalt shows maximum sorption when eluting with $9 M$ hydrochloric acid, while zinc is maximally held on the resin with $2 M$ hydrochloric acid as eluent. When eluting the column with $1 M$ hydrochloric acid zinc is strongly adsorbed and cobalt will pass through. According to KRAUS AND MOORE³⁰, zinc can be eluted afterwards with $0.005 M$ hydrochloric acid. However, other investigators state that it is impossible to recover zinc quantitatively even with very dilute hydrochloric acid, as the elution curve shows tailing. Therefore, it is advisable to use dilute sodium hydroxide, ammonia, nitric acid or acetic acid as eluent. The first experiments were carried out with dilute sodium hydroxide, but after evaporation of the eluate, the large amount of sodium chloride produced rendered dissolution difficult. Moreover, sodium hydroxide causes clogging of the column. Finally, $1 M$ acetic acid was chosen for eluting zinc from the resin.

A Pyrex glass tube (20×1 cm) fitted with a removable funnel and a fused-in filter plate was used as column.

In order to investigate the zinc yield, various elutions were performed on 1 g cobalt samples with the addition of known activities of ^{65}Zn . Comparison of the recovered activity in the eluate and of the activity originally added gave the zinc yield. Possible interference from nitrate or sulphate ions was checked by carrying out similar separations using $\text{CoSO}_4 \cdot 7\text{H}_2\text{O}$ and $\text{Co}(\text{NO}_3)_2 \cdot 6\text{H}_2\text{O}$, respectively. The results are summarised in Table 1. The percentage yield was $98.19 \pm 0.92\%$.

Losses during evaporation and redissolution of the eluate, were checked by treating a series of $10^{-6} M$ zinc solutions in $1 M$ acetic acid as described. The zinc could be recovered quantitatively. The residue was redissolved in 5 ml $0.05 M$ hydrochloric acid, and 5 ml $0.1 M$ ammonium acetate was added. This prevents possible loss of zinc, as a part of the acetate can be changed into oxide when evaporating at rather high temperatures.

(b) *Manganese*. Various procedures can be considered for the cobalt-manganese

separation: extraction^{19,32,33}, precipitation as hydroxide³⁴ or sulphide^{35,36}, distillation as permanganate^{5,37}, electrochromatographic techniques³⁸, controlled-potential electrolysis and ion-exchange separation^{30,31}. The latter procedure was used. Manganese shows only slight sorption above 5 M hydrochloric acid; cobalt, on the other hand, is

TABLE 1

ZINC RECOVERY AFTER SEPARATION
(1 g cobalt compound; $\pm 10 \mu\text{g}$ zinc)

Product	Activity added counts/min.	Activity found counts/min.	Yield (%)
$\text{CoCl}_2 \cdot 6 \text{ H}_2\text{O}$	91796	88027	95.89
$\text{CoCl}_2 \cdot 6 \text{ H}_2\text{O}$	89702	88422	98.57
$\text{CoCl}_2 \cdot 6 \text{ H}_2\text{O}$	92493	92084	99.56
$\text{Co}(\text{NO}_3)_2 \cdot 6 \text{ H}_2\text{O}$	91557	90278	98.60
$\text{CoSO}_4 \cdot 7 \text{ H}_2\text{O}$	91406	89887	98.34

TABLE 2

MANGANESE RECOVERY AFTER SEPARATION
(1 g cobalt compound)

Product	Activity added counts/min.	Activity found counts/min.	Yield (%)
$\text{CoCl}_2 \cdot 6 \text{ H}_2\text{O}$	56758	58088	102.34
$\text{CoCl}_2 \cdot 6 \text{ H}_2\text{O}$	544827	550108	100.97
$\text{CoCl}_2 \cdot 6 \text{ H}_2\text{O}$	546759	531861	97.28
$\text{CoSO}_4 \cdot 7 \text{ H}_2\text{O}$	543652	548760	100.94
$\text{Co}(\text{NO}_3)_2 \cdot 6 \text{ H}_2\text{O}$	544304	557940	102.51

strongly adsorbed above 4 M hydrochloric acid. When eluting with 6 M acid manganese passes through the column, while cobalt slowly migrates. The distribution factor is not infinite, but cobalt was not observed to interfere in any analysis thus proving the efficiency of the separation. Nickel and iron(II) are the only elements eluted simultaneously with manganese. Nickel reduces at a rather more positive potential and does not interfere in the polarographic determination. Iron(II) can easily be oxidised by hydrogen peroxide to the trivalent state, which is strongly adsorbed on an anion-exchange resin. The column, 30×3 cm, contained about 100 g of resin.

The quantitative recovery of manganese by elution with 6 M hydrochloric acid was checked by carrying out a series of elutions on a 1 g sample, adding carrier free ^{54}Mn as tracer. The results for $\text{CoCl}_2 \cdot 6 \text{ H}_2\text{O}$, $\text{Co}(\text{NO}_3)_2 \cdot 6 \text{ H}_2\text{O}$ and $\text{CoSO}_4 \cdot 7 \text{ H}_2\text{O}$, are shown in Table 2. The recovery was $100.81 \pm 1.41\%$.

After elution, the solution was evaporated under an infrared lamp. The direct polarographic determination of manganese after redissolving the residue was impossible owing to the presence of reducible organic compounds eluted from the resin, which completely masked the manganese reduction wave. Therefore, the destruction of organic matter was necessary. The residue was usually mineralised by heating with sulphuric acid on a hot-plate. To ensure complete destruction, the crucible was placed in a muffle

furnace at 400° for 1 h. As control, a series of manganese solutions was treated similarly and afterwards analysed. The results showed quantitative recovery. Nitric acid cannot be used for the mineralisation owing to the volatility of manganese(II) nitrate.

4. Procedure

(a) *Zinc*. Equilibrate the column with 50 ml of 1 M hydrochloric acid and add 1 g cobalt dissolved in the minimum volume of 1 M hydrochloric acid. Elute the cobalt with 50 ml of 1 M hydrochloric acid and afterwards remove zinc with 50 ml of 1 M acetic acid. Evaporate the zinc eluate to dryness and dissolve the residue in 5 ml of 0.05 M hydrochloric acid and 5 ml of 0.1 M ammonium acetate. Record a pulse polarogram and determine the zinc by the standard addition method.

(b) *Manganese*. Equilibrate the column with 100 ml of 6 M hydrochloric acid and add 1 g of cobalt dissolved in the minimum volume of 6 M hydrochloric acid. Elute with 125 ml of 6 M hydrochloric acid and collect the last 75 ml containing all the manganese. Evaporate the eluate to dryness and add 2 ml sulphuric acid. Remove excess acid by heating on a hot-plate ($\pm 300^\circ$). Place the residue in a furnace at 400° for 1 h and then dissolve the residue in 10 ml of 0.1 M lithium chloride. Record a pulse polarogram and determine the manganese by the standard addition method.

RESULTS

The method was applied to the analysis of synthetic samples prepared by adding known quantities of zinc and manganese to a cobalt solution freed from these elements by a preliminary ion-exchange separation. The results are summarised in Tables 3 and 4.

TABLE 3

DETERMINATION OF ZINC IN COBALT

(1 g sample; final volume, 10 ml)

Zn added (μg)	Zn found (μg)	Yield (%)	Zn added (μg)	Zn found (μg)	Yield (%)
1.63	1.58	96.93	6.54	6.01	91.90
3.27	3.11	95.11	6.54	7.06	107.95
3.27	3.16	96.64	6.54	6.11	93.43
6.54	6.08	92.96	16.35	15.76	96.39

TABLE 4

DETERMINATION OF MANGANESE IN COBALT

(1 g sample; final volume, 10 ml)

Mn added (μg)	Mn found (μg)	Yield (%)	Mn added (μg)	Mn found (μg)	Yield (%)
0.98	0.93	94.90	19.56	18.64	95.30
4.89	4.81	98.36	48.90	47.96	98.08
9.78	9.40	96.11			

Finally, a number of analyses were carried out on various commercially available cobalt compounds, to check the efficiency of the method (Table 5). Every analysis was at least duplicated giving results reproducible within 5% at the 1-p.p.m. level.

TABLE 5

DETERMINATION OF ZINC AND MANGANESE IN COMMERCIALLY AVAILABLE COBALT SAMPLES
(1 g sample; final volume, 10 ml)

<i>Product</i>	<i>Grade</i>	<i>Zinc</i> (<i>p.p.m.</i>)	<i>Manganese</i> (<i>p.p.m.</i>)
CoCl ₂ · 6 H ₂ O	analytical	1.63	3.19
CoCl ₂ · 6 H ₂ O	analytical	3.75	4.73
CoCl ₂ · 6 H ₂ O	analytical	3.21	6.58
Co(NO ₃) ₂ · 6 H ₂ O	analytical	4.12	11.48
CoSO ₄ · 7 H ₂ O	analytical	8.71	14.27
Co metal	pure	118.4	68.14

The blank value for zinc was $2.5 \cdot 10^{-7} M$, even after very careful purification of the reagents. This value is still relatively high with regard to the detection limit of zinc by pulse polarography ($10^{-8} M$ corresponds to a peak height of ± 10 mm at a drop-time of 4 sec and at maximum sensitivity of the polarograph). As a doubling of the peak height with regard to the blank (*i.e.*, $2.5 \cdot 10^{-7} M$) can be measured fairly accurately, this concentration can be determined (representing 0.15 p.p.m. zinc for a 1 g sample and a final volume of 10 ml).

For manganese, the blank value was $5 \cdot 10^{-8} M$. This value prevents attainment of the detection limit of manganese, which is about the same as for zinc. Assuming that the same concentration can still be determined accurately, the detection limit can be estimated at 0.03 p.p.m. manganese in a 1 g sample and a final volume of 10 ml.

The sensitivity for both elements is satisfactory and the percentage of zinc or manganese in the commercial cobalt samples analysed is far greater than the detection limit of the procedures used.

SUMMARY

A pulse polarographic method for determining traces of zinc and manganese in cobalt and its compounds is described. Interference due to the reduction of the cobalt matrix was eliminated by a prior separation on an anion exchange resin. The yield was controlled with the radio-isotopes, ⁶⁵Zn and ⁵⁴Mn, and a quantitative recovery was obtained for both elements. After separation, zinc was determined in an acetate medium; for manganese, 0.1 M lithium chloride was chosen as supporting electrolyte. A blank value prevented the attainment of the pulse polarographic detection limit for zinc and manganese, being about $10^{-8} M$ for both elements. The method enables as little as 0.15 p.p.m. of zinc and 0.03 p.p.m. of manganese to be determined in a 1 g sample. A number of analyses carried out on synthetic and various commercially available cobalt samples showed satisfactory sensitivity and accuracy.

REFERENCES

- 1 R. S. YOUNG, *Metallurgia*, 36 (1947) 347.
- 2 R. CARSON, *Analyst*, 86 (1961) 198.
- 3 T. A. KRIUKOWA, S. I. SINJAKOWA AND T. W. AREFJEWKA, *Polarographische Analyse*, VEB Deutscher Verlag für Grundstoffenindustrie, Leipzig, 1964, pp. 220 and 226.
- 4 A. G. HYBINETTE, *Svensk Kem. Tidskr.*, 57 (1945) 6; *C.A.*, 40 (1946) 2411.
- 5 A. SPEECKE AND K. MAES, *Radiochemical Methods of Analysis*, 1 (1965) 51.
- 6 L. WALDBAUER AND N. M. WARD, *Ind. Eng. Chem. Anal. Ed.*, 14 (1942) 727.
- 7 C. M. DOZINEL, *Ing. Chem.*, 173 (1958) 53.
- 8 O. C. VELICHKO, *Zavodsk. Lab.*, 22 (1956) 1307; *C.A.*, 51 (1957) 11170h.
- 9 V. L. GINZBURG, I. N. GRAMENITSKII, S. S. KASHLINSKAYA AND D. M. LIVSHITS, *Izv. Akad. Nauk SSSR*, 19 (1955) 211; *C.A.*, 50 (1956) 3891h.
- 10 J. H. MCCLURE AND R. E. KITSON, *Anal. Chem.*, 25 (1953) 867.
- 11 G. C. BARKER AND A. W. GARDNER, *A.E.R.E. Report C/R 2297* (1958); *Anal. Chim. Acta*, 18 (1958) 118; *Z. Anal. Chem.*, 173 (1960) 79.
- 12 A. LAGROU AND F. VERBEEK, *J. Electroanal. Chem.*, 10 (1965) 68.
- 13 A. LAGROU AND F. VERBEEK, *J. Electroanal. Chem.*, 19 (1968) 411.
- 14 E. TEMMERMAN AND F. VERBEEK, *J. Electroanal. Chem.*, 12 (1966) 158.
- 15 A. LAGROU, J. VANHEES AND F. VERBEEK, *Z. Anal. Chem.*, 224 (1967) 310.
- 16 E. TEMMERMAN, Personal communication.
- 17 YOSHIAKI MIURA, *Japan Analyst*, 8 (1959) 5.
- 18 C. PEKER, M. HERLEM AND J. BADOZ-LAMBLING, *Z. Anal. Chem.*, 224 (1967) 284.
- 19 G. B. JONES, *Anal. Chim. Acta*, 11 (1954) 88.
- 20 E. HAMAMOTO, *Collection Czech. Chem. Commun.*, 6 (1934) 325.
- 21 D. MONNIER, E. MARTIN AND W. HAERDI, *Anal. Chim. Acta*, 34 (1966) 346.
- 22 P. P. TSYB, *Zavodsk. Lab.*, 16 (1950) 1419; *C.A.*, 45 (1951) 10130f.
- 23 HISAJI KATO, *J. Chem. Soc. Japan*, 55 (1934) 213.
- 24 J. R. CALDWELL AND H. V. MOYER, *J. Am. Chem. Soc.*, 57 (1935) 2375.
- 25 E. A. OSTROUMOV, *Ann. Chim. Anal. Chim. Appl.*, 19 (1937) 173; *C.A.*, 32 (1938) 3723g.
- 26 E. A. OSTROUMOV, *Zavodsk. Lab.*, 6 (1937) 1058; *C.A.*, 32 (1938) 1208.
- 27 M. I. TROITSKAYA AND A. P. KUSHNER, *Obogashch. i Met. Tsvet. Metal.*, 143 (1953); *C.A.*, 53 (1959) 14838d.
- 28 H. A. MAHLAN, G. W. LEDICOTTE AND F. L. MOORE, *Anal. Chem.*, 26 (1954) 1939.
- 29 I. G. SHAFRAN, T. K. ZELENOVA AND I. A. SIROTINA, *Sb. Statei Vses. Nauchn.-Issled. Inst. Khim. Reaktivov i Osobo Chistykh Kim. Veshchestv*, 24 (1961) 217; *C.A.*, 57 (1962) 1544a.
- 30 G. E. MOORE AND K. A. KRAUS, *J. Am. Chem. Soc.*, 72 (1950) 5792; 74 (1952) 843; 75 (1953) 1460.
- 31 K. A. KRAUS AND F. NELSON, *Symposium on Ion-Exchange and Chromatography in Analytical Chemistry*, 1956, *Am. Soc. Testing Mater., Spec. Tech. Publ.*, 195 (1958).
- 32 E. B. SANDELL, *Colorimetric Determination of Traces of Metals*, Interscience Publishers Inc., New York, 3rd ed., 1959.
- 33 D. WILLIAMS AND R. V. ANDES, *Ind. Eng. Chem. Anal. Ed.*, 17 (1945) 28.
- 34 G. DENK, H. ASTLER AND J. WURBS, *Z. Anorg. Allgem. Chem.*, 333 (1964) 29.
- 35 H. KATO, *J. Chem. Soc. Japan*, 55 (1934) 337.
- 36 R. B. HARN, C. H. SANDERS AND G. GUTNIKOV, *J. Chem. Educ.*, 37 (1960) 412.
- 37 J. PIJCK AND J. HOSTE, *Anal. Chim. Acta*, 31 (1964) 159.
- 38 R. GIJBELS, L. DE MEYER AND J. HOSTE, *Anal. Chim. Acta*, 31 (1964) 159.

THE DETERMINATION OF TRACES OF THALLIUM IN CADMIUM BY PULSE POLAROGRAPHY

E. TEMMERMAN AND F. VERBEEK

Laboratory for Analytical Chemistry, University of Ghent (Belgium)

(Received May 30th, 1968)

Copper, lead, zinc, iron and thallium are the main impurities in pure commercial cadmium products and are usually found in concentrations ranging from 0.01 to 0.0002 %. Cadmium may contain even smaller amounts of silver, nickel, arsenic, tin, antimony, tellurium, bismuth, cobalt, manganese, indium and mercury. However, a purity control of cadmium products generally implies the determination of thallium which can be done by photometry¹⁻⁶, emission spectrography⁷⁻¹⁶ and polarography¹⁷⁻²⁵.

Photometric determinations are carried out mostly with the colorimetric reagents rhodamine B^{4,5} and methyl or crystal violet^{1,2,6}, after a previous separation by ether extraction of the thallium halide complex, or co-precipitation of thallium(III) hydroxide with manganese dioxide. As low as 1 p.p.m. thallium in cadmium can be determined³.

Emission spectrography allows a direct determination of thallium in cadmium down to about 5 p.p.m. Smaller contents necessitate a preliminary separation.

In many supporting electrolytes, the presence of lead(II), arsenic(III) or tin(II) and also excess cadmium(II) can interfere with the polarographic reduction of thallium(I). In d.c. polarography it is not easy to obtain a clearly defined reduction wave for thallium(I) in the presence of large amounts of these elements; lead especially is often present in excess. PROKOF'EV²³ determined down to 40 p.p.m. thallium in cadmium directly, using 6.5-7 M ammonium hydroxide, 0.3 M sodium hydroxide as supporting electrolyte, in the presence of sufficient tartrate to keep cadmium in solution, and potassium iron(II) cyanide to avoid interference of copper. A sodium hydroxide electrolyte was necessary to prevent the interference of lead. ENSSLIN *et al.*²⁵ used an ammoniacal supporting electrolyte for the direct determination of traces of thallium in cadmium. As the concentration of the interfering traces is rather large and because of the low detection limit of a direct method, most other investigators have separated thallium from the cadmium matrix, to obtain concentration enrichment. Ether extraction of a thallium halide has been used, followed by the polarographic determination in an ammoniacal, chloride or bromide supporting electrolyte.

This investigation deals with the determination of thallium in cadmium and its compounds by means of the sensitive pulse polarographic technique developed by BARKER and coworkers²⁶. The determination of bismuth, copper and lead has already been described in a previous paper²⁷ and that of antimony, arsenic, tin, indium, nickel, zinc, cobalt, manganese and iron will be discussed in following papers.

EXPERIMENTAL

1. Apparatus and reagents

Pulse polarograph Southern type A 1700 Mark II. The measurement of peak heights and working conditions of this instrument were described previously²⁷. The derivative method of operation was used.

pH-meter Radiometer type PH M 22.

Water was distilled twice in a quartz apparatus and stored in polyethylene flasks.

Mercury, nitrogen, hydrochloric acid, ammonium hydroxide, nitric acid and acetic acid were purified as previously described²⁷.

All other reagents were analytical-grade and used without further purification.

Thallium stock: prepared from analytical-grade thallium(I) sulphate and standardised gravimetrically as thallium(I) chromate.

2. Polarographic data

Thallium(I) shows well defined reduction waves in various supporting electrolytes at about -0.5 V vs. the saturated calomel electrode (SCE). The possibility of a direct determination was examined. For the determination of thallium in high purity cadmium compounds, a preliminary separation is necessary to obtain a concentration enrichment.

(a) *Direct determination.* An EDTA supporting electrolyte seemed to be appropriate: the half-wave potential of thallium(I) is fairly constant in most base electrolytes because of the poor complexing tendency of this element. Thus, below pH 6 it is almost unaffected by EDTA²⁸, which forms very stable complexes with most di- and trivalent cations, shifting their half-wave potentials to more negative values. However, the interference of ions that are normally reduced at more positive potentials than thallium(I) must be considered, as their half-wave potentials will also undergo this negative shift. As the value of these shifts depends on the acidity, a pH control is essential.

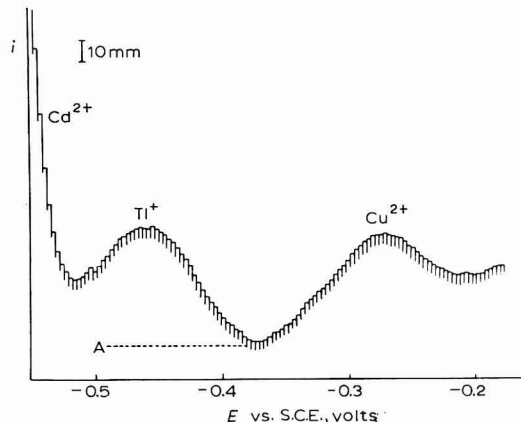


Fig. 1. Pulse polarogram of $2.5 \cdot 10^{-6} M$ Tl(I) and Cu(II) in 1 M CdCl₂-1.1 M EDTA at pH 4.25 (4.55 p.p.m. Tl in cadmium). Conditions: sensitivity 1/5; 35 mV; 9 integrations; 30 min/V; recorder 1 in./min.

The maximal potential difference between the thallium(I) peak and the cadmium(II) reduction was observed in the pH-range 3–13, at a 10% molar excess of EDTA with respect to cadmium. To ensure a reasonable sensitivity, 1 M cadmium (as chloride, sulphate or nitrate)–1.1 M EDTA (ammonium salt) was used. This mixture is soluble at pH ≥ 4.25 . The latter value appeared to be the most favourable; the copper(II)–thallium(I) peak potential difference was still about 200 mV, while no reduction peaks of bismuth(III), antimony(III), tin(II) and lead(II) appeared between the thallium(I) peak and the start of the cadmium(II) reduction. At higher pH-values, the copper(II) and thallium(I) peaks approach each other. A typical pulse polarogram of thallium(I) and copper(II) recorded in the cadmium–EDTA mixture is given in

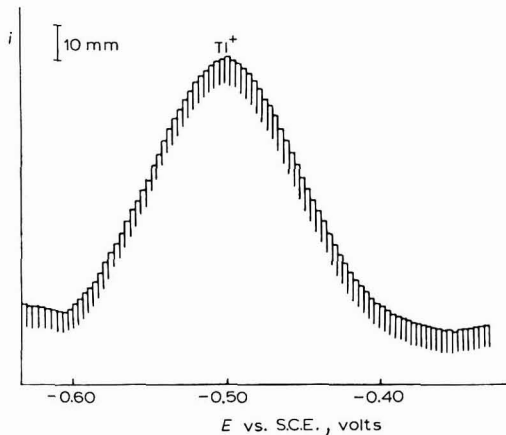


Fig. 2. Pulse polarogram of $1.16 \cdot 10^{-5} M$ Tl(I) in $0.3 M$ HA – $0.3 M$ NH_4Ac – $0.05 M$ EDTA (3.95 p.p.m. Tl in analytical-grade cadmium—sample 2 from Table 3). Conditions: sensitivity 1/40; 35 mV; 3 integrations; 12 min/V; recorder 1 in./min.

Fig. 1. The pulse polarographic sensitivity of thallium(I) in this medium is limited to $\pm 5 \cdot 10^{-7} M$ (corresponding to a detection limit of about 1 p.p.m. thallium in cadmium) because the maximal instrumental amplification cannot be used owing to interference from the cadmium(II) reduction, the thallium(I) peak being masked by the slope of the sharply rising cadmium(II) peak.

A linear relationship between concentration and peak height of thallium(I) was established by recording a calibration curve in the $5 \cdot 10^{-7}$ – $10^{-5} M$ range. The standard addition method was applied for all determinations.

(b) *Determination after separation.* After removal of the bulk of the cadmium, an EDTA-containing supporting electrolyte of pH about 4.5 appeared to be appropriate in view of the interfering elements (especially lead) that could still be present; an ammonium acetate, acetic acid buffer was convenient. A $0.3 M$ buffer and $0.05 M$ EDTA were used. A typical pulse polarogram is shown in Fig. 2. In this medium, the copper(II)–thallium(I) peak potential difference is about 140 mV, that of thallium(I)–antimony(III) 250 mV, and that of thallium(I)–bismuth(III) 170 mV, while cadmium(II), lead(II) and tin(IV) are reduced at potentials sufficiently negative to eliminate their interference. The ions of each pair are reduced in the sequence given.

Thallium(I) can be detected at concentrations down to about $4 \cdot 10^{-8} M$ (peak height, ± 10 mm at maximal instrumental amplification and a drop time of 4 sec).

This corresponds to a detection limit of 0.008 p.p.m. thallium in cadmium for a 10-g sample and a final volume of 10 ml.

A calibration curve in the $5 \cdot 10^{-7}$ – $10^{-5} M$ range showed a linear relationship, concentration–peak height, for thallium(I). All determinations were performed by the standard addition method.

3. Separation techniques

Since the thallium(I) reduction in an EDTA medium was mainly free from interferences, only the cadmium–thallium separation was investigated.

Various methods were considered for separating thallium from a cadmium matrix: extraction^{3,4,19,22–24}, co-precipitation with manganese dioxide^{16,29}, or ion exchange².

Ether extraction of a thallium halide is often used because of its simplicity. However, as a prerequisite to a pulse polarographic determination, this procedure is rather time-consuming, as a destruction is required since the polarogram cannot be recorded directly after evaporation of the ether solution, because interfering reactions occur at the DME, associated with an unstable base line. This is probably due to organic impurities in ether. This is also the case for ion exchange.

Co-precipitation of thallium(III) hydroxide with manganese dioxide, formed by the reaction of manganese(II) ion and potassium permanganate in hot dilute nitric acid solution, seemed to be promising as manganese(II) does not interfere with the thallium reduction because of its much more negative half-wave potential.

LUKE³⁰ stated that thallium can be quantitatively collected from nitric acid solutions as strong as 10%. Only the bulk of the cadmium was to be separated and the precipitations were therefore carried out from 0.06 M nitric acid solution so that thallium and antimony could eventually be isolated together³¹. Tin, and part of the arsenic, bismuth, lead and iron accompany thallium and antimony in the co-precipitate, but none of these elements interferes with the polarographic determination of thallium.

The manganese dioxide precipitate was dissolved in a hydrochloric acid–hydrazine sulphate mixture, which also reduces thallium(III) to (I).

4. Procedure

(a) *Direct determination.* Treat 2.8 g (1.1 g) of cadmium metal with 30 ml (12 ml) of hydrochloric acid 25%. Heat to boiling, add a few drops of nitric acid to complete dissolution and then evaporate almost to dryness. Cool, dissolve the residue in a minimum amount of water, add a few drops of 1% hydrazine sulphate solution while stirring and a 10% molar excess of EDTA with regard to cadmium. Neutralise to pH 4.25 with ammonium hydroxide with stirring until complete dissolution. Transfer to a 25-ml (10-ml) volumetric flask and dilute to the mark. De-aerate a part of the solution; record a pulse polarogram from –0.3 V vs. SCE and determine thallium by the standard addition method.

For cadmium compounds, dissolve an amount equivalent to 2.8 g cadmium in water, acidify to pH 3, add hydrazine sulphate and continue as above.

The neutralisation process requires some time, as at room temperature and in a volume of about 20 ml the cadmium–EDTA mixture is nearly at the limit of solubility, and heating of the solution gives an unstable base line.

(b) *Determination after separation.* Treat a suitable sample weight of cadmium metal with a minimum amount of nitric acid 25%. After decomposition, dilute to 250–600 ml with hot water to obtain a nitric acid concentration of about 0.06 M. Add 1 ml of 1% potassium permanganate solution and heat gently to boiling. Add, successively, two 1-ml portions of 1% manganese(II) nitrate solution and boil for 2 min after each addition. After cooling to 60–70°, filter through a finely sintered glass filter and wash thoroughly with water. Discard the filtrate. Dissolve the manganese dioxide precipitate with 15 ml of 2 M hydrochloric acid–1% hydrazine sulphate solution. After evaporating almost to dryness, transfer with 0.3 M acetic acid–0.3 M ammonium acetate–0.05 M EDTA mixture to a 10-ml volumetric flask and dilute to the mark. De-aerate a portion of the solution; record a pulse polarogram from –0.3 V vs. SCE and determine thallium by the standard addition method.

For cadmium compounds the same procedure is followed after dissolving the sample in water and adding nitric acid.

When analysing cadmium chloride, a manganese dioxide precipitate is sometimes formed before the addition of manganese(II) solution (reduction of permanganate). This can be prevented by first adding manganese(II).

RESULTS

Various quantities of thallium have been determined, with and without previous separation, in a number of synthetic samples prepared by adding known amounts of thallium to a cadmium solution, freed from thallium by a preliminary coprecipitation with manganese dioxide. The results are summarized in Tables 1 and 2.

TABLE 1

DIRECT DETERMINATION OF THALLIUM IN CADMIUM
(1 M Cd–1 M EDTA at pH 4.25)

<i>Added</i>		<i>Found</i>	
<i>Tl</i> (M · 10 ⁶)	<i>Tl in Cd</i> (p.p.m.)	<i>Tl</i> (M · 10 ⁶)	<i>Yield (%)</i>
6.30	11.45	6.35	100.8
		6.24	99.05
		6.52	103.5
		6.33	100.5
3.15	5.73	3.22	102.2
		1.64	97.6
		1.03	103.0
1.68	3.05	0.560	112.0
		0.533	106.6
		0.545	109.0
1.00	1.82		
0.500	0.91		

Finally, samples of commercially available cadmium and cadmium compounds were analysed to check the practicability of the method. The results are shown in Table 3. The direct determination was possible only for three samples. After separation, the thallium contents found were all well above the detection limit for a sample weight of 5 g and a final volume of 10 ml. The results of direct and indirect determinations were in good agreement. No blank values were observed.

TABLE 2

DETERMINATION OF THALLIUM IN CADMIUM AFTER SEPARATION
(2.8 g sample; 0.3 M acetate buffer-0.05 M EDTA; final volume, 10 ml)

<i>Tl added</i>		<i>Tl found</i>	
(μ g)	(<i>p.p.m.</i>)	(μ g)	<i>Yield</i> (%)
20.44	7.27	20.63	100.93
10.22	3.64	10.13	99.12
2.04	0.73	2.11	103.43
1.02	0.36	0.93	91.18
0.51	0.18	0.56	109.80
0.20	0.07	0.23 ⁵	117.50

TABLE 3

DETERMINATION OF THALLIUM IN COMMERCIALLY AVAILABLE CADMIUM SAMPLES
(5-g sample; final volume, 10 ml)

<i>Product</i>	<i>Grade</i>	<i>Thallium</i> (<i>p.p.m.</i>)
cadmium	pure	16.35
		16.23 ^a
cadmium	analytical	3.95
		4.14 ^a
cadmium	analytical	0.290
CdCl ₂ ·2½ H ₂ O	analytical	0.090
CdCl ₂ ·2½ H ₂ O	analytical	0.036
Cd(NO ₃) ₂ ·4 H ₂ O	very pure	0.048
Cd(NO ₃) ₂ ·4 H ₂ O	pure	2.82
		3.01 ^a
3 CdSO ₄ ·8 H ₂ O	analytical	0.163

^a Direct determination in 1 M cadmium, 1.1 M EDTA at pH 4.25.

SUMMARY

Traces of thallium in cadmium and cadmium compounds have been determined by pulse polarography. A direct method, without previous separation, allows the determination of about 1 p.p.m. at pH 4.25 in the presence of a 10% molar excess of EDTA with respect to cadmium. After separation by co-precipitation with manganese dioxide, thallium could be determined in an acetate buffer-EDTA mixture down to 0.008 p.p.m. thallium in cadmium for a sample weight of 10 g and a final volume of 10 ml.

Both methods were applied satisfactorily to the analysis of a number of synthetic and commercially available cadmium products.

REFERENCES

- 1 S. A. LOMONOSOV, V. N. PODCHAINOVA AND V. E. RYBINA, *Zavodsk. Lab.*, 31 (1965) 420.
- 2 L. B. GINZBURG AND E. P. SHKROBOT, *Zavodsk. Lab.*, 21 (1955) 1289.
- 3 H. POHL, Z. *Erzbergbau, Metallhüttenw.*, 9 (1956) 530.
- 4 J. F. WOOLLEY, *Analyst*, 83 (1958) 477.

- 5 R. E. VAN AMAN AND J. H. KANZELMEYER, *Anal. Chem.*, 33 (1961) 1128.
- 6 C. G. SCHEMELEVA, *Fiz. Khim. Methody Analiza i Kontrolya Proizv. (Rostovsk. Univ.) Sb.*, (1961) 151.
- 7 M. SCALISE, *Met. Ital.*, 44 (1952) 153.
- 8 F. W. LAMB, *Am. Soc. Testing Mater. Proc.*, 35 (1935) 71.
- 9 N. A. PORTKHUNOVA, L. K. LARINA AND N. S. BAKALDINA, *Sb. Nauchn. Tr. Vses. Nauchn. Issled. Gornu-Met. Inst. Tsvetn. Metal.*, 7 (1962) 380.
- 10 G. SEMPELS, *Spectrochim. Acta*, 3 (1948) 346.
- 11 V. S. KOMISSARENKO, *Zavodsk. Lab.*, 16 (1950) 1260.
- 12 L. P. SHKLOVER, *Zavodsk. Lab.*, 28 (1962) 686.
- 13 N. A. PORKHUNOVA, *Sb. Tr. Vses. Nauchn. Issled. Inst. Tsvetn. Metal.*, (1956) 197.
- 14 E. A. LAVROVA AND A. V. KUZNETSOVA, *Zavodsk. Lab.*, 31 (1965) 50.
- 15 G. SCACCIATI AND A. D'ESTE, *Met. Ital.*, 47 (1955) 259.
- 16 W. GEILMANN AND K. H. NEEB, *Z. Anal. Chem.*, 165 (1959) 251.
- 17 R. CARSON, *Analyst*, 83 (1958) 472.
- 18 V. A. TSIMMERGAKL AND Z. A. KRASNOVA, *Ukr. Khim. Zh.*, 25 (1959) 501.
- 19 T. V. AREF'eva, R. G. PATS AND A. A. POZDNYAKOVA, *Sb. Nauchn. Tr. Gos. Nauchn. Issled. Inst. Tsvetn. Metal.*, 10 (1955) 358.
- 20 A. M. USTIMOV AND Z. L. BULANOVA, *Zavodsk. Lab.*, 31 (1965) 420.
- 21 G. RASPI AND F. PERGOLA, *Chim. Ind. (Milan)*, 45 (1963) 1517.
- 22 Z. ZAGORSKI AND O. KEMPINSKI, *Chem. Anal. Warsaw*, 1 (1956) 273.
- 23 E. K. PROKOF'EV, *Zavodsk. Lab.*, 27 (1961) 530.
- 24 R. POPPER, *Chem. Prumysl*, 13 (1963) 527.
- 25 F. ENSSLIN, H. DREYER AND K. ABRAHAM, *Metall u. Erz.*, 39 (1942) 184.
- 26 G. C. BARKER AND A. W. GARDNER, *A.E.R.E. Report C/R 2297* (1958); *Anal. Chim. Acta*, 18 (1958) 118; *Z. Anal. Chem.*, 173 (1960) 79.
- 27 E. TEMMERMAN AND F. VERBEEK, *J. Electroanal. Chem.*, 12 (1966) 158.
- 28 P. BOUTEN, F. VERBEEK AND J. EECKHAUT, *Anal. Chim. Acta*, 17 (1957) 339.
- 29 V. M. VLADIMIROVA AND N. K. DAVIDOVICH, *Metody Analiza Khim. Reaktivov Preparatov, Gos. Kom. Sov. Min. SSSR po Khim.*, 4 (1962) 116.
- 30 C. L. LUKE, *Anal. Chem.*, 31 (1959) 1680.
- 31 E. TEMMERMAN AND F. VERBEEK, unpublished results.

J. Electroanal. Chem., 19 (1968) 423-429

POLAROGRAPHIC DETERMINATION OF THE AGGREGATION NUMBER OF DYES AND THE EFFECT OF ADDITIVES ON THE AGGREGATION

WAHID U. MALIK AND PURAN CHAND

Chemical Laboratories, University of Roorkee, Roorkee (India).

(Received April 26th, 1968)

Recently, HILSON AND MCKAY¹ have reported a polarographic method for determining the aggregation number of dyes. Since many additives like urea, formamide and methanol, etc., influence the aggregation number through hydrogen bonding with water molecules, it was thought worthwhile to find whether the method can be extended to determine the aggregation number in the presence of various additives. In this communication the effect of urea, formamide and methanol on the aggregation number of congo red and crystal violet is reported.

EXPERIMENTAL

Reagents

Congo red ($C_{32}H_{22}N_6Na_2O_6 \cdot 6 H_2O$) and crystal violet ($C_{25}H_{30}ClN_3 \cdot 2 H_2O$) were BDH products and were purified by recrystallization. The solutions were prepared in doubly-distilled water (all-glass).

Urea (A.R.) and formamide (Riedel) were used. Methanol was purified by redistillation.

Glycine and citrate buffers used in the reduction of the dyes were of the following compositions:

Glycine buffer pH 6.00: Potassium chloride, 0.025 M; glycine, 0.0025 M.

Citrate buffer pH 4.40: Potassium chloride, 0.01 M; tri-sodium citrate, 0.005 M; citric acid, 0.005 M;

Apparatus

Polarographic measurements were carried out using a Heyrovsky polarograph (LP 55A) operated manually in conjunction with a Scalamp Pye galvanometer. A normal polarographic capillary (Gallenkamp) with drop-time 4.30 sec was used. The mercury reservoir was kept at a constant height (60.0 cm) throughout the measurements. A saturated calomel electrode was used as reference electrode. The measurements were carried out at $25 \pm 0.1^\circ$ using a thermostatic water bath.

Procedure

Working solutions were prepared by mixing different amounts of the concentrated aqueous solutions of the dye with a fixed amount of the appropriate buffer (4.0 ml), and then diluting to 10.0 ml with water. The solutions were allowed to stand overnight after the addition of the substance to be studied. Polarograms were taken

by passing purified nitrogen through the solutions for about 10 min. One set of observations was taken for each dye without the additive.

RESULTS AND DISCUSSION

Assuming that the horizontal line in the plot of $-\Delta \log_{10} i_d$ vs. $\log_{10} C$ corresponds to an aggregation number equal to one and any deviation from it indicates the aggregation of the dye molecule¹, the following information regarding the molecular state of the dye at different concentrations and in the presence of various additives is obtained.

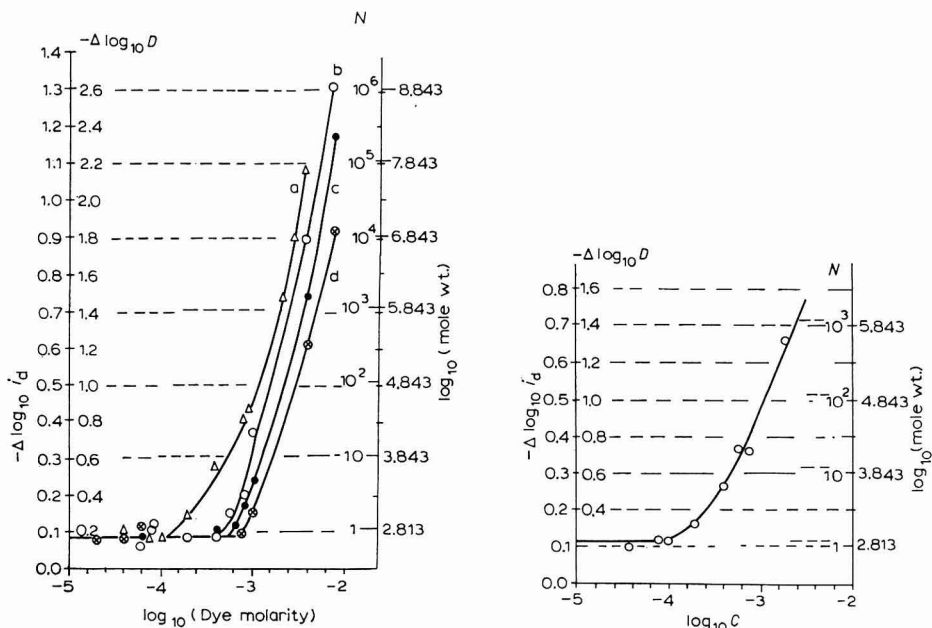


Fig. 1. Effect of urea on aggregation number of congo red. (a), Congo red; (b), +1; (c), +3; (d), +6 M urea. N = aggregation number.

Fig. 2. Effect of 10% methanol on aggregation number of congo red. N = aggregation number.

TABLE 1

EFFECT OF UREA AND FORMAMIDE ON THE AGGREGATION NUMBER OF CONGO RED

Dye concn. ($\cdot 10^{-4} M$)	Urea (M)				Formamide (M)		
	0.0	1.0	3.0	6.0	0.6	1.2	2.4
2.0	2	I	I	I	I	I	I
4.0	7	I	I	I	I	I	I
6.0	13	2	I	I	2	I	I
8.0	32	3	2	I	3	2	I
10.0	40	20	5	2	4	3	I
20.0	1437	361	51	14	144	114	10
40.0	(tendency to precipitate)	8080	1437	322	3216	2277	287

Congo red

It is seen from Fig. 1, curve a, that congo red remains in the unaggregated form below $1.0 \cdot 10^{-4} M$. Above this concentration, there is a steep rise in the $-\Delta \log_{10} i_d$ vs. $\log_{10} C$ curve, showing that the aggregation number varies widely within a narrow concentration range.

The results given in Table 1 show that a five-fold increase in concentration results in a very large increase (from 7 to 1437) in the aggregation number. Furthermore, the aggregation number is very much affected by the presence of the additives. Thus the aggregation number of a $10.0 \cdot 10^{-4} M$ congo red solution is reduced from 40 to 20 in presence of 1 M urea and the dye exists as a dimer in 6 M urea. Similarly, the aggregation number of $20.0 \cdot 10^{-4} M$ congo red solution is reduced from 1437 to 10 in 2.4 M formamide.

Methanol also affects the aggregation number, but its effect can only be realised at higher dye concentrations ($20.0 \cdot 10^{-4} M$) where a marked change from 1437 to 443 is observed with 10% alcohol (Fig. 2).

Crystal violet

The aggregational behaviour of crystal violet is quite different from that of congo red. From the plot of $-\Delta \log_{10} i_d$ vs. $\log_{10} C$ (Fig. 3), it is seen that the dye remains in an unaggregated form below $4.0 \cdot 10^{-5} M$ whereas congo red remains in an unaggregated form up to a much higher concentration, *viz.*, $1.0 \cdot 10^{-4} M$. In this case

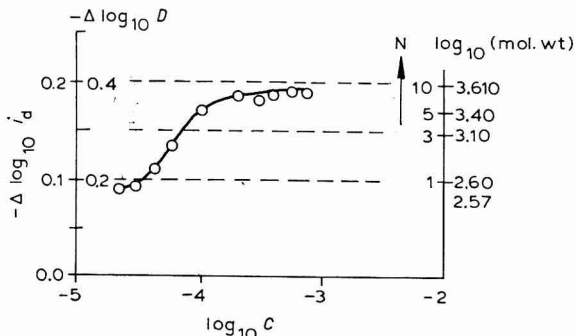


Fig. 3. Aggregation number of crystal violet alone. N = aggregation number.

the deviation from the horizontal line is very little and the aggregation number does not go beyond 6 even with a three-fold increase in dye concentration. Moreover, unlike congo red, the aggregation number does not continue to increase with dye concentration but reaches a constant value at a certain concentration. Also, the effect of additives on the aggregation of crystal violet is remarkably high, so that in presence of 3 M urea, and 1.2 M formamide, the dye exists as a dimer (Table 2).

The addition of methanol to the dye also brings about a reduction in the aggregation number. But here again, like congo red, this behaviour is observed at higher concentrations.

The effect of additives on the dye aggregation is more clearly observed by computing the data on aggregation point and dye concentration for an aggregate of

TABLE 2

EFFECT OF UREA, FORMAMIDE AND METHANOL ON THE AGGREGATION NUMBER OF CRYSTAL VIOLET

Dye concn. ($\cdot 10^{-4} M$)	Urea (M)				Formamide (M)		Methanol %	
	0.0	1.0	3.0	6.0	0.6	1.2	10	20
0.4	I	I	I	I	I	I	I	I
0.6	2	I	I	I	I	I	I	I
0.8	3	I	I	I	I	I	I	I
1.0	5	I	I	I	5	I	I	I
2.0	6		I	5	I	I	I	I
3.0	6	6	2	5	2	3	I	

TABLE 3

EFFECT OF UREA AND FORMAMIDE ON THE AGGREGATION POINT AND CONCENTRATION OF AN AGGREGATE OF 1000 MOLECULES OF CONGO RED

Additive	Additive concn. (M)	Aggregation point ($\cdot 10^{-4} M$)	Concn. of an aggregate ($\cdot 10^{-4} M$)
Urea	0.0	1.0	20.0
	1.0	4.0	22.7
	3.0	6.0	36.4
	6.0	8.0	50.0
Formamide	0.6	2.0	31.7
	1.2	4.0	36.4
	2.4	10.0	50.0

TABLE 4

EFFECT OF UREA, FORMAMIDE AND METHANOL ON THE AGGREGATION POINT AND CONCENTRATION OF AN AGGREGATE OF 5 MOLECULES OF CRYSTAL VIOLET

Additive	Additive concn. (M)	Aggregation point ($\cdot 10^{-4} M$)	Concn. of an aggregate ($\cdot 10^{-4} M$)
Urea	0.0	0.4	1.0
	1.0	1.0	2.4
	3.0	2.0	5.0
	6.0	2.5	5.0
Formamide	0.6	0.6	1.0
	1.2	2.0	4.0
Methanol	10%	2.0	4.0
	20%	4.0	6.0

a fixed number (1000 molecules in the case of congo red and 5 molecules in the case of crystal violet) of dye molecules.

From Table 3 it is evident that both the aggregation point and dye concentration for an aggregate is increased with increasing addition of additive. Similar behaviour is observed with crystal violet (see Table 4).

The increase in the aggregation point (and thus also the concentration of the

dye required to aggregate the fixed number of molecules) can be attributed to the breaking of the water structure by the addition of urea, formamide, and methanol. Their addition not only brings about the weakening of hydrophobic bonding between the molecules of the dye aggregate, but results in enhanced peptization. At higher concentrations where the dye would normally be precipitated, its dispersion in non-aggregated form takes place by the addition of substances that are known to shift the $n \text{ H}_2\text{O} \rightleftharpoons (\text{H}_2\text{O})_n$ equilibrium towards the left-hand side.

The different additives affect the aggregation point to different extents. This may be attributed to factors like polymerization, dielectric constant, viscosity, interfacial tension, etc., of the additive solutions. For example, amides that are polymerized at a lower concentration than urea cannot be used in larger quantities to suppress aggregation.

Similarly in the water-methanol system, few methanol molecules may penetrate into the aggregate owing to the partition equilibrium bringing about disaggregation. The addition of large amounts, however, affects the solvent property, and precipitation of the dye takes place with the result that the aggregation point cannot be shifted to higher dye concentration.

The effect of urea seems to be quite general in preventing the aggregation of dye molecules of very different chemical constitutions. GHOSH AND MUKERJEE² observed that the solubility of Orange OT, a highly insoluble non-ionic azo dye is increased by a factor of roughly 10 in 10 M urea. ALEXANDER AND STACEY³ investigated several highly aggregating acidic and basic dyes and found that urea usually causes extensive disaggregation. Further, GHOSH AND MUKERJEE pointed out that in the presence of urea, the transfer of methylene blue into a solid form or into a non-aqueous environment, or the association of methylene blue to form aggregates, are all less favourable because of less gain in entropy. They observed a marked lowering in the aggregation of pinacyanol chloride in the presence of urea.

ACKNOWLEDGEMENT

The authors are grateful to C.S.I.R. (India) for the award of a fellowship to one of us (P.C.) to carry out this work.

SUMMARY

The effect of the additives, urea, formamide and methanol on the aggregation of congo red and crystal violet have been studied polarographically. The aggregation number of the dyes has been found to be very much lowered in the presence of varying amounts of the additives; these increase the aggregation point and also the concentration of the dye required to aggregate a fixed number of molecules. This has been attributed to the breaking of the water structure.

REFERENCES

- 1 P. J. HILSON AND R. B. MCKAY, *Trans. Faraday Soc.*, 61 (1965) 375.
- 2 A. K. GHOSH AND P. MUKERJEE, *J. Phys. Chem.*, 67 (1963) 193.
- 3 P. ALEXANDER AND K. A. STACEY, *Proc. Roy. Soc. (London)*, A212 (1952) 274.

SHORT COMMUNICATIONS**Polarographic studies on the binding of copper(II) and cadmium(II) with ovalbumin**

A number of workers^{1–6} have used the polarographic technique for studying the binding of metal ions to both the globular and keratin types of proteins. A literature survey indicates that, so far, little work has been done on the binding of metal ions to ovalbumin, which is a protein of high biological activity and is easily available in a well characterised form. The present communication reports on the polarographic investigation of the binding of Cu²⁺ and Cd²⁺ with ovalbumin.

Experimental

Reagents and solutions. A solution of ovalbumin (E. Merck) was prepared in doubly-distilled water. The solution was centrifuged and its concentration determined by drying a known aliquot in an air oven at 105°. Solutions of AnalaR cupric chloride and cadmium chloride were prepared in doubly-distilled water. The copper content of the stock solution was determined gravimetrically; cadmium was estimated complexometrically with EDTA using eriochrome black T as indicator. A 1.0 M solution of AnalaR potassium chloride was used for maintaining the ionic strength at 0.15.

Ammonium acetate-acetic acid and ammonium chloride-ammonia buffers were prepared by mixing ammonium acetate and acetic acid (each 0.2 M) and ammonium chloride and ammonia (each 0.5 M), respectively.

Polarographic measurements were made with a Heyrovsky LP 55A polarograph in conjunction with a Pye Galvanometer in the external circuit. The polarograph was used manually. An H-shaped polarographic cell was found to be suitable for de-aeration of the protein solution without denaturation. Purified nitrogen was passed for 15–20 min in each case to remove oxygen. Triply-distilled mercury (A.R.) was used for the dropping electrode. The capillary used had a flow rate of 2.2 mg/sec with a drop-time of 3.5 sec. The temperature of the solution was maintained at 30±0.1° by keeping the cell immersed in a water thermostat.

The reversibility of the waves was tested by TOMES' method⁷.

Results and discussion

The molecular weight of ovalbumin was taken as 45,000. The number of metal ions bound per protein molecule (V_M) was computed from Tanford's equation:

$$i_d/(i_{d0}) = (C_F + kC_b)/C_0$$

where C_F , C_b and C_0 are the free, bound and total metal concentrations, $i_d/(i_{d0})$ is the ratio of diffusion currents in the presence and absence of protein for a given system and k is a constant which can be evaluated from the limiting value of $i_d/(i_{d0})$. The values of k for copper and cadmium, obtained from Figs. 1A and 2A are 0.3 and 0.7, respectively. The results for hydrogen ion equilibria studies of ovalbumin have been taken from literature⁸.

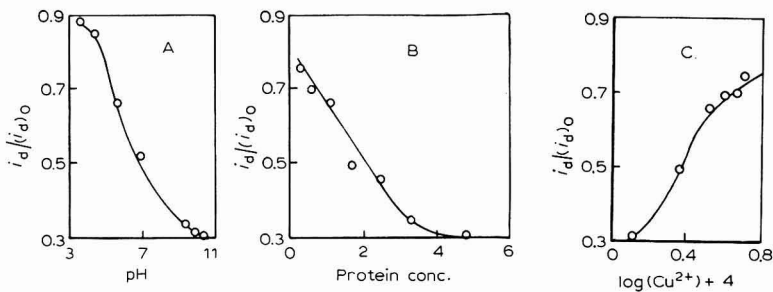


Fig. 1. Copper-ovalbumin system. A. Effect of pH. Protein concn., $1.111 \cdot 10^{-4} M$; Cu^{2+} concn., $3.333 \cdot 10^{-4} M$; ionic strength, 0.15. B. Effect of protein concn. Cu^{2+} concn., $3.333 \cdot 10^{-4} M$; ionic strength, 0.15; pH of acetate buffer, 5.57; protein concn. varied (0.000, 0.277, 0.555, 1.111, 1.666, 2.500, $3.333 \cdot 10^{-4} M$, 4.755). C. Effect of metal ion concn. Protein concn., $1.111 \cdot 10^{-4} M$; pH of acetate buffer, 5.57; ionic strength, 0.15; Cu^{2+} concn. varied ($1.333 \cdot 10^{-4} M$, $2.333 \cdot 10^{-4} M$, $3.333 \cdot 10^{-4} M$, $3.999 \cdot 10^{-4} M$, $4.666 \cdot 10^{-4} M$, $5.333 \cdot 10^{-4} M$).

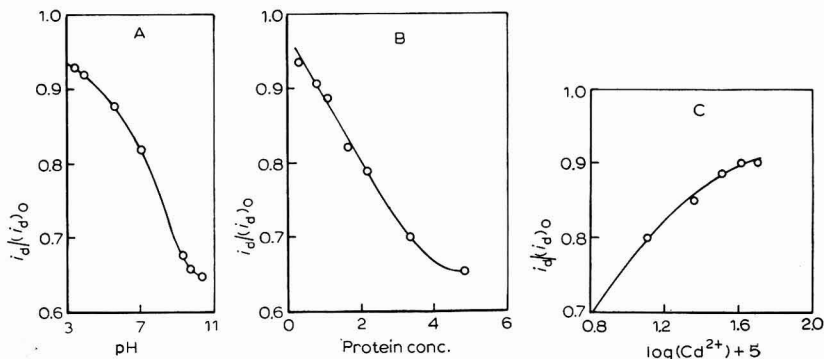


Fig. 2. Cadmium-ovalbumin system. A. Effect of pH. Protein concn., $1.111 \cdot 10^{-4} M$; Cd^{2+} concn., $3.333 \cdot 10^{-4} M$; ionic strength, 0.15. B. Effect of protein concn. Cd^{2+} concn., $3.333 \cdot 10^{-4} M$; ionic strength, 0.15; pH of acetate buffer, 5.57; protein concn. varied (0.000, 0.277, 0.555, 1.111, 1.666, 2.222, $3.333 \cdot 10^{-4} M$, 4.755). C. Effect of metal ion concn. Protein concn., $1.111 \cdot 10^{-4} M$; pH of acetate buffer, 5.57; ionic strength, 0.15; Cd^{2+} concn. varied ($0.666 \cdot 10^{-4} M$, $1.333 \cdot 10^{-4} M$, $2.333 \cdot 10^{-4} M$, $3.333 \cdot 10^{-4} M$, $3.999 \cdot 10^{-4} M$, $4.999 \cdot 10^{-4} M$).

Copper-ovalbumin system. It is clear from Fig. 1A that although there is small decrease in the diffusion current in the pH-range 3.5–4.4, a large decrease is observed at pH 5.57, with a subsequent increase in C_b . At pH 5.57, all the carboxyl groups of ovalbumin will be deprotonated and thus will be available for interaction with the metal ions. The results show that copper ions are bound to the carboxyl groups of the protein. The intrinsic association constant (K) has been calculated by Scatchard's equation and the log K -value of 2.23 for metal-carboxyl interaction is similar to that of the first association constant of the copper-acetate complex⁹.

At pH-values above 5.5, imidazole groups from histidine residues lose their protons and are thus available for interaction. The large decrease in diffusion current at pH 7.0 indicates clearly that cupric ions are taking part in an interaction with the imidazole groups of the protein. The log K -value of 3.35 for the interaction of Cu^{2+} with the imidazole groups of the protein is, however, somewhat smaller than the logarithm of the first association constant of the copper-imidazole system⁹.

Cadmium-ovalbumin system. Figure 2A shows clearly the binding of cadmium ions to the carboxyl as well as to the imidazole groups of the protein, since an appreciable decrease in diffusion current is observed at pH 5.57 and 7.0. The log *K*-values calculated by Scatchard's equation for the cadmium-carboxyl and cadmium-imidazole systems of the protein are 1.93 and 2.90, respectively.

The order of reactivity of these metals with the carboxyl as well as imidazole groups of the protein is:



A comparison of the log *K*-values for different systems is given in Table 1.

TABLE 1

COMPARISON OF LOG *K*-VALUES FOR DIFFERENT SYSTEMS

<i>Ligand</i>	<i>Method</i>	<i>log K (carboxyl groups)</i>		<i>log K (imidazole groups)</i>	
		<i>Cu²⁺</i>	<i>Cd²⁺</i>	<i>Cu²⁺</i>	<i>Cd²⁺</i>
Ovalbumin	Polarographic	2.23 ^a	1.93 ^a	3.35 ^a	2.90 ^a
T. Gelatin	Equilibrium dialysis	2.18 ^b	1.96 ^b	3.40 ^b	—
Acetate	—	2.16 ^c	1.30 ^c	—	—
Imidazole	—	—	—	4.36 ^c	2.80 ^c

^a Present studies. ^b Ref. 10. ^c Ref. 9.

Acknowledgement

One of the authors (M.R.J.) thanks the U.G.C., New Delhi for financial assistance.

Department of Chemistry,
University of Roorkee,
Roorkee, U.P. (India)

WAHID U. MALIK
M. R. JINDAL

- 1 C. TANFORD, *J. Am. Chem. Soc.*, 74 (1952) 211.
- 2 C. TANFORD AND J. EPSTEIN, *J. Am. Chem. Soc.*, 76 (1954) 2170.
- 3 M. S. N. RAO AND H. LAL, *J. Am. Chem. Soc.*, 80 (1958) 3222.
- 4 H. A. SAROFF AND H. J. MARK, *J. Am. Chem. Soc.*, 75 (1953) 1420.
- 5 W. U. MALIK AND M. MUZAFFARUDDIN, *J. Electroanal. Chem.*, 6 (1963) 214-220.
- 6 W. U. MALIK AND SALAHUDDIN, *J. Electroanal. Chem.*, 5 (1963) 147-151.
- 7 J. TOMES, *Collection Czech. Chem. Commun.*, 9 (1937) 12.
- 8 R. K. CANNAN, A. KIBRICK AND A. M. PALMER, *Ann. N.Y. Acad. Sci.*, 41 (1941) 243; R. K. CANNAN, *Chem. Rev.*, 30 (1942) 395.
- 9 *Advances in Protein Chemistry*, edited by M. L. ANSON, K. BAILEY AND J. T. EDSALL, Academic Press, New York, 11 (1956) 351.
- 10 W. U. MALIK AND M. MUZAFFARUDDIN, *Australian J. Chem.*, 18 (1965) 1397-1404.

Received March 5th, 1968; in revised form, May 3rd, 1968

J. Electroanal. Chem., 19 (1968) 436-438

Adsorptionseffekte bei Bildung von Quecksilber-Alkylverbindungen im Zuge polarographischer Reduktionsprozesse

Wie an anderer Stelle kurz berichtet¹ bewirkt eine Reaktion primär gebildeter Radikale mit dem Kathoden-Quecksilber bei polarographischer Reduktion von Methylvinylketon eine charakteristische Beeinflussung der Tropfzeitkurven.

Für das Methylvinylketon (Butenon) wurde szt. gezeigt, dass die Reduktion an Hg-Elektroden in sauerem Medium in einem einelektronigen Prozess zu einer Quecksilber-Alkylverbindung führt². Potentiostatische Elektrolysen in präparativem Ausmass liessen als Reduktionsprodukt $\text{Hg}(\text{CH}_2\text{CH}_2\text{COCH}_3)_2$ feststellen.

Elektrokapillarkurven des Quecksilbers — durch Tropfzeitmessung — zeigen bei der Reduktion organischer Stoffe gegenüber jenen in der Grundlösung (ohne Depolarisator) in der Regel einen geänderten Verlauf, und zwar derart, dass vor der Reduktion, also bei Potentialen positiver als das Reduktionspotential, eine Erniedrigung der Grenzflächenspannung (Verkürzung der Tropfzeit) eintritt, während nach der Reduktion die Tropfzeitkurven meist keinen merklichen Unterschied gegenüber der reinen Grundlösung aufweisen. Das heisst, dass allgemein der Depolarisator im Zustand "Ox" stärker am Hg adsorbiert ist als im Zustand "Red". Bei Ketonen entspricht das der grösseren Lösungstendenz der resultierenden OH-Verbindungen in den wässrigen Lösungen. Ein solcher Verlauf lässt sich am Beispiel des Benzophenons aufzeigen (Abb. 1). Die beachtliche Erniedrigung der Grenzflächenspannung vor der Reduktion weist auf die starke Adsorption des Depolarisators hin, während bei negativeren Potentialen, die eine Durchreduktion bewirken, keine merklichen Tropfzeitverkürzungen auftreten. Am Tropfenende liegt danach praktisch keine merkliche Adsorption des Reduktionsprodukts vor. Dieser Befund steht auch im Einklang mit seinerzeitigen Untersuchungsergebnissen betreffend die Inhibition der Nitrogruppenreduktion durch adsorbierte Fremdstoffe, wobei das Benzophenon nur bis zu seiner eigenen Reduktion als Inhibitor wirkt³.

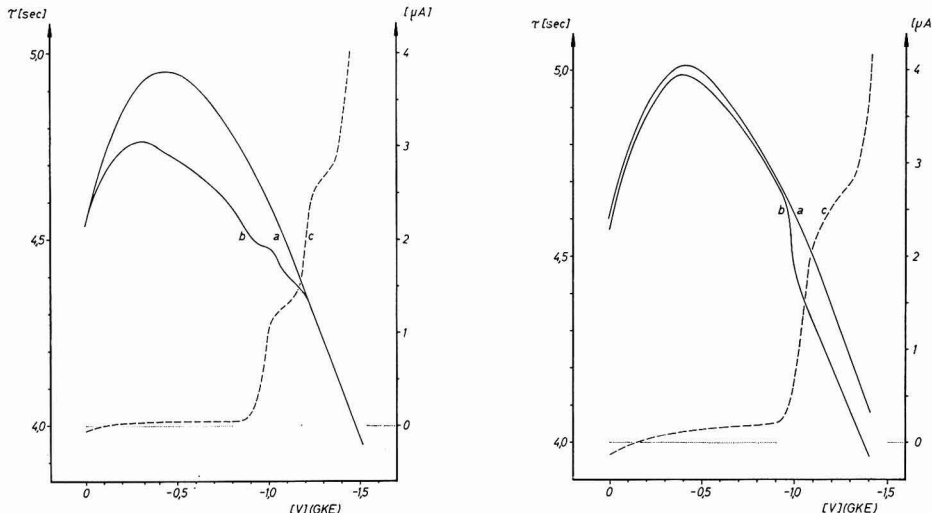


Abb. 1-2. Tropfzeitkurven (b) und Polarogramme (c) von: (1) $5 \cdot 10^{-4} M$ Benzophenon; (2) $10^{-3} M$ Methylvinylketon; in Citratpuffer pH 3.2, 20% Methanol. Kurve (a): Grundlösung Citratpuffer.

Anders liegen die Verhältnisse bei dem konjugiert ungesättigten Methylvinylketon. Hier ist eine entgegengesetzte Änderung der Tropfzeitkurve im Zuge der Reduktion festzustellen (Abb. 2). Während in saueren Lösungen im Zustand "Ox" keine wesentliche Erniedrigung der Grenzflächenspannung auftritt (Hinweis auf nur geringe Adsorption), kommt es im Potentialbereich der einelektronigen Reduktion des Ketons zu einer starken Erniedrigung der Grenzflächenspannung (Tropfzeitverkürzung). Es entspricht dies der Adsorption des Primärprodukts, bzw. der gebildeten Quecksilber-Alkylverbindung. Dieser Befund steht in Übereinstimmung mit Ergebnissen von BENESCH UND BENESCH⁴, die bei der Reduktion organischer Quecksilberverbindungen auch eine beachtliche Adsorption feststellten. Die Änderung der Grenzflächenspannung findet ihre Parallele in den Wechselstrompolarogrammen nach Breyer, die als Mass für die Doppelschichtkapazität bei Vorliegen von "Ox" und "Red" heranziehbar sind. Während die Kapazitätserniedrigung gegenüber den Grundlösungen bei Benzophenon im positiveren Potentialbereich (wo "Ox" vorliegt) auftritt, wird sie im Falle des Methylvinylketons im Bereich des Reduktionsproduktes—also negativer als das Halbstufenpotential — beobachtet (siehe Abb. 3a und 3b).

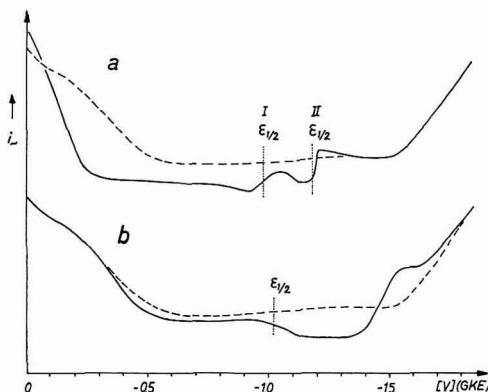


Abb. 3. Wechselstrompolarogramme (a) von Benzophenon und (b) von Methylvinylketon (jeweils $5 \cdot 10^{-4} M$ in Citratpuffer pH 3.25, 20% Methanol). Die gestrichelte Kurve bezieht sich auf die zugehörige Grundlösung.

Die Veränderungen der Tropfzeitkurven—wie auch die Wechselstrompolarogramme—sind danach in entsprechenden Fällen zum Nachweis von radikalstabilisierenden Merkierungsreaktionen heranziehbar.

Chemisches Institut der Phil.-Theol. Hochschule, Bamberg (Deutschland) L. HOLLECK

- 1 L. HOLLECK, *Intern. Congr. of Polarography, Kyoto, 1966*, Polarographic Society of Japan, Kyoto, Abstr. S. 18.
- 2 L. HOLLECK UND D. MARQUARDING, *Naturwissenschaften*, 49 (1962) 468; D. MARQUARDING Diplomarbeit, Univ. Hamburg, 1961.
- 3 L. HOLLECK UND H. J. EXNER, *Z. Naturforsch.*, 6a (1951) 763.
- 4 R. E. BENESCH UND R. BENESCH, *J. Phys. Chem.*, 56 (1952) 648.

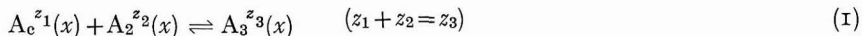
Eingegangen am 25 Mai, 1968

Ion-pairing in strong electric fields

There is, at present, increasing evidence to show that ion-pairing constitutes a concomitant rate-determining factor in electrode kinetics¹. Diagnosis of such ion association relies merely on the concept of reduced electrostatic interactions with the diffuse layer ψ -potential owing to the decreased charge of the depolarizing species.

However, no serious consideration has been given so far to the problem of occurrence of water structure enforced ion-pairing in an electric field. Only field-induced dissociation has been sometimes invoked², but this effect by itself would amount to decreasing ion-pairing at high field strengths at the electrode, to values inconsistent with the experimental facts recorded by GIERST *et al.*¹. In order to discuss briefly this question no attention will be paid, in the following tentative treatment, either to the influence of specific electrode-bound water or to particular double-layer models or to the difficult task of determining activity coefficients in the field³.

Let us, therefore, examine an ion-pairing reaction at equilibrium



where z_n is the ionic charge of species A_n ($n=1, 2, 3$), and $\psi(x)$ is the electrostatic potential at position x . The corresponding local macroscopic field, $E(x)$, and polarization, $P(x)$, are directed along the x -axis. On $x=x_b$, at some distance from x , $\psi(x_b)$, $E(x_b)$ and $P(x_b)$ vanish. In the treatment it will be further postulated that $P(x)$ decomposes at equilibrium into

$$P(x) = P_0(x) + P_i(x) \quad (2)$$

The polarization, $P_0(x)$, pertains exclusively to the medium (solvent, A_1 and A_2) surrounding A_3 . The term $P_i(x)$ then corresponds to the actual average internal dipole moment per unit volume of the pairs A_3 in the field. From the suggested definition of $P_0(x)$ we get:

$$P_0(x)/E(x) = [\epsilon_0(x) - 1]/4\pi \quad (3)$$

For the study at high field strengths of the integral dielectric permittivity, $\epsilon_0(x)$, related to $P_0(x)$, a theoretical expression due to BOOTH⁴⁻⁶ is used:

$$(\epsilon_0(x) - \epsilon_0^\infty) = (\epsilon_0^0 - \epsilon_0^\infty)(3/y)L(y) \quad (4)$$

where $L(y) \equiv \operatorname{ctnh} y - y^{-1}$, $y = (bE^2)^{1/2}$, and $\epsilon_0^0(x)$ and ϵ_0^∞ are, respectively, the static permittivity at zero field strength and the limit of ϵ_0 for water when orientation polarization becomes saturated ($\epsilon_0^\infty \approx 5.5$). In pure water b is $5.65 \cdot 10^{-8}$ e.s.u.⁻². The ionic strength dependence of b will be needed. It is therefore assumed that

$$b = h(\epsilon_0^0(x) - \epsilon_0^\infty)^l \quad (1 \leq l \leq 2) \quad (5)$$

where, according to the results in pure water, $h = 5.65 \cdot 10^{-8}(73)^{-l}$ e.s.u.⁻².

Some reasons for adopting eqn. (5) are embodied in the facts that (a) at small field and ionic strengths eqn. (4) combined with (5) enables some qualitative agreement with theoretical expressions to be reached⁵ for the slope of $\epsilon_0^0(x)$ vs. E ,

and (b) the onset of dielectric saturation occurs at increasing E with increasing ionic strengths, as expected theoretically⁵ and from frequency response measurements in aqueous electrolyte solutions⁷. The latter experiments have further led to the assumption of a linear concentration-dependence of $\varepsilon_0^0(x)$ at ionic concentrations, c_n , less than $2 M^*$, thus

$$\varepsilon_0^0(x) = \varepsilon_s^0 + \sum_n c_n(x) (\partial \varepsilon_0^0 / \partial c_n)_{T,p} \quad \text{for } n' \neq n \quad (6)$$

where p is the hydrostatic pressure, ε_s^0 the dielectric constant of pure water and δ_n are usually negative quantities yielding a more or less important decrement of $\varepsilon_0^0(x)$, whether A_n is ordering the solvent in its own field or is acting as a solvent structure disturbing center, or producing a large cavity of small dipole moment.

In order to calculate the free energy density, $f(x)$, a path can be imagined leading first to $P_i(x)$, keeping $P_0(x) = 0$, and generating afterwards some charging of $P_0(x)$ from zero to its final value. In this way, the first step virtually amounts to switching off $E(x)$ around A_3 . Consequently, the chemical potential would be

$$\begin{aligned} (\partial f(x) / \partial c_n)_{T,P} &= \mu_n^0(T, P_i(x), \sum_n c_n(x)) + \\ &RT \ln a_n(P_i(x)) + \left[\partial / \partial c_n \left(\int_0^{P_0(x)} E(x) dP(x) \right)_{T,P} \right]_{n', s \neq n} \end{aligned} \quad (7)$$

Equation (7) is valid for $n = 1, 2, 3$ and s , s denoting the solvent. The quantities, μ_n^0 and a_n , correspond to the standard chemical potential and to the activity, both being defined in a system where A_3 takes its inner equilibrium configuration in $E(x)$ even though the solvent remains virtually unaffected by $E(x)$. Introduction of eqn. (3) into (7) gives⁸:

$$\begin{aligned} \mu_n(T, P(x), \sum_n c_n(x)) &= \mu_n^0(T, P_i(x), \sum_n c_n(x)) + \\ &RT \ln a_n(P_i(x)) - \frac{1}{8\pi} \int_0^{E^2} \left(\frac{\partial \varepsilon_0}{\partial c_n} \right)_{T, \sum_n c_n(x), E} dE^2 \quad (n = 1, 2, 3, s) \end{aligned} \quad (8)$$

Furthermore, the integrand in eqn. (8) becomes

$$(\partial \varepsilon_0 / \partial c_n)_{T, \sum_n c_n(x), E} = \delta_n + (v_n/v_s) (\partial \varepsilon_0 / \partial c_s)_{T, \sum_n c_n(x), E} \quad (9)$$

where v_n and v_s are, respectively, the partial molar volume of A_n and of the solvent.

The diffusion equilibrium condition is written as follows:

$$(v_n/v_s) \mu_s(x) + \mu_n(x_b) = (v_n/v_s) \mu_s(x_b) + \mu_n(x) + z_n F \psi(x) \quad (n = 1, 2, 3) \quad (10)$$

The dissociation equilibrium constant is obtained in terms of activities in not too concentrated solutions if eqns. (1), (4), (5), (6), (8), (9) and (10) are used, thus

$$K_a(x) = a_1(x) a_2(x) / a_3(x) = K_a(x_b) F_3(E(x)) \exp \left[\frac{3\delta}{8\pi RT b} \left(lyL(y) - 2(l-1) \log \left(\frac{\sinhy}{y} \right) \right) \right] \quad (11)$$

* Non-linear effects have been considered by NÜRNBERG who kindly communicated us his data.

where $\delta = \delta_1 + \delta_2 - \delta_3$ and $F_3(E(x)) = \exp [\mu_3^0(x) - \mu_3^0(x_b)]/RT$.

The value of $F_3(E(x))$ can be reduced to some suitable form by assuming Onsager's theory of dissociation at high field strengths. This theory ultimately relies on pure electrostatic enforced ion-pairing in absence of ionic atmosphere effects. Furthermore, it makes no provision for solvation in the external field, which leads to increasing free energy (if $\delta_n \ll 0$) as indicated in eqn. (8). For a binary electrolyte, the relative increase of dissociation rate becomes, according to ONSAGER AND WIEN⁹:

$$F_3(E(x)) = J_1\{2i[E(x)|z_1|^3/(kT)^2\varepsilon_0^0(x)]^{1/2}\}/2i\{E(x)|z_1|^3/(kT)^2\varepsilon_0^0(x)\}^{1/2} \quad (12)$$

where J_1 is the Bessel function of order one. Referring to eqn. (11), it is observed that the effect of $F_3(E(x))$ might be overruled and the process reversed towards association if $\delta \ll 0$. The values of $\log K_a(x)/K_a(x_b)$ have been plotted *versus* E for different conditions in Figs. 1 and 2*, and it can be seen that Onsager's dissociation

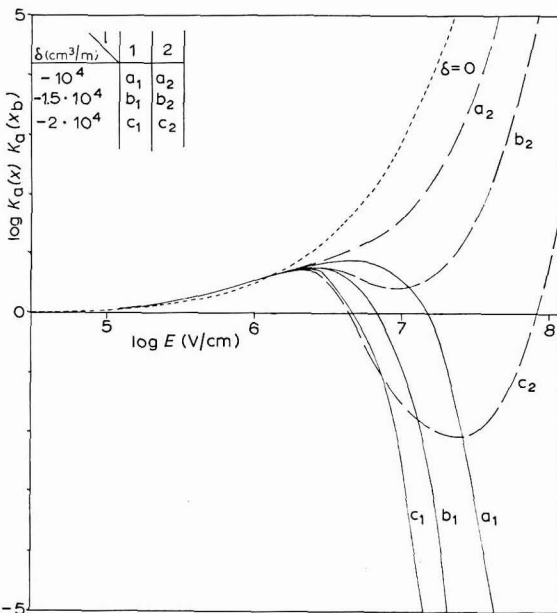


Fig. 1. Log $K_a(x)/K_a(x_b)$ vs. the electric field for $z=1$ and $T = 25^\circ$, $|z_1| = 1$, $\langle \varepsilon_0^0(x) - \varepsilon_0^\infty \rangle = 73 + 15 \cdot 10^{-3} \delta$.

effect subsists at fields $< 10^6$ V cm⁻¹. However, at larger field strengths and very negative values of δ , the reverse trend towards association prevails and goes through a maximum, provided that $l \approx 2$. At the maximum, therefore only for $l \rightarrow 2$, the onset of dielectric saturation due to $E(x)$ acts in such a way as to keep ε_0 almost unaffected by ionic solvation, thus sharply reducing any further occurrence of solvent enforced ion-pairing.

* In order to compute roughly the concentration effect on y in eqn. (11) and on $\varepsilon_0^0(x)$ in eqn. (12), eqn. (6) has been used assuming arbitrarily that, in average at x , $\sum_n \delta_n c_n(x) \approx \delta 15 \cdot 10^{-3}$.

Therefore, in Figs. 1 and 2, at small field strengths, dissociation for finite δ is slightly above that for $\delta=0$. NÜRNBERG has used for $c(x)$ a corrected Gouy-Chapman distribution².

This rough calculation indicates that at the electrode near the outer Helmholtz layer boundary where the field strength might be quite large ($\approx 10^7$ V/cm), association would occur, as indicated by GIERST¹, depending on the abilities of the ions to interact with the solvent. The converse applies to the case of dissociation rates of weak acids measured by means of fast electrochemical relaxation methods², since then the average field strength in the thin reaction layer remains comparatively small.

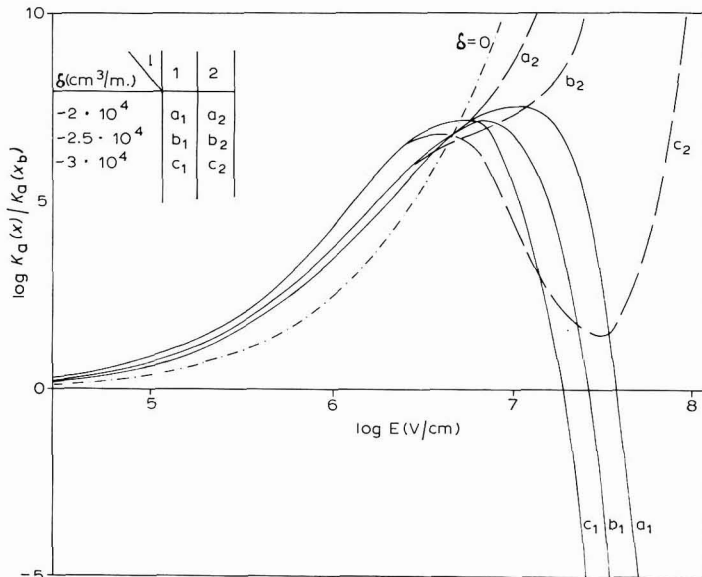


Fig. 2. Log $K_a(x)/K_a(x_b)$ vs. the electric field for $z=2$ and $T = 25^\circ$, $|z_1| = 2$, $\langle \epsilon_0^0(x) - \epsilon_0^\infty \rangle = 73 + 1.5 \cdot 10^{-3} \delta$.

The calculations need further implementation as follows:

(i) By improving the model for $F_3(E)$. For example, the presence of ϵ_0^0 in eqn. (12) is doubtful. An estimate of this effects results from the plot in Fig. 2 which is also valid for the conditions $z=1$ provided that $\epsilon_0^0/8$ be inserted in eqn. (12) instead of ϵ_0^0 .

(ii) By estimating the role of the activity coefficients implicated in $a_n[P_1(x)]$. If, in high field strengths, the ionic atmosphere is broken up, this calculation would rely essentially on interactions of the cavity field type³.

(iii) By considering that protolysis of water at very high field strengths narrows the limits of applicability of eqn. (4).

Acknowledgement

The authors greatly appreciate the help of Mrs. STROSBERG-LEUWENKROON who performed several calculations used in this work.

They are also indebted to Professor L. GIERST and to Professor H. W. NÜRNBERG for stimulating discussions.

Faculty of Science,
Free University of Brussels (Belgium)

A. JENARD
H. D. HURWITZ

- 1 L. GIERST, L. VANDENBERGHEN, E. NICOLAS AND A. FRABONI, *J. Electrochem. Soc.*, 113 (1966) 1025.
- 2 H. W. NÜRNBERG, *Discussions Faraday Soc.*, 39 (1965) 136.
- 3 G. M. BELL AND S. LEVINE, *Chemical Physics of Ionic Solutions*, edited by B. E. CONWAY AND R. G. BARRADAS, John Wiley, New York, 1966, p. 409.
- 4 D. C. GRAHAME, *J. Chem. Phys.*, 18 (1950) 903; 21 (1953) 1054.
- 5 F. BOOTH, *J. Chem. Phys.*, 19 (1951) 391, 1327, 1615.
- 6 E. GLUECKAUF, *Chemical Physics of Ionic Solutions*, edited by B. E. CONWAY AND R. G. BARRADAS, John Wiley, New York, p. 67.
- 7 J. HASTED, D. RITSON AND C. COLLIE, *J. Chem. Phys.*, 16 (1948) 1.
- 8 A. SANFELD AND R. DEFAY, *Physica*, 30 (1964) 2232.
- 9 H. S. HARNEY AND B. B. OWEN, *The Physical Chemistry of Electrolytic Solutions*, Reinhold Pub. Corp., New York, 3rd ed., 1958, pp. 138 and 321.

Received June 21st, 1968

J. Electroanal. Chem., 19 (1968) 441-445

Computer program for the error function of complex argument

The error function complement of a complex argument is obtained, for certain range of parameters, in the solution of some diffusion problems in electrode kinetics. This is often the case when charging of the double layer is considered in non-steady-state perturbation methods. Such a function with complex argument had to be computed in a recent study, using the galvanostatic single pulse method, of the Hg(I)/Hg reaction with specific adsorption of reactant¹. A Fortran IV sub-routine was prepared to allow computer analysis of experimental results. Detailed tables of the exponential error function complement of complex argument are available², but they cannot be used directly in a computer analysis.

The sub-routine is based on a seventh-order interpolation between a limited number of values, taken from the tables of FADDEYEVA AND TERENT'EV². The program gives values accurate within $4 \cdot 10^{-6}$ at high speed. A CDC 6600 computer computes 1000 values within 1 sec. A write-up and the program itself is available*.

Acknowledgement

This work was supported by the Office of Naval Research.

New York University,
Department of Chemistry,
New York, 10003 (U.S.A.)

D. J. KOOIJMAN

¹ D. J. KOOIJMAN, *J. Electroanal. Chem.*, 19 (1968) 365.

² V. N. FADDEYEVA AND N. M. TERENT'EV, *Tables of Values of the Exponential Error Function Complement for Complex Argument*, Pergamon Press, New York, 1961.

Received May 27th, 1968

* Order NAPS Document 00054 from ASIS National Auxiliary Publications Service, c/o CCM Informations Sciences, Inc., 22 West 34th Street, New York, N.Y. 10001; remitting \$ 1.00 for microfiche or \$ 3.00 for photocopies.

The dependence of the separation factor for the hydrogen evolution reaction upon potential: Mechanism evidence for transition metal substrates

In the electrolytic hydrogen evolution reaction, recent work by BOCKRIS AND MATTHEWS¹ showed that the separation factor of hydrogen and tritium on mercury electrodes varies with the potential. This variation seems to depend upon a change in shape of the potential energy barrier of the rate-determining proton discharge step with potential, resulting in a change in the degree of tunnelling for proton and tritium.

Here, results of an examination of the potential-dependence of the separation factor when a variety of electrode catalysts is used are discussed. Generalizations are (Table 1):

(1) If the metals under consideration are in the group of "soft" metals (*e.g.*, Hg, Sn, Cd), for which a rate-determining proton transfer step has been established^{2,3}, then there is a variation of the separation factor with potential similar to that observed by BOCKRIS AND MATTHEWS (except for the special case of Cd prepared by etching in HNO_3).

(2) If the metals concerned are the transition metals (*e.g.*, Ni, Ag), there is a negligible variation of the separation factor with potential except when there is a

TABLE I

SEPARATION FACTORS AND TAFEL PARAMETERS FOR A NUMBER OF METALS AT ROOM TEMPERATURE

Metal	Solution	Separation factor variation with potential?	Overpotential range (mV)	Magnitude of separation factor	$-b$ (mV)	$-\log_{10}$ current (A cm^{-2})
Tin	1.0 N HCl	Yes	-655 to -1000	8.2-3.6	120	10.2
Tin ^a	1.0 N NaOH	No	-950 to -1100	8.0	116 220	8.0 5.4
Cadmium ^b	1.0 N HCl	Yes	-990 to -1120	6.2-4.5	115	9.5
Cadmium ^c	1.0 N HCl	No	-920 to -1120	6.8	120	10.2
Mercury	1.0 N HCl	Yes	-920 to -1150	8.8-6.2	115	12.0
Mercury	1.0 N HCl + 1.0 N $(\text{C}_3\text{H}_7)_4\text{HCl}$	Yes	-1100 to -1200	6.6-5.3	110	12.4
Mercury	1.0 N HClO_4	Yes	-940 to -1150	8.4-5.8	112	11.9
Mercury	0.5 N H_2SO_4	Yes	-950 to -1150	8.6-5.7	113	12.3
Silver ^d	1.0 N HCl	No	-660 to -1000 -220 to -360	6.3 18	68 115	7.2 5.4
Silver	1.0 N NaOH	No	-480 to -950	21	121	6.6
Nickel	1.0 N HCl	No	-560 to -800 -395 to -715	18	113	5.8
Nickel	1.0 N NaOH	No	-250 to -385	4.6	100	5.5
Iron	1.0 N HCl	No	-450 to -455 -500 to -580 -580 to -700	3.9 5.0 15.9	120	5.5
Tungsten ^d	1.0 N HCl	No	-380 to -575	3.7	66 116	7.6 5.7
Tungsten ^d	1.0 N NaOH	No	-405 to -775	6.7	70 122	7.0 6.6
Platinum	1.0 N HCl	No	-45 to -190	6.7	28	3.0

^a At high overpotentials, SnH_4 is being formed.

^b Surface prepared by heating in H_2 at 200°.

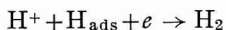
^c Surface prepared by chemical etching in conc. HNO_3 .

^d Separation factor changes occur at the potential where the Tafel slope is constant.

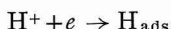
change in mechanisms of reaction, a change in the rate-determining step, or both.

Possible causes of the variation of the separation factor (s) (cf. ref. 3) with potential such as: (i) collection inefficiency of hydrogen and tritium; (ii) the existence of various exchange reactions; (iii) specific adsorption effects; and (iv) limiting diffusion of tritium, were eliminated. Thus, the existence of a dependence of s on potential seems to occur with systems having only a simple discharge step as the rate-determining process. Under such conditions, the classical factor of the separation factor is almost potential-independent, and the variation of the separation factor with potential can be explained¹ by a variation of the quantum mechanical contribution (a highly mass sensitive factor) of the separation factor with potential.

For those metals in which the separation factor is independent of potential over a certain potential range but then changes to another value at a certain potential and remains constant, it seems likely that a change of mechanism, rate-determining step, or both, cause the change of separation factor. For these metals, one must conclude that the quantum mechanical tunnelling contribution to the separation factor is constant with potential. Such a lack of the effect of proton tunnelling may arise from the different form of the potential energy surface associated with the rate-determining step:



(probable for transition metals²), compared with that for:



(probable for metals such as Hg, Sn, Cd, Pb²).

Acknowledgement

Thanks are due to Dr. S. SRINIVASAN for discussion, and to the National Aeronautics and Space Administration for financial support, under contract (NsG-325) 4-03114-3-5133.

*Electrochemistry Laboratory,
University of Pennsylvania.
Philadelphia, Pa. 19104 (U.S.A.)*

J. O'M. BOCKRIS
E. GILEADI
R. HAYNES

1 J. O'M. BOCKRIS AND D. B. MATTHEWS, *Electrochim. Acta*, 11 (1966) 143.

2 B. E. CONWAY AND J. O'M. BOCKRIS, *J. Chem. Phys.*, 26 (1957) 532.

3 J. O'M. BOCKRIS, S. SRINIVASAN AND D. B. MATTHEWS, *Discussions Faraday Soc.*, 39 (1965) 239.

Received April 11th, 1968

BOOK REVIEWS

Journal of Radioanalytical Chemistry, Elsevier, Amsterdam, Subscription £8.50d—six issues per annum, expected to give a volume of 450–500 pages.

This is a new journal for the communication of original papers, short communications, preliminary reports, and letters to the editor. The scope of the journal as envisaged by the editors comprises activation analysis, radiometric analysis, radio-reagent analysis and radiometric titration, isotope dilution analysis, β -, γ -, X-ray and neutron absorption and back-scattering, analytical separations involving radionuclides, instrumentation and automation for radioanalytical chemistry.

The specimen copy (Vol. 1, No. 1) contains five papers, a short communication, an editorial article about the activation analysis research laboratory, Texas, U.S.A., a bibliography of six topics in radioanalysis, a list of seventeen papers received and a "tear out" reprint of the bibliography for card-index purposes.

The presentation of the journal is excellent, and in this issue papers have been contributed in English (3), French (1) and German (1).

A. COUPER, University of Bristol

J. Electroanal. Chem., 19 (1968) 448

Atomic and Nuclear Chemistry, Vol. I. Atomic theory and structure of the atom, by T. A. H. PEACOCKE, Pergamon Press, Oxford, xv+140 pages, price 25 s.

This volume forms part of the Intermediate Chemistry Division of the Commonwealth and International Library, and is the first part of a two-volume treatise.

The author develops the subject along historical lines, starting as far back as the ideas of LEUKIPPOS and DEMOKRITOS. There is sufficient relevant personal detail of such people as DALTON, PROUST, NEWLANDS and MOSELEY, etc., to make the narrative both interesting and lively. The evolution of our present-day knowledge of the nuclear atom is put in a very digestible form, and this reviewer recommends this little book to a much wider readership than the sixth form audience proposed in the preface.

In addition to getting an excellent "birds-eye-view" of the development and current state of knowledge of atomic theory, the reader will pick up such interesting tit-bits as that test-tubes, rubber tubing and desiccators were all invented by BERZELIUS; that DE BROGLIE's tutor considered his prediction that electrons should show interference effects as unwise to include in his thesis; and that NEWLANDS' paper on octaves of elements was refused by the Chemical Society amid ridicule. Thus does science grow, and this book is an answer to those who would wish to teach atomic theory solely in accepted contemporary ideas.

The second volume of this work is to contain more experimental work, especially in the field of radiochemistry, and promises to be a satisfying complement to Vol. I.

E. W. ABEL, University of Bristol

J. Electroanal. Chem., 19 (1968) 448

**JOURNAL OF ELECTROANALYTICAL CHEMISTRY AND INTERFACIAL
ELECTROCHEMISTRY, VOL. 19 (1968)**

AUTHOR INDEX

ARMSTRONG, R. D.	233	HAYTER, J. B.	181	PAYNE, R.	1
ASTLEY, D. J.	325	HELLO, O.	37	PERDU, F.	310
BARCLAY, D. J.	318	HOLLECK, L.	439	POIRIER D'ANGÉ D'ORSAY, E.	
BATICLE, A. M.	310	HURWITZ, H. D.	441	335	
BAUER, H. H.	15	JENARD, A.	441	POSEY, F. A.	99
BEG, M. A.	175	JENKINS, H. W.	385	PRAVDIĆ, V.	267
BEHR, B.	373	JINDAL, M. R.	436	RACE, W. P.	233
BOCKRIS, J. O'M.	446	JONES, J. R.	297	ROWLINSON, J. A.	297
BRAND, M. J. D.	157	KABIR-UD-DIN	175	SATTAR, M. A.	351
BRANICA, M.	259	KAMATH, V. N.	137, 249	SAWYER, D. T.	405
BRAUN, S.	23	KHAN, A. A.	175	SCHWARZER, O.	391
BREITER, M. W.	131	KOOIJMAN, D. J.	365, 445	SENGUPTA, M.	199
BREUKEL, J. S. M. C.	85	LAGROU, A.	125, 413	SCHELLER, F.	187
BRITZ, D.	15	LAL, H.	137, 249	SLUYTERS, J. H.	73, 85, 305
ČAJA, J.	267	LANDSBERG, R.	187, 391	SLUYTERS-REHBACH, M.	73, 85, 305
CHAND, P.	431	LANTZ, P. M.	99	SPITZER, H.-J.	187
CONWAY, B. E.	351	LANZA, P.	275, 289	TARASZEWSKA, J.	373
ČUKMAN, D.	267	LEVART, E.	335	TEMMERMAN, E.	423
DELAHAY, P.	61	McCULLOUGH, J. G.	111	THIRSK, H. R.	233, 325
FLEET, B.	157	MACOVSKI, M. E.	219	TIMMER, B.	73, 305
GELB, R. I.	215	MALIK, W. U.	431, 436	VERBEEK, F.	125, 413, 423
GILEADI, E.	446	MAMANTOV, G.	385	VETTERL, V.	169
GOLDMAN, J. A.	205	MANNING, D. L.	385	VIG, S. K.	147
GOOLSBY, A. D.	405	MANOUŠEK, O.	147	VIRES, W. T. DE	41, 55
HALE, J. M.	315	MEITES, L.	111	ZUMAN, P.	147
HARRISON, J. A.	325	MEYER, R. E.	99	ŽUTIĆ, M.	259
HAYNES, R.	446	MÜLLER, S.	187		

JOURNAL OF ELECTROANALYTICAL CHEMISTRY AND INTERFACIAL ELECTROCHEMISTRY, VOL. 19 (1968)

SUBJECT INDEX

- Acetophenones,
reduction of some — (Jones, Rowlinson) 297
- A.c. polarography,
base-current depressions in — (Britz, Bauer) 15
- Additives,
effect of — on the aggregation number of dyes (Malik, Chand) 431
- Adsorption,
— and faradaic impedance (Sluyters *et al.*) 305
(Baticle, Perdu) 310
- Aggregation number, of dyes,
detn. of — and the effect of additives on it (Malik, Chand) 431
- Alkyl, see mercury-alkyl compounds
- Base-current depression,
a.c. polarographic — not due to adsorption (Britz, Bauer) 15
- Benzene derivatives, see *o,p*-disubstituted b.d.
- Booth theory,
— of electrophoresis of liquid drops (Sengupta) 199
- Boundary, see moving boundary
- Cadmium,
detn. of traces Tl in — (Temmerman, Verbeek) 423
binding of —^{II} with ovalbumin (Malik, Jindal) 436
- Carbon dioxide,
films on platinized Pt in — soln. (Kamath, Lal) 249
oxidation of films in — on platinized Pt (Kamath, Lal) 137
oxidation of reduced — and other species on platinized Pt (Breiter) 131
- Carbon monoxide, chemisorbed,
oxidation of — and other species on platinized Pt (Breiter) 131
- Channel flow, see double-electrode ...
- Chemical softness,
— and specific adsorption at electrodes (Barclay) 318
- Chloride ion,
analysis of — on the Ag electrode (Meyer *et al.*) 99
- Chronopotentiometry, see constant-current chr., programmed-current chr.
- Cinnamic acids, see 4-cyanocinnamic acids
- Cobalt,
detn. of traces Ni in — (Lagrou, Verbeek) 125
- detn. of traces Mn and Zn in — (Lagrou, Verbeek) 413
- Cobalt^{II}-hydroxycyanomolybdates^{IV},
composition of — (Kabir-ud-Din *et al.*) 175
- Complex argument, see error function
- Complexes, see stability constants
- Constant-current chronopotentiometry,
double-layer charging in — at a Hg-film electrode (de Vries) 41
- Copper^{II},
binding of — with ovalbumin (Malik, Jindal) 436
- Copper^{II}-hydroxycyanomolybdate^{IV},
composition of — (Kabir-ud-Din *et al.*) 175
- 4-Cyanocinnamic acid,
polarography of — and its ethyl ester (Brand, Fleet) 157
- 1,3-Diaminopropane, see silver-1,3-diaminopropane system
- Differential capacitance measurement,
a self-timing bridge for — (Hayter) 181
- Dimer-monomer reduction,
polarographic wave for — with strong adsorption (Gelb) 215
- Disk electrodes, partially covered,
dependence of the limiting current on — (Scheller *et al.*) 187
- o,p*-Disubstituted benzene derivatives,
two-electron step reduction of — (Zuman *et al.*) 154
- Double-electrode in a channel flow,
product transport in a — (Braun) 23
- Double-layer,
structure of — at anodically-polarized Hg electrodes in OH⁻ soln. (Armstrong *et al.*) 233
- Dyes, aggregation number of,
detn. of — and the effect of additives on it (Malik, Chand) 431
- Electric fields, strong,
ion-pairing in — (Jenard, Hurwitz) 441
- Electrochemical rate constants,
potential dependence and upper limits of — (Hale) 315
- Electrode, see double-electrode, ideal reversible e., mercury-film e., mercury-mercury^I e., nickel oxide e., platinum e.
- Electrode kinetics,
— and double-layer structure (Sluyters *et al.*) 85

- Electrophoresis,
theory of —— of liquid drops (Sengupta) 199
- Error function, of complex argument,
computer program for —— (Kooijman) 445
- Faradaic impedance,
adsorption and —— (Sluyters *et al.*) 305
(Baticle, Perdu) 310
- Fluorides, molten,
the Ni-Ni^{II} couple in —— (Jenkins *et al.*) 385
- Formic acid,
films on platinized Pt in —— (Kamath, Lal) 249
oxidation of films in —— on platinized Pt (Kamath, Lal) 137
- Galvanic cells,
impedance of —— (Timmer *et al.*) 73
- Glycine, see silver-glycine system
- Hydrogen evolution reaction,
separation factor/potential dependence for —— (Bockris *et al.*) 446
- Hydrolysable ligand,
metal ion reduction in the presence of a —— (Macovschi) 219
- Hydroxocyanogen compounds,
amperometric and conductometric studies of —— (Kabir-ud-Din *et al.*) 175
- Hydroxylamine,
oxidation of —— on Pt and Au in DMSO (Goolsby, Sawyer) 405
- Hypochlorous acid,
reduction of —— and its anion on Pt (Schwarzer, Landsberg) 391
- Ideal reversible electrode,
admittance of —— with adsorption (Delahay) 61
- Impedance, operational,
use of —— in transient methods (Levart, Poirier) 335
- Indium^{III}-indium amalgam electrode,
impedance of —— in KSCN and KCl soln. (Timmer *et al.*) 73
- Ion-pairing,
— in strong electric fields (Jenard, Hurwitz) 441
- Ligands, nature of,
a method for the definition of the —— (Lanza) 275, 289
- Liquid drops,
electrophoresis of —— (Sengupta) 199
- Manganese,
detn. of traces —— and Zn in Co (Lagrou, Verbeek) 413
- Mercury,
oxidation of —— in KCl soln. (Behr, Taraszewska) 373
- Mercury-alkyl compounds,
adsorption effects in the formation of —— (Holleck) 439
- Mercury electrode, anodically-polarized,
structure of double layer at —— in OH⁻ soln. (Armstrong *et al.*) 233
- Mercury-film electrode,
constant-current chronopotentiometry at —— (de Vries) 41
- Mercury-mercury^I electrode,
kinetics of the —— with specific adsorption (Kooijman) 365
- Metal ions, simple or complexed,
eqn. of polarographic waves of —— (Macovschi) 219
reduction of —— in the presence of a hydrolysable ligand (Macovschi) 219
- Metal layers,
formation of —— (Astley *et al.*) 325
- Methanol,
films on platinized Pt in —— (Kamath, Lal) 249
oxidation of films in —— on platinized Pt (Breiter) 131
(Kamath, Lal) 137
- Monomer, see dimer-monomer,
Moving boundary analysis,
(Hello) 37
- Nickel,
detn. of traces —— in Co (Lagrou, Verbeek) 125
- Nickel^{II}-hydroxocyanomolybdate^{IV},
composition of —— (Kabir-ud-Din *et al.*) 175
- Nickel-nickel^{II} couple,
e.m.f. measurements on —— in fluorides (Jenkins *et al.*) 385
- Nickel oxide electrode,
thin film oxide layers on —— (Conway, Sattar) 351
- Niobium^V,
reduction of —— in HCl soln. at Hg electrodes (McCullough, Meites) 111
- Nucleosides,
polarography of —— (Vetterl) 169
- Ovalbumin,
binding of Cu^{II} and Cd^{II} with —— (Malik, Jindal) 436
- Platinized platinum,
oxidation of films on —— in CH₂OH, HCOOH and CO₂ soln. (Kamath, Lal) 249
- Platinum electrode,
reduction of HClO and ClO⁻ on —— (Schwarzer, Landsberg) 391
- Potassium chloride soln.,
oxidation of Hg in —— (Behr, Taraszewska) 373
- Programmed-current chronopotentiometry,
double-layer charging in —— (de Vries) 55

- Rate constants, see electrochemical r.c.
- Redox reactions, homogeneous and symmetrical,
a titration curve eqn. for —— (Goldman) 205
- Reversible electrode, see ideal r.e.
- Self-timing bridge, employing phase detection,
a —— for differential capacitance measurement (Hayter) 181
- Silver^I-1,3-diaminopropane system,
evaluation of stability constants of —— (Lanza) 289
- Silver^I-glycine system,
evaluation of stability constants of —— (Lanza) 275
- Silver-silver chloride system,
chronopotentiometry of —— (Meyer *et al.*) 99
- Sodium bicarbonate soln.,
oxidation of U^{IV} in —— (Cukman *et al.*) 267
- Specific adsorption at electrodes,
chemical softness and —— (Barclay) 318
- Stability constants, of complexes,
an acidimetric criterion for —— (Lanza) 275, 289
- Thallium,
detn. of traces —— in Cd (Temmerman, Verbeek) 423
- Thallium^I-thallium amalgam reaction,
interpretation of data for —— (Baticle, Perdu) 310
- Time-domain reflectometry,
application of —— for electrode processes (Payne) 1
- Titration curve eqn., general,
a —— for homogeneous and symmetrical redox reactions (Goldman) 205
- Transient methods,
use of the operational impedance in —— (Levart, Poirier) 335
- Transition-metal substrates,
hydrogen evolution reaction for —— (Bockris *et al.*) 446
- Uranium^{IV},
oxidation of —— in NaHCO₃ soln. (Cukman *et al.*) 267
- Uranyl peroxodicarbonato ion,
double-layer effect on reduction of —— (Zutic, Branica) 259
- Zinc,
detn. of traces —— and Mn in Co (Lagrou, Verbeek) 413
- Zinc^{II}-hydroxocyanomolybdate^{IV},
composition of —— (Kabir-ud-Din *et al.*) 175
- Zinc^{II}-zinc amalgam electrode reaction,
potential dependence of the —— (Sluyters *et al.*) 85

CONTENTS

The formation of metal layers D. J. ASTLEY, J. A. HARRISON AND H. R. THIRSK (Newcastle upon Tyne, Great Britain)	325
Etude théorique de l'utilisation de l'impédance opérationnelle dans les méthodes transitoires E. LEVART ET E. POIRIER d'ANGÉ d'ORSAY (Bellevue, France)	335
Electrochemistry of the nickel oxide electrode. Part VIII. Stoichiometry of thin film oxide layers B. E. CONWAY AND M. A. SATTAR (Ottawa, Ont., Canada)	351
Kinetics of the Hg(I)/Hg electrode with consideration of specific adsorption D. J. KOOIJMAN (New York, N.Y., U.S.A.)	365
On the anodic oxidation of mercury in KCl solutions B. BEHR AND J. TARASZEWSKA (Warsaw, Poland)	373
E.m.f. measurements on the nickel-nickel(II) couple in molten fluorides H. W. JENKINS, G. MAMANTOV AND D. L. MANNING (Knoxville and Oak Ridge, Tenn., U.S.A.)	385
Zur Reduktion der Hypochlorsäure und ihres Anion an Platin-Elektroden O. SCHWARZER UND R. LANDSBERG (Merseburg, Deutschland)	391
The electrochemical oxidation of hydroxylamine at platinum and gold electrodes in dimethyl-sulfoxide A. D. GOOLSBY AND D. T. SAWYER (Riverside, Calif., U.S.A.)	405
Determination of traces of zinc and manganese in cobalt by pulse polarography A. LAGROU AND F. VERBEEK (Ghent, Belgium)	413
The determination of traces of thallium in cadmium by pulse polarography E. TEMMERMAN AND F. VERBEEK (Ghent, Belgium)	423
Polarographic determination of the aggregation number of dyes and the effect of additives on the aggregation W. U. MALIK AND P. CHAND (Roorkee, U.P., India)	431
<i>Short communications</i>	
Polarographic studies on the binding of copper(II) and cadmium(II) with ovalbumin W. U. MALIK AND M. R. JINDAL (Roorkee, U.P., India)	436
Adsorptionseffekte bei Bildung von Quecksilber-Alkylverbindungen im Zuge polarographischer Reduktionsprozesse L. HOLLECK (Bamberg, Deutschland)	439

(Continued on the next page)

(Continued from previous page)

Ion-pairing in strong electric fields A. JENARD AND H. D. HURWITZ (Brussels, Belgium)	441
Computer program for the error function of complex argument D. J. KOOIJMAN (New York, N.Y., U.S.A.)	445
The dependence of the separation factor for the hydrogen evolution reaction upon potential: Mechanism evidence for transition metal substrates J. O' M. BOCKRIS, E. GILEADI AND R. HAYNES (Philadelphia, Pa., U.S.A.)	446
<i>Book reviews</i>	448
<i>Author index</i>	449
<i>Subject index</i>	450

COPYRIGHT © 1968 BY ELSEVIER SEQUOIA S.A., LAUSANNE
PRINTED IN THE NETHERLANDS

RADIATION RESEARCH REVIEWS

Editors: G. O. PHILLIPS (Salford) and R. B. CUNDALL (Nottingham)
Consultant Editor: F. S. DAINTON, F. R. S. (Nottingham)

The objective of RADIATION RESEARCH REVIEWS is to secure from leading research workers throughout the world review papers giving broad coverage of important topics on the physical and chemical aspects of radiation research. The main emphasis will be on experimental studies, but relevant theoretical subjects will be published as well.

Tabulated data helpful to workers in the field will also be included.

RADIATION RESEARCH REVIEWS appears in four issues per approx. yearly volume. Subscription price per volume Dfl. 90.00 plus Dfl. 3.00 postage or equivalent (£10.9.6 plus 7s. or US\$25.00 plus US\$.85).

For further information and specimen copy write to:



**Elsevier
Publishing
Company**

P.O. Box 211, AMSTERDAM The Netherlands

531 E

25 Nov 2512

